

**Ministry of Higher Education & Scientific Research
Ninevah University
College of Electronics Engineering
Communication Engineering Department**



An Investigation on F-OFDM Spectrum Efficiency for 5G systems

By

Zhraa Zuheir Yahya

M.Sc. Thesis

In

Communication Engineering

Supervised by

Asst. Prof. Dr. Dia M. Ali

2022 A.D.

1443 A.H.

**Ministry of Higher Education & Scientific Research
Ninevah University
College of Electronics Engineering
Communication Engineering Department**



An Investigation on F-OFDM Spectrum Efficiency for 5G systems

A thesis Submitted

By

Zhraa Zuheir Yahya

To

The Council of the College of Electronic Engineering
Ninevah University

As a Partial Fulfillment of the Requirements
for the Degree of Master of Science

In

Communication Engineering

Supervised by

Asst. Prof. Dr. Dia M. Ali

بِسْمِ اللَّهِ الرَّحْمَنِ الرَّحِيمِ

﴿يَسْتَبْشِرُونَ بِنِعْمَةٍ مِّنَ اللَّهِ وَفَضْلٍ وَأَنَّ اللَّهَ لَا يُضِيعُ أَجْرَ الْمُؤْمِنِينَ﴾

صَدَقَ اللَّهُ الْعَظِيمُ

سورة آل عمران آية (171)

ACKNOWLEDGMENTS

First and foremost, praise and thanks be to Allah, Who has given me strength, patience, and ability to do this thesis.

I would like to express my sincere gratitude and thank to my supervisor Asst. Prof. Dr. Dia M. Ali for his continuous guidance, useful suggestions, constant encouragement and assistance to me throughout preparing this research. It was a great opportunity for me to work with him.

I would like to express my gratitude and thanks to the former Head of the Communications Engineering Department, Asst. Prof. Dr. Younis M. Abbosh, and the current Head, Asst. Prof. Dr. Mahmud A. Mahmud. I would also like to thank all the staff members of the Communication Engineering Department who have provided me with science and knowledge throughout the preparatory year. Thanks to all those who have given me advice and provided me with useful information during the research period.

Last but not least, I want to express my heartfelt gratitude to my dear father (may Allah rest his soul) for his unflinching support and encouragement of me till the last days of his life. I would also like to thank the rest of my family for their inspiration and support.

Zhraa Zuheir Yahya

ABSTRACT

According to the 3rd Generation Partnership Project (3GPP) and International Telecommunication Union (ITU) standards, the Fifth Generation (5G) networks will have to deal with heterogeneous services and requirements. One important challenge of the next generation (5G) is the effective use of the spectrum, which requires a flexible physical layer design to boost the Spectrum Efficiency (SE) for a wide range of applications over radio resources. The current thesis introduces a quasi-orthogonal waveform called Filtered-Orthogonal Frequency Division Multiplexing (F-OFDM) for spectral localization and asynchronous transmission capability. Two modeling scenarios (equal and unequal sized sub-bands) have been proposed utilizing Matlab-Simulink and LabVIEW NXG. Several Window-Sinc filter forms have been used to limit user/service spectrum leakage, and to enhance the performance, two window function forms have been proposed. Simulation results showed that the F-OFDM using proposed window 2 accomplished 5.2% and 5.8% higher SE than the conventional OFDM in the first and second scenarios, respectively. Furthermore, the two simulators exhibited the same Bit Error Rate (BER) behavior, and their performances diverged from those of OFDM at higher Signal-to-Noise Ratio (SNR) values. The Peak-to-Average Power Ratio (PAPR) has also increased slightly as a result of the filter influence. The Universal Software Radio Peripheral (USRP) X310, one of the Software Defined Radio (SDR) hardware technology products, has been used to perform the proposed transceiver models in a real-world indoor environment. The testbed was implemented using a single USRP device and a Personal Computer with other equipment. A practical operation was conducted at 915 MHz and 3.4 GHz carrier frequencies to demonstrate the flexibility of the SDR technology. The acquired SE enhancements were 5% and 5.6% for the first and second scenarios, respectively, which validates the simulation results obtained.

TABLE OF CONTENTS

| Subject | | Page |
|--|---|-------------|
| ACKNOWLEDGMENTS | | I |
| ABSTRACT | | II |
| TABLE OF CONTENTS | | III |
| LIST OF FIGURES | | VI |
| LIST OF TABLES | | X |
| LIST OF ABBREVIATIONS | | XI |
| LIST OF SYMBOLS | | XIII |
| CHAPTER ONE-INTRODUCTION | | |
| 1.1 | Overview | 1 |
| 1.2 | Literature Review | 2 |
| 1.3 | Statement of the Problem | 6 |
| 1.4 | Aims of the Thesis | 6 |
| 1.5 | Thesis Organization | 7 |
| CHAPTER TWO-SPECTRUM EFFICIENCY TECHNIQUES FOR 5G | | |
| 2.1 | Introduction | 8 |
| 2.2 | 5G Fundamentals | 8 |
| 2.3 | Spectrum for 5G | 9 |
| 2.4 | 5G Spectrum Efficiency Enhancement Techniques | 10 |
| 2.5 | OFDM Technology Basics | 12 |
| 2.5.1 | OFDM Transceiver Structure | 15 |
| 2.5.2 | OFDM Signal Generation | 16 |
| 2.5.3 | OFDM Block Structure | 17 |
| 2.5.3.1 | Pilot Symbols Configuration | 18 |
| 2.5.4 | Channel Estimation | 19 |
| 2.5.5 | Synchronization | 20 |
| 2.5.6 | OFDM Implementation Issues | 21 |
| 2.5.6.1 | Peak-to-Average Power Ratio (PAPR) | 21 |

| | | |
|---|--|----|
| 2.5.6.2 | Sidelobes | 22 |
| 2.6 | Required Waveform Specifications for 5G | 23 |
| 2.7 | Candidates 5G Waveforms | 24 |
| 2.8 | Filtered-OFDM (F-OFDM) | 25 |
| 2.8.1 | F-OFDM Transceiver Scheme | 26 |
| 2.8.2 | Sub-band Filter Characteristics | 28 |
| CHAPTER THREE- F-OFDM MODELING, SIMULATION AND RESULTS | | |
| 3.1 | Introduction | 29 |
| 3.2 | Model Assumptions | 29 |
| 3.3 | First Approach MATLAB-Simulink F-OFDM Methodology | 32 |
| 3.3.1 | OFDM System Model (Simulink) | 32 |
| 3.3.2 | F-OFDM System Model (Simulink) | 35 |
| 3.3.3 | F-OFDM and OFDM Results and Comparisons (Simulink) | 39 |
| 3.3.4 | F-OFDM Sub-banding (Simulink) | 43 |
| 3.3.4.1 | Equal-Sized Sub-bands F-OFDM (Simulink) | 43 |
| 3.3.4.2 | Equal-Sized Sub-bands Results and Comparisons (Simulink) | 45 |
| 3.3.4.3 | Unequal-Sized Sub-bands F-OFDM (Simulink) | 49 |
| 3.3.4.4 | Unequal-Sized Sub-bands Results and Comparisons (Simulink) | 49 |
| 3.4 | Second Approach LabVIEW NXG F-OFDM Methodology | 54 |
| 3.4.1 | OFDM System Model (LabVIEW) | 54 |
| 3.4.2 | F-OFDM System Model (LabVIEW) | 57 |
| 3.4.3 | F-OFDM and OFDM Results and Comparisons (LabVIEW) | 60 |
| 3.4.4 | F-OFDM Sub-banding (LabVIEW) | 63 |
| 3.4.4.1 | Equal-Sized Sub-bands F-OFDM (LabVIEW) | 63 |
| 3.4.4.2 | Equal-Sized Sub-bands Results and Comparisons (LabVIEW) | 65 |

| | | |
|---|---|-----|
| 3.4.4.3 | Unequal-Sized Sub-bands F-OFDM (LabVIEW) | 69 |
| 3.4.4.4 | Unequal-Sized Sub-bands Results and Comparisons (LabVIEW) | 69 |
| 3.5 | Results Discussion and Comparisons | 73 |
| CHAPTER FOUR- F-OFDM IMPLEMENTATION BASED SOFTWARE DEFINED RADIO | | |
| 4.1 | Introduction | 78 |
| 4.2 | Software Defined Radio Fundamentals | 78 |
| 4.2.1 | SDR Advantages | 81 |
| 4.2.2 | SDR Disadvantages | 82 |
| 4.3 | Ettus Research™ USRP-X310 | 82 |
| 4.3.1 | USRP X310 Specifications | 84 |
| 4.3.2 | USRP Signal Workflow | 85 |
| 4.3.3 | USRP Configuration in LabVIEW NXG | 86 |
| 4.4 | F-OFDM Practical Implementation | 88 |
| 4.4.1 | Hardware Requirements | 88 |
| 4.4.2 | Equal-Sized Sub-bands F-OFDM Practical Implementation | 88 |
| 4.4.3 | Unequal-Sized Sub-bands F-OFDM Practical Implementation | 99 |
| 4.4.4 | Spectrum Efficiency Enhancement | 104 |
| CHAPTER FIVE- CONCLUSION RESULTS AND SCOPE FUTURE DEVELOPMENT | | |
| 5.1 | Conclusion | 105 |
| 5.2 | Future Works | 107 |
| REFERENCES | | 108 |
| APPENDIX-A | | A-1 |
| APPENDIX-B | | B-1 |

LIST OF FIGURES

| Figure | Title | Page |
|---------------|---|-------------|
| 2.1 | Anticipated IMT usage categories for 2020 and beyond | 9 |
| 2.2 | Frequency bands for 5G system | 10 |
| 2.3 | OFDM spectrum | 13 |
| 2.4 | Cyclic prefix concept | 14 |
| 2.5 | OFDM transceiver structure | 16 |
| 2.6 | Pilots arrangement types: (a) Block pilot (b) Comb pilot (c) Lattice pilot | 19 |
| 2.7 | Mixed numerologies design | 24 |
| 2.8 | Methods of sub-band filtering: (a) Per RB (b) Per user (c) Per service | 26 |
| 2.9 | F-OFDM transceiver block diagram: (a) Transmit side (b) Receive side | 27 |
| 3.1 | Flowchart of minimizing the guard band between the sub-bands | 31 |
| 3.2 | OFDM block (Simulink) | 32 |
| 3.3 | A snapshot constellation diagrams of various modulation orders in Simulink: (a) 16-QAM, (b) 64-QAM, (c) 128-QAM, (d) 256-QAM, (e) 512-QAM | 33 |
| 3.4 | IFFT process subsystem | 34 |
| 3.5 | FFT process subsystem | 34 |
| 3.6 | Time-Frequency domain representation of the utilized window functions | 35 |
| 3.7 | Magnitude and phase response of the Gaussian window filter | 36 |
| 3.8 | Magnitude and phase response of the Nuttall window filter | 37 |
| 3.9 | Magnitude and phase response of the Hanning window filter | 37 |
| 3.10 | Magnitude and phase response of the Blackman window filter | 37 |
| 3.11 | Magnitude and phase response of the BlackmanHarris window filter | 38 |
| 3.12 | Magnitude and phase response of the Proposed window 1 filter | 38 |
| 3.13 | Magnitude and phase response of the Proposed window 2 filter | 38 |

| | | |
|------|---|----|
| 3.14 | Impulse response of 513 samples length of the utilized digital filter | 39 |
| 3.15 | MATLAB-Simulink block diagram of one sub-band F-OFDM | 39 |
| 3.16 | F-OFDM power spectrum compared with OFDM spectrum using different Window-Sinc filters (MATLAB-Simulink) | 40 |
| 3.17 | BER performance of F-OFDM compared with OFDM using 16-QAM Simulink results | 41 |
| 3.18 | BER performance of F-OFDM compared with OFDM using 64-QAM Simulink results | 41 |
| 3.19 | BER performance of F-OFDM compared with OFDM using 128-QAM Simulink results | 42 |
| 3.20 | BER performance of F-OFDM compared with OFDM using 256-QAM Simulink results | 42 |
| 3.21 | BER performance of F-OFDM compared with OFDM using 512-QAM Simulink results | 42 |
| 3.22 | Sub-bands F-OFDM waveform in MATLAB-Simulink | 44 |
| 3.23 | Power spectrum of equal-sized sub-bands OFDM (Simulink) | 45 |
| 3.24 | Power spectrum of equal-sized sub-bands F-OFDM using Blackman window filter (Simulink) | 46 |
| 3.25 | Power spectrum of equal-sized sub-bands F-OFDM using proposed window 1 filter (Simulink) | 46 |
| 3.26 | Power spectrum of equal-sized sub-bands F-OFDM using proposed window 2 filter (Simulink) | 46 |
| 3.27 | Average BER of equal-sized sub-bands (Simulink) | 47 |
| 3.28 | Normalized SE of equal-sized sub-band F-OFDM compared to OFDM (Simulink) | 48 |
| 3.29 | Average PAPR of equal-sized sub-band F-OFDM (Simulink) | 48 |
| 3.30 | Power spectrum of unequal-sized sub-bands OFDM (Simulink) | 50 |
| 3.31 | Power spectrum of unequal-sized sub-bands F-OFDM using Blackman window filter (Simulink) | 50 |
| 3.32 | Power spectrum of unequal-sized sub-bands F-OFDM using proposed window 1 filter (Simulink) | 50 |
| 3.33 | Power spectrum of unequal-sized sub-bands F-OFDM using proposed window 2 filter (Simulink) | 51 |
| 3.34 | Average BER of unequal-sized sub-bands sizes (Simulink) | 51 |

| | | |
|------|--|----|
| 3.35 | Normalized SE of unequal-sized sub-bands F-OFDM compared to OFDM (Simulink) | 52 |
| 3.36 | Average PAPR of unequal-sized sub-bands F-OFDM (Simulink) | 53 |
| 3.37 | OFDM diagram window in LabVIEW NXG | 55 |
| 3.38 | A snapshot constellation diagrams of various modulation orders in LabVIEW: (a) 16-QAM, (b) 64-QAM, (c) 128-QAM, (d) 256-QAM, (e) 512-QAM | 56 |
| 3.39 | Interfacing process between MATLAB function and LabVIEW NXG | 58 |
| 3.40 | F-OFDM diagram window in LabVIEW NXG | 59 |
| 3.41 | F-OFDM power spectrum compared with OFDM spectrum using different window-sinc filters (LabVIEW) | 60 |
| 3.42 | BER performance of F-OFDM compared with OFDM using 16-QAM LabVIEW results | 61 |
| 3.43 | BER performance of F-OFDM compared with OFDM using 64-QAM LabVIEW results | 61 |
| 3.44 | BER performance of F-OFDM compared with OFDM using 128-QAM LabVIEW results | 62 |
| 3.45 | BER performance of F-OFDM compared with OFDM using 256-QAM LabVIEW results | 62 |
| 3.46 | BER performance of F-OFDM compared with OFDM using 512-QAM LabVIEW results | 62 |
| 3.47 | Sub-bands F-OFDM waveform in LabVIEW NXG | 64 |
| 3.48 | Power spectrum of equal-sized sub-bands OFDM (LabVIEW) | 65 |
| 3.49 | Power spectrum of equal-sized sub-bands F-OFDM using Blackman window filter (LabVIEW) | 66 |
| 3.50 | Power spectrum of equal-sized sub-bands F-OFDM using proposed window 1 filter (LabVIEW) | 66 |
| 3.51 | Power spectrum of equal-sized sub-bands F-OFDM using proposed window 2 filter (LabVIEW) | 66 |
| 3.52 | Average BER of equal-sized sub-bands (LabVIEW) | 67 |
| 3.53 | Normalized SE of equal-sized sub-bands F-OFDM compared to OFDM (LabVIEW) | 68 |
| 3.54 | Average PAPR of equal-sized sub-bands F-OFDM (LabVIEW) | 68 |
| 3.55 | Power spectrum of unequal-sized sub-bands OFDM (LabVIEW) | 69 |

| | | |
|------|---|----|
| 3.56 | Power spectrum of unequal-sized sub-bands F-OFDM using Blackman window filter (LabVIEW) | 70 |
| 3.57 | Power spectrum of unequal-sized sub-bands F-OFDM using proposed window 1 filter (LabVIEW) | 70 |
| 3.58 | Power spectrum of unequal-sized sub-bands F-OFDM using proposed window 2 filter (LabVIEW) | 70 |
| 3.59 | Average BER of unequal-sized sub-bands sizes (LabVIEW) | 71 |
| 3.60 | Normalized SE of unequal-sized sub-bands F-OFDM compared to OFDM (LabVIEW) | 72 |
| 3.61 | Average PAPR of unequal-sized sub-bands F-OFDM (LabVIEW) | 72 |
| 3.62 | The power spectrum comparison among OFDM, F-OFDM and UFMC waveforms | 73 |
| 3.63 | Average BER comparison for: (a) OFDM, (b) F-OFDM (Blackman), (c) F-OFDM (Proposed Window1), (d) F-OFDM (Proposed Window2) | 74 |
| 4.1 | SDR transmitter block diagram | 80 |
| 4.2 | SDR receiver block diagram | 81 |
| 4.3 | USRP-X310: (a) photograph (b) Front panel (c) Back panel | 83 |
| 4.4 | USRP X310 components | 84 |
| 4.5 | USRP network connection | 85 |
| 4.6 | USRP nodes configuration in LabVIEW NXG: (a) transmitter (b) receiver | 87 |
| 4.7 | F-OFDM equal-sized sub-bands transmit signal process through USRP | 89 |
| 4.8 | LabVIEW NXG diagram of transmit/receive signal setup | 90 |
| 4.9 | F-OFDM equal-sized sub-bands received signal process through USRP | 92 |
| 4.10 | Testbed of the equal-sized sub-bands waveform F-OFDM | 93 |
| 4.11 | Transmit/Receive process summary for equal-sized sub-bands F-OFDM | 94 |
| 4.12 | Equal-sized sub-bands waveform transmit signal spectrum and constellation diagrams: (a) OFDM (b) F-OFDM | 95 |
| 4.13 | Equal-sized sub-bands waveform receive signal spectrum and constellation diagrams: (a) OFDM (b) F-OFDM | 96 |

| | | |
|------|---|-----|
| 4.14 | Equal-sized sub-bands waveform power spectrum at 915 MHz: (a) OFDM (b) F-OFDM | 97 |
| 4.15 | Equal-sized sub-bands waveform power spectrum at 3.4 GHz: (a) OFDM (b) F-OFDM | 98 |
| 4.16 | Unequal-sized sub-bands waveform transmit signal spectrum and constellation diagrams: (a) OFDM (b) F-OFDM | 100 |
| 4.17 | Unequal-sized sub-bands waveform receive signal spectrum and constellation diagrams: (a) OFDM (b) F-OFDM | 101 |
| 4.18 | Unequal-sized sub-bands waveform power spectrum at 915 MHz: (a) OFDM (b) F-OFDM | 102 |
| 4.19 | Unequal-sized sub-bands waveform power spectrum at 3.4 GHz: (a) OFDM (b) F-OFDM | 103 |
| 4.20 | Normalized SE for the equal-sized and unequal-sized sub-bands F-OFDM in practical | 104 |

LIST OF TABLES

| Table | Title | Page |
|--------------|--|-------------|
| 3.1 | SE enhancements for F-OFDM using a variety of used window functions | 75 |
| 3.2 | Minimum Guard band between the equal-sized sub-bands | 75 |
| 3.3 | Minimum Guard band between the unequal-sized sub-bands | 76 |
| 3.4 | Comparison the performance of the proposed waveform to some relevant works | 77 |
| 4.1 | Transmitting/Receiving setting parameters for USRP | 91 |

LIST OF ABBREVIATIONS

| Abbreviation | Name |
|--------------|---|
| 3GPP | 3rd Generation Partnership Project |
| 4G | Fourth Generation |
| 5G | Fifth Generation |
| ACLR | Adjacent Channel Leakage Ratio |
| ADC | Analog to Digital Converter |
| API | Application Programming Interface |
| AWGN | Additive White Gaussian Noise |
| BER | Bit Error Rate |
| CFO | Carrier Frequency Offset |
| CP | Cyclic Prefix |
| D2D | Device-to-Device communication |
| DAC | Digital to Analog Converter |
| DC | Direct Current |
| DDC | Digital Down Conversion |
| DDCE | Decision Directed Channel Estimation |
| DFT | Discrete Fourier transform |
| DFT-S-OFDMA | Discrete Fourier transform- Spread- Orthogonal Frequency Division Multiple Access |
| DUC | Digital Up Converter |
| eMBB | enhance Mobile Broad Band |
| FBMC | Filter Bank Multicarrier |
| FFT | Fast Fourier Transform |
| FIR | Finite Impulse Response |
| F-OFDM | Filtered-Orthogonal Frequency Division Multiplexing |
| FC-F-OFDM | fast-convolution-based filtered OFDM |
| FPGA | Field Programmable Gate Array |
| GFDM | Generalized Frequency Division Multiplexing |
| GigE | Gigabit Ethernet |
| GPP | General Purpose Processor |
| IBM | Interpolated Band-pass Method |
| ICI | Inter Carrier Interference |
| IDFT | Inverse Discrete Fourier Transform |
| IFFT | Inverse Fast Fourier Transform |
| IMT | International Mobile Telecommunications |
| INI | Inter Numerology Interference |
| IoT | Internet of Things |
| IQ | In-phase and Quadrature components |
| ISI | Inter Symbol Interference |
| ITU | International Telecommunication Union |

| | |
|-------|---|
| IUI | Inter-User-Interference |
| LDPC | Low Density Parity Check |
| MIMO | Multiple-Input Multiple-Output |
| mMTC | massive Machine Type Communication |
| NI | National Instruments |
| NOMA | Non-Orthogonal Multiple Access |
| OOBE | Out-Of-Band Emission |
| OFDM | Orthogonal Frequency Division Multiplexing |
| OQAM | Offset Quadrature Amplitude Modulation |
| PA | Power Amplifier |
| PACE | Pilot Aided Channel Estimation |
| PAPR | Peak-to-Average Power Ratio |
| PC | Personal Computer |
| PSK | Phase Shift Keying |
| PTS | Partial Transmit Sequence |
| QAM | Quadrature Amplitude Modulation |
| QoS | Quality of Service |
| RB | Resource Block |
| RF | Radio Frequency |
| SCMA | Sparse Code Multiple Access |
| SDR | Software Defined Radio |
| SE | Spectrum Efficiency |
| SLM | Selective mapping |
| SMA | SubMiniature version A |
| SNR | Signal-to-Noise Ratio |
| UFMC | Universal Filter Multicarrier |
| UHD | USRP Hardware Driver TM |
| URLLC | Ultra Reliable and Low Latency Communications |
| USRP | Universal Software Radio Peripheral |
| VI | Virtual Instrument |
| ZP | Zero prefix |

LIST OF SYMBOLS

| Symbol | Name |
|------------------------|--|
| $\tilde{\xi}_l(n)$ | F-OFDM Signal for the lth -sub-band |
| $\tilde{s}_m(t)$ | Transmitted OFDM Signal at Extended Time Interval |
| $BW_{g,i}$ | Minimum Guard Band between the Sub-bands |
| BW_u | Utilized Bandwidth |
| $C_{sub,n}$ | Capacity of each Sub-band |
| H_k | Channel Frequency Response |
| N_u | Number of used Subcarriers |
| T_{CP} | Cyclic Prefix Samples Length |
| T_s | OFDM Symbol Duration |
| Z_k | Additive White Gaussian Noise |
| $f_d(n)$ | Time-Domain Representation of Sinc Function Impulse Response |
| $f_l(n)$ | Digital Filter Impulse Response for lth -sub-band |
| f_{max} | Maximum Doppler Frequency |
| f_s | Sampling Frequency |
| n_u | Location of the Active Subcarrier for each Sub-band |
| $s_{m,k}$ | Modulated Data Symbols |
| $s_m(n \frac{T_s}{N})$ | Discrete-Time Transmitted OFDM Signal |
| $s_m(t)$ | Transmitted OFDM Signal |
| $X_{m,k}$ | OFDM Received Signal |
| Y_i | Complex Amplitude from i Paths |
| τ_i | Delay Time from i Paths |
| $f_l^*(-n)$ | Digital Filter Impulse Response for the received lth -sub-band |
| N | Number of Subcarriers |
| SE | Spectrum Efficiency |
| T | OFDM Signal Time Interval |
| $w(n)$ | Time-Domain Window Function |
| Δf | Subcarriers Space |
| SUB | Total Number of Sub-bands |
| sub | Sub-band Index |
| n_k | Additive White Gaussian Noise |

CHAPTER ONE

INTRODUCTION

1.1 Overview

In recent years, the traffic volume on wireless communication networks has extensively increased due to the demand for existing and new diversified services as well as an enormous increase in the number of users. For these reasons, it has become crucial to use the available spectrum more efficiently [1]. To accomplish all of those objectives, 5G (the developed wireless mobile generation) is being designed to incorporate a variety of existing technologies and new innovative techniques [2].

To enable extreme mobile broadband, 5G involves millimeter-wave spectral resources that are used in addition to the existing frequency bands, ranging from sub-1 GHz to 100 GHz. The vital issue concerning the available spectrum, particularly at lower frequencies, is Spectrum Efficiency (SE), which is defined as the maximum data rate that can be delivered within a given bandwidth measured in bit per second per Hertz (bit/s/Hz). The main objective of 5G is to significantly improve the SE by adopting new strategies to maximize connection density and deliver higher capacity [3]-[4].

The modulation waveform is one of the key technological components in the physical layer that significantly contributes to improve the SE in the utilized frequency band. In the Fourth Generation (4G), 90% of the spectrum is used for data transmission, and the rest (10%) are allocated as the guard band. In a 5G system, 94% to 99% of the available spectrum used for data transfer. The spectrum of the current Orthogonal Frequency Division Multiplexing (OFDM) technology (the approved downlink scheme for the 4G application) decays outside the allocated bandwidth due to the sidelobes, making it unsuitable for 5G applications. Many alternative multicarrier waveforms are being suggested for 5G spectrum confinement, solving the

high impact of Out-Of-Band Emission (OOBE) and repression interference leakage from neighboring channels using the filtration principle [3]-[5].

1.2 Literature Review

Several techniques have been emerged to satisfy the demands of the 5G network. The works listed below are relevant to this purpose:

In 2013, J. Li, E. Bala, and R. Yang [6] proposed a filter based on Resource Block (RB), which divides the entire available spectrum into blocks and the filter performed for block of subcarriers with an efficient polyphase implementation method. For varying Adjacent Channel Interference (ACI) situations, the performance was compared with OFDM and Filtered-OFDM (F-OFDM). The RB-F-OFDM outperforms F-OFDM when ACI is increased and lowers OOBE attainment. The study also contained reduction of Peak-to-Average Power Ratio (PAPR) using Selective Mapping (SLM) and Partial Transmit Sequence (PTS).

In 2015, J. Abdoli, M. Jia, and J. Ma [7] proposed an F-OFDM waveform to attain the required spectrum localization while keeping a permissible limit of Inter-Symbol-Interference/Inter-Carrier-Interference (ISI/ICI). The proposed F-OFDM enables asynchronous transmission of filtered orthogonal frequency division multiple access (F-OFDMA)/Filtered-Discrete Fourier Transform-Spread OFDMA (F-DFT-S-OFDMA) at each transmitter with a spectrum shaping filter to minimize the sidelobe leakage, and the receiver employs a bank of filters to reject Inter-User-Interference (IUI).

In the same year, X. Zhang et al. [8] described the general construction of F-OFDM with significant design aspects such as the filter design and guard tone. A comparison of waveform contenders for 5G was also included in the study demonstrating the merits of F-OFDM such simple equalizer at the receiver, the ability to be compatible with the Multiple-Input Multiple-Output (MIMO) technology, canceling the need for synchronized

transmission, and it offers forward and backward compatible. The authors claimed that the simulation model with four different kinds of services indicates that F-OFDM offers 46% higher information gains than the conventional OFDM.

In 2016, X. Cheng et al. [9] proposed a digital Finite Impulse Response (FIR) filter-based window function approach to evaluate the performance of F-OFDM applying distinctive time-domain window functions. They claimed that the suggested scheme was straightforward to configure and possesses a very low OOB, while maintaining the same bit error rate (BER) performance as conventional OFDM.

In the same year, D. Wu et al. [10] presented a field test design and implementation of F-OFDM. According to their results, F-OFDM has lower spectrum leakage and higher SE than conventional OFDM. The ability of F-OFDM to support multiple asynchronous sub-band transmissions was also demonstrated, with a performance loss caused by neighboring but asynchronous transmissions confirmed to be insignificant.

In 2017, J. Wang et al. [5] demonstrated the performance of three key technologies for the 5G system: Sparse code multiple access (SCMA), Polar codes, and F-OFDM based on the field trial testbed by NTT DOCOMO and HUAWEI. They claimed that the results of F-OFDM performance improved in terms of throughput and SE by 7.47%.

In the same year, R. Gerzaguet et al. [11] introduced a Block Filtered-OFDM to support asynchronous multi-user connections and spectrum localization. Their results of the proposed waveform offered the same performance in terms of SE and BER compared to the conventional Cyclic Prefix (CP)-OFDM with complexity cost and a simple equalizer at the receiver.

Again in the same year, C. An, B. Kim, and H. Ryu [12] proposed four various forms of window F-OFDM waveform based on the variation position

of the filter and the framework of the waveform which may help to increase the SE and decrease the OOB. When comparing simulation results to Filter Bank Multicarrier (FBMC) performance, they found that window F-OFDM has lower OOB at two forms of the proposed designs.

Also in the same year, L. Yang and Y. Xu [13] proposed an F-OFDM waveform with two sub-bands employing the Nuttall-Blackmanharris window filter as a candidate waveform for 5G. Various window functions were used to evaluate F-OFDM performance. The results of simulation were compared with the Hamming window and OFDM. They observed that, as compared to OFDM, their proposed filter scheme has the lower OOB and the same performance in terms of BER.

In 2018, L. Zhang et al. [14] presented the mathematical model and derived the conditions for attaining free interference, and one tap channel equalization used for the F-OFDM scheme. A multirate F-OFDM is also presented in the study, which reduces the complexity and cost of a communication system.

In 2019, M. Yang, Y. Chen, and L. Du [15] proposed an F-OFDM waveform with two sub-bands (users) in uplink asynchronous transmission to achieve the BER objective and SE enhancement using window-sinc filter. For various numerologies between the users, the authors derived the theoretical computation of BER on ISI, ICI and IUI. The filter parameters and guard band were optimized to enhance the performance and outperforms the conventional OFDM.

In the same year, S. Gokceli et al. [16] measured the OOB and ACLR for fast-convolution-based filtered-orthogonal frequency division multiplexing (FC-F-OFDM) using the (Universal Software Radio Peripheral) USRP RIO. According to their measurements, FC-F-OFDM processing outperformed windowed overlap-and-add OFDM processing in

terms of spectral containment. The study only dealt with the spectrum leakage without receiving the data.

Again in the same year, S. Roy and A. Chandra [17] presented a novel F-OFDM technique based on an FIR filter with a narrow bandwidth and an Interpolated Band-pass Method (IBM). They conclude that their simulation results show that the F-OFDM with an IBM achieves lower OOB with better BER than the F-OFDM.

In 2020, K. S. Chandran and C. K. Ali [18] proposed index modulation F-OFDM waveform with two sub-bands of different parameters to combat the effect of Inter-Numerology-Interference (INI) between the sub-bands. The obtained simulation results show that the performance of the mixed numerology waveform improved in terms of BER in comparison to conventional OFDM due to the reduced interference.

In the same year, M. A. Taher, H. S. Radhi, and A. K. Jameil [19] proposed the idea of convolution of two window functions in the time domain with various digital filter designs to improve the performance of F-OFDM and increase SE. They conclude since that there are no restrictions on the symbol size or on the order of Quadrature Amplitude Modulation (QAM) in the obtained filter design, the proposed filter outperforms preceding designs in terms of SE.

In 2021, M. Liu et al. [20] proposed a generic function model to design time domain window functions used for F-OFDM system. For different sidelobe attenuation rates, the optimized window functions were modified using a rising index. The results of designed window functions show that lower OOB was achieved and the same BER performance was obtained compared to the classical window functions.

In the same year, S. Mukhtar and G. R. Begh [21] proposed F-OFDM for Non-Orthogonal Multiple Access (NOMA) scheme in both uplink and downlink. The BER performance was analyzed over different channels,

through which the results showed that the F-OFDM is a better than that of OFDM by 2dB and 1dB for downlink and uplink, respectively.

1.3 Statement of the Problem

The main characteristics of the 5G telecommunication system are the ability to provide multi-services over different frequency bands. The most important challenge, especially at the lower frequencies (Sub-6 GHz), is the efficient use of the spectrum. 5G necessarily requires SE enhancement for extra bandwidth, capacity improvement, and ubiquitous coverage in both indoor and outdoor environments. Waveform style is considered to be one of the most important components for the physical layer of any communication system, as it has a significant influence on performance. However, due to the inflexibility and the scarcity of spectral resources of the conventional OFDM waveform, such 5G requirements are not satisfied. A new multicarrier waveform is required to reduce the spectrum leakage, minimize the guard band consumption, support asynchronous transmission, and allow multiplexing of different numerologies for different service requirements.

1.4 Aims of the Thesis

The main objectives of this research are outlined as follows:

1. Study the performance of the OFDM technology-based filtering for SE enhancement at Sub-6 GHz in the 5G system.
2. Modeling, simulation and evaluating the performance of the F-OFDM waveform using MATLAB-Simulink (Version 2020b) and Laboratory Virtual Instrument Engineering Workbench Next Generation (LabVIEW NXG) Communications System Design Suite with some comparisons to find the best approach.
3. Justifying the simulation results using a real time practical implementation for some designed transceiver scenarios of the F-OFDM waveform using the Software Defined Radio (SDR) technology.

1.5 Thesis Organization

This thesis consists of five chapters. The contents of each chapter are as follows:

Chapter One gives an overview to 5G, a literature review, statement of the problem, and the aims of the thesis.

Chapter Two describes the fundamentals, the available frequency bands, techniques that considerably improve the SE in the 5G system, and the basic overview of OFDM. In addition, the required specifications of the new waveform, the waveforms candidate, and the basic concept of the F-OFDM scheme are explained.

Chapter Three presents modeling, simulation, analysis, and comparisons of the F-OFDM waveform in two scenarios of design using MATLAB-Simulink and LabVIEW NXG software simulators.

Chapter Four describe the fundamentals of SDR technology and the Ettus ResearchTM USRP X310 platforms. Furthermore, practical implementation of the proposed waveform using USRP-X310 is covered.

Chapter Five contains conclusion and suggestions for future works.

CHAPTER TWO

SPECTRUM EFFICIENCY TECHNIQUES FOR 5G

2.1 Introduction

The next generation of wireless communication networks (5G) requires innovative and recently developed SE techniques. In this chapter, the fundamentals, the available frequency bands, techniques that considerably improve the SE in the 5G system, and the basic overview of OFDM technology are covered. Furthermore, the required specifications of the new waveform, the waveforms candidate, and the basic concept of the F-OFDM scheme have been discussed.

2.2 5G Fundamentals

The massive increases in a data exchange and the number of connected devices with the demand for a greater experience bandwidth, in addition to the shortcomings in the performance of 4G techniques, have prompted the design of 5G mobile networks to satisfy the services requirements of the applications in 2020 and beyond [22]. To deal with a much wider range of applications, the 5G system must be more versatile and adaptive to the developed technologies [23].

The International Telecommunication Union (ITU) defines the 5G services and applications for International Mobile Telecommunications (IMT) 2020 and beyond into three usage categories as shown in figure (2.1):

1. Enhance Mobile Broadband (eMBB): This usage category addresses increasing user data rates capabilities and improving system capacity.
2. Massive Machine Type Communication (mMTC): This category addresses a significant increase in connected devices without regard to data rates, high device battery life, and lower cost, such as Internet of Things (IoT) applications.

3. Ultra Reliable and Low Latency Communications (URLLC): This category has strict requirements for capabilities such as latency, throughput, and availability. Such examples include autonomous vehicles [24].

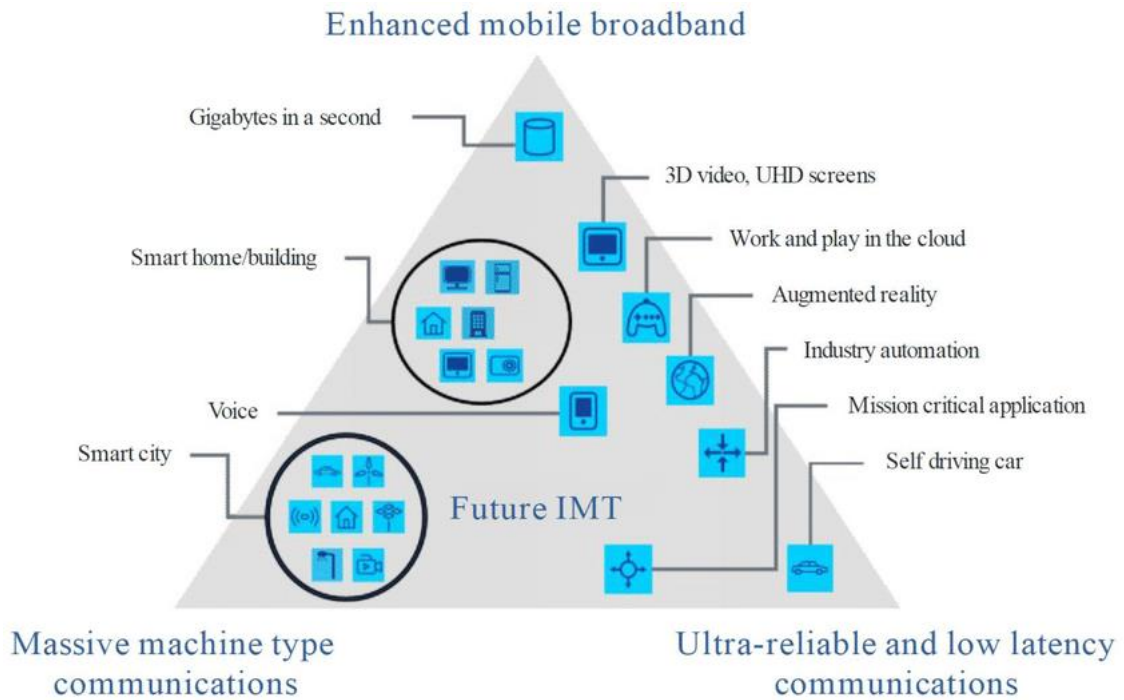


Figure (2.1) Anticipated IMT usage categories for 2020 and beyond [24].

2.3 Spectrum for 5G

Based on the usage categories, the 5G system fragments the spectrum for more flexible management capability. The new generation uses a variety of new frequency bands: licensed, unlicensed, and shared to supplement the currently utilized wireless frequencies [22].

The frequency bands used in the 5G network are divided into three groups (Low, mid, and high bands) [25] as shown in figure (2.2):

1. Low band: Frequencies at Sub-1 GHz, enable widespread coverage area in urban, suburban, and rural areas. The spectrum is suitable for IoT applications.

2. The Mid band: Frequencies between 1-6 GHz, offers a good compromise between coverage and capacity. The spectrum is more suitable for urban area due to a good propagation and penetration characteristics in the indoor environment.
3. High band: Frequencies above 24 GHz up to 100 GHz of spectrum provide additional bandwidth, greater data rate transmission and lower latency [26]-[27]-[28].

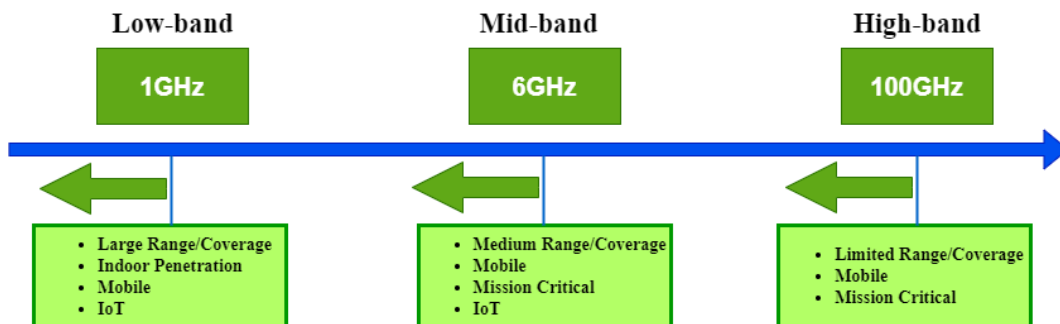


Figure (2.2) Frequency bands for 5G system [28].

2.4 5G Spectrum Efficiency Enhancement Techniques

Several innovative SE improvement techniques are used in the 5G system, which are discussed below:

1. Device-to-Device communication (D2D): One of the techniques which helps to reduce the burden on the 5G spectrum, and higher SE can be attained if the interferences are kept to a minimum and reliance on minimum Quality of Service (QoS). D2D operates in two modes: Inband (licensed), and Outband (unlicensed). The licensed mode have two types: underlay and overlay. In underlay communication, same cellular radio resources are shared between cellular users and D2D users while in overlay communication D2D users are provided with dedicated radio resources. The Inband mode is more efficient for spectrum utilization and less communication latency [30].
2. Massive Multiple-Input Multiple-Output (mMIMO): MIMO technology offers a higher SE without increasing the utilized bandwidth by using the

spatial multiplexing category. Many data signals can be sent over the same radio channel simultaneously by exploiting multipath propagation. The capacity of the 5G system will expand linearly as the number of antenna elements increases (hundreds to thousands), resulting in greater SE [31].

3. Full-Duplex communication: The full-duplex mode is a bidirectional communication by simultaneously transmitting and receiving over the same carrier frequency. The challenge related to full-duplex is the signal of self-interference, which refers to that signal that comes from the device transmitter itself (with a maximum power) to its receiver that interferes with the desired receive signal (weak signal power). Propagation, analogue and digital are the three domains used to suppress the self-interference signal. Full duplex has the ability to double the SE when it is utilized [22].
4. New Modulation and Coding Scheme: Channel coding is vital for efficient and reliable transmission. Polar and Low-Density Parity Check (LDPC) are the most effective coding schemes for 5G system. The Polar code is used as a channel coding scheme in both the uplink and downlink for control channels, while the LDPC coding technique is employed as a coding scheme for data channels on both the uplink and downlink. Both approaches contribute to boosting 5G SE [32].
5. New Waveforms: Waveforms play a vital role in lowering the OOB and hence improving the SE. The most important waveforms that have been proposed are: F-OFDM, Universal Filter Multicarrier (UFMC), Filter Bank Multicarrier (FBMC), and Generalized Frequency Division Multiplexing (GFDM) [5].
6. New Multiple Access Technique: SCMA is a non-orthogonal multiple access scheme, in which sparse codewords from codebooks of numerous users overlap in code and power domains, and the users share the same

time-frequency domains [33]. In the SCMA scheme, the utilization of multidimensional constellation achieves higher SE [34].

2.5 OFDM Technology Basics

In most modern wireless communication systems, increasing the data transmission rates is a priority required to improve system efficiency. For single carrier transmission systems, the impact of channel delay spread due to multipath propagation causes the duration of the received symbol to be extended, resulting in some overlap with previously received symbols. This overlapping, (commonly referred to as the ISI [35]), distorts the symbols at the receiver, and limits the data rates. In addition, an imbalanced frequency response (frequency-selective channels) complicates the design of the equalizer at the receiver. Furthermore, increasing symbol duration beyond the delay spread time to eliminate ISI caused a waste of spectrum resources [28]. To overcome these restrictions, attention was paid to the idea of multicarrier transmission, which was first proposed in the 1960s [36]. One of the special forms of multicarrier transmission is the OFDM, which was used for the first time in the 1971s by Weinstein and Ebert [37].

OFDM breaks the data streams into smaller, lower-data-rate substreams, which are then transmitted via orthogonal narrowband subcarriers as shown in figure (2.3). The orthogonality concept permits subcarriers to overlap without mutual interference, and by determining symbol duration, T_s will determine subcarrier space Δf ($T_s \Delta f = 1$) resulting in higher data rates, and improved bandwidth utilization [36].

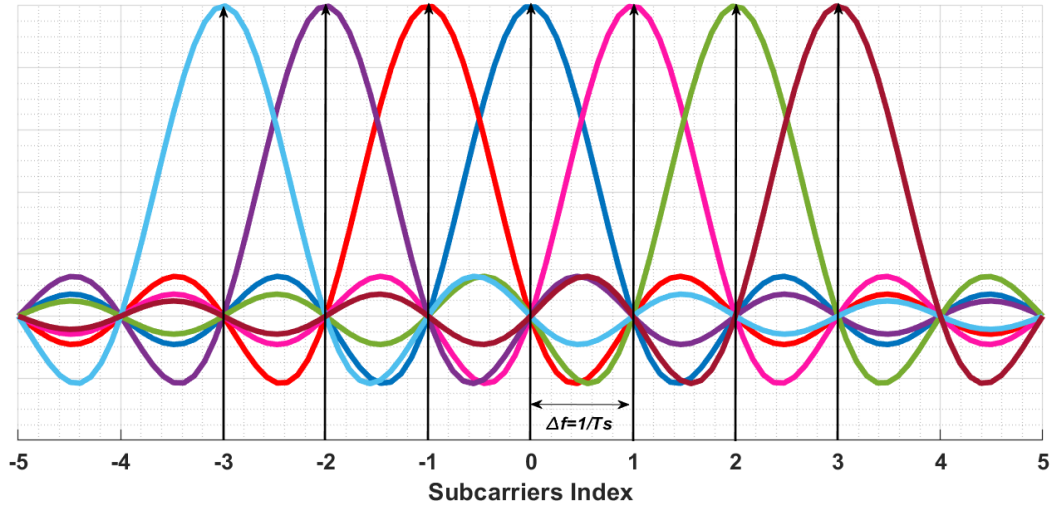


Figure (2.3) OFDM spectrum.

The subcarrier spacing Δf is chosen to be less than the channel coherence bandwidth to deal with flat fading channel, and to design a one-tap equalizer to compensate the distorted frequency response [22]. The duration of the OFDM symbol should be smaller than the coherence time of the channel, which is proportional to the maximum Doppler frequency f_{max} ($f_{max}T_s \ll 1$), where the channel fluctuates rapidly compared to the OFDM symbol duration, leading to performance deterioration of OFDM BER [35]-[38].

The propagation through the multipath channel causes ISI between the consecutive OFDM symbols, and as a result, orthogonality is lost between the subcarriers, resulting in ICI. A simple approach to combating the effect of ISI/ICI is to increase the time interval of the OFDM symbol by adding a redundancy to the beginning of the symbol, namely a CP or guard interval (T_{CP}) as shown in figure (2.4). At the receiver, this portion is discarded prior to the FFT process. The ratio of symbol extensions related to the frequency band and the scenario of deployment is usually taken in the last quarter time samples of the OFDM symbol [22]. The length of the CP must be a greater than the delay spread of the wireless channel and less than the OFDM symbol duration to decrease the overhead [28].

The effects of short CP length cause interference and degraded communication system performance. The increased unnecessary extension may result in a reduction in resources, and drop system throughput [38].

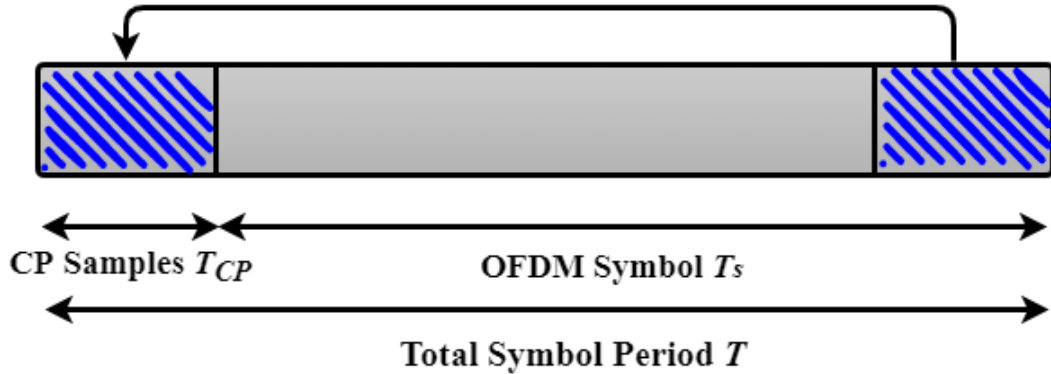


Figure (2.4) Cyclic prefix concept.

The OFDM technology, as the single carrier transmission, is more sensitive to the time-frequency variation in wireless channels. Time-varying impairments can be induced resulting from Carrier Frequency Offset (CFO) caused by mismatched frequency oscillators between the transmitter and receiver sides, or by Doppler frequency shift. Frequency varying impairments result from timing offset, or from the channel delay spread [36].

The OFDM symbol duration is proportional to the subcarriers number used within the available bandwidth. As a result, a small number of subcarriers is preferred over a larger number to reduce the impact of ISI. The number of used subcarriers and the CP extent are related to the desired BER, allocated spectrum, as well as the available power for the transmission [38].

2.5.1 OFDM Transceiver Structure

The basic operation of the OFDM transceiver is depicted in figure (2.5). At the transmitter, coding and interleaving are applied to the baseband digital data for a reliable transmission. Following that, the digital modulation process the streams of data with various modulation forms (M- Phase Shift Keying (PSK), M-QAM, etc.). At this point, a serial-to-parallel converter is applied to the complex symbols to configure the OFDM signal, the IFFT algorithm is used to preserve the orthogonality between the subcarriers. CP is inserted into the OFDM symbol after the process of parallel-to-serial conversion. The complete digital OFDM signal is converted to analog form through a Digital-to-Analog Converter (DAC) and then up-converted to Radio Frequencies (RF) for transmission over the wireless channel. The opposite process is used on the receiver side. The received signal is down-converted to the baseband frequency, and an Analog-to-Digital Converter (ADC) is applied to obtain the digital signal forms. The CP samples is removed from the received signal, and converted to the parallel format using a serial-to-parallel converter. An FFT process is used to demodulate the OFDM signal. Subsequently, the demodulation is performed based on the transmit constellation, decoded, and de-interleaved to recover the digital transmit bitstreams [39].

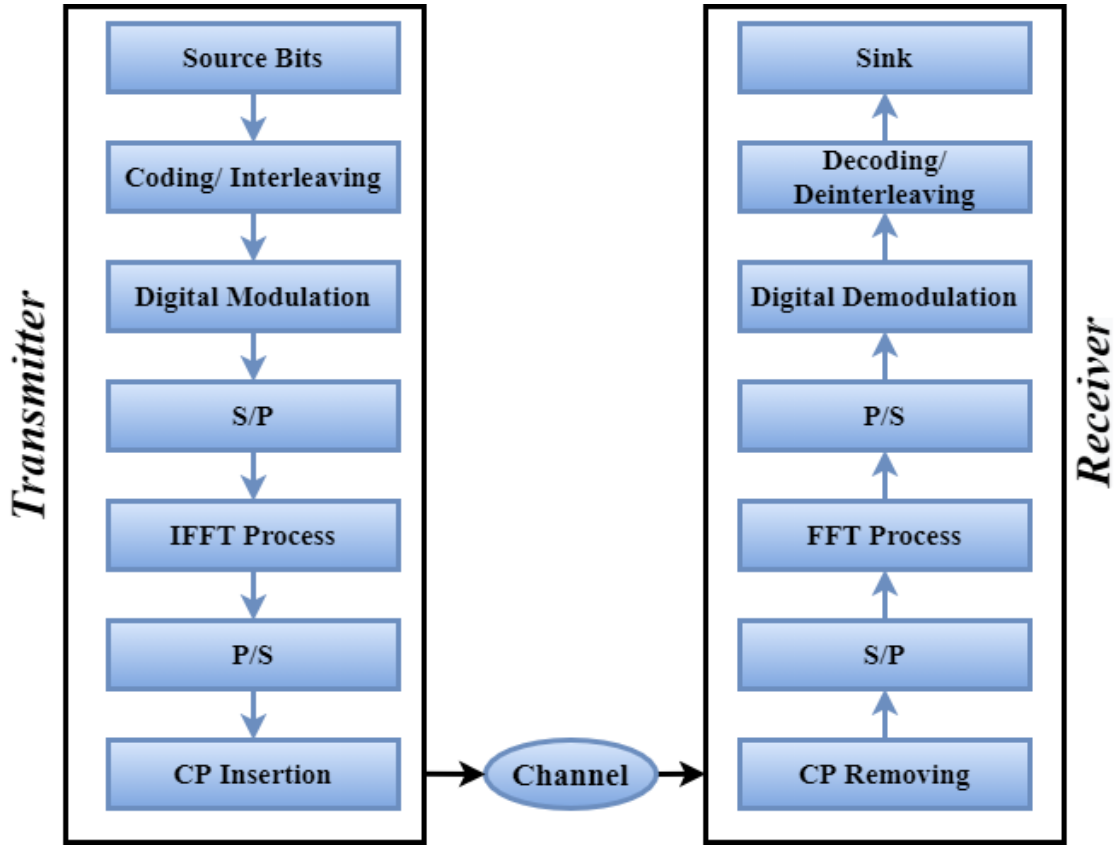


Figure (2.5) OFDM transceiver structure.

2.5.2 OFDM Signal Generation

If $\{s_{m,k}\}_{k=0}^{N-1}$ is a modulated symbols transmitted at the m th OFDM block, then the OFDM signal can be expressed as:

$$s_m(t) = \sum_{k=0}^{N-1} s_{m,k} e^{j2\pi k \Delta f t}, \quad 0 \leq t \leq T_s \quad (2.1)$$

where, N is the number of subcarriers in OFDM Block. At the receiver, the modulated symbols can be detected if there is no channel distortion:

$$s_{m,k} = \frac{1}{T_s} \int_0^{T_s} s_m(t) e^{-j2\pi k \Delta f t} \quad (2.2)$$

A discrete-time description of the transmitted signal can be obtained by sampling the continuous signal at $t = \frac{T_s}{N}$, equation (2.1) can be expressed as:

$$s_m\left(n \frac{T_s}{N}\right) = \sum_{k=0}^{N-1} s_{m,k} e^{j2\pi k \Delta f n \frac{T_s}{N}} = \sum_{k=0}^{N-1} s_{m,k} e^{j2\pi \frac{kn}{N}} \quad (2.3)$$

where, n is the discrete sampling points. The signal in equation (2.1) represents the Inverse Discrete Fourier Transform (IDFT) of the transmitted symbols and can be efficiently calculated by IFFT. At the receiver, the original symbols is recovered by applying FFT instead of integration.

Note that CP is inserted at the beginning of the OFDM symbol with time T_{CP} , the OFDM signal time interval is extended to $T=T_{CP}+T_s$, then the transmitted signal $\tilde{s}_m(t)$ is expressed as:

$$\tilde{s}_m(t) = \sum_{k=0}^{N-1} s_{m,k} e^{j2\pi k \Delta f t}, \quad -T_{CP} \leq t \leq T_s \quad (2.4)$$

At the receiver, the signal ($X_{m,k}$) can be written as:

$$X_{m,k} = H_k \tilde{s}_{m,k} + n_k \quad (2.5)$$

where, H_k is the channel frequency response and can be represented by:

$$H_k = \sum_i Y_i e^{-j2\pi k \Delta f \tau_i} \quad (2.6)$$

where, τ_i and Y_i are the delay and the complex amplitude of the i th path, respectively. n_k is the impact of Additive White Gaussian Noise (AWGN) [36].

2.5.3 OFDM Block Structure

Modulated data, Direct Current (DC) subcarriers, zero insertion, and what are known as “pilot signals”, are contribute to constructing the OFDM block. The OFDM block size must equal the IFFT/FFT size. Usually, the DC component does not typically carry information because of the fact that low-frequency signals are challenging to deal with an analog circuits. When the transmitter modulates the DC subcarrier, the receiver will discard it and rely on the error correction coding to retrieve the information from it.

Alternatively, the allocated spectrum shifts by a half subcarrier bandwidth yields no subcarriers at the DC [28]. A portion of the OFDM signal contains subcarriers that are not loaded with information and are used as a guard band to prevent interference. The pilots are a known signal to both transmitter and receiver used for synchronization and channel estimation [36].

2.5.3.1 Pilot Symbols Configuration

There are three types of arrangements of pilot symbols used for channel estimation in the OFDM technology, as following:

1. **Block pilot:** In this type, the pilot symbols are inserted into all subcarriers of the OFDM symbol, and periodically transmitted for time-domain channel estimation. The time interval for the periodic position of pilots must be at the coherence time of the channel. The Block pilot is used to track the time-varying characteristics of the channel, and it is considered not sensitive to frequency selective channels due to the pilot inserted into all subcarriers at the OFDM symbol. The Block pilot is sometimes called the preamble and its arrangement illustrated in figure (2.6-a).
2. **Comb Pilot:** In this type, the pilot symbols are inserted between the modulated data in the OFDM block, which is used for frequency domain channel estimation. The Comb pilot is appropriate for fast-fading channels. The distance between successive comb pilots must be at the coherence bandwidth, which is inversely proportional to the delay spread of the wireless channel. The arrangement of this type illustrated in figure (2.6-b).
3. **Lattice Pilot:** In this type, the pilots are embedded in different OFDM subcarriers of different OFDM blocks (scattered) for tracking time-varying and frequency selective channel characteristics [40]. Figure (2.6-c) illustrates the arrangement of this type.

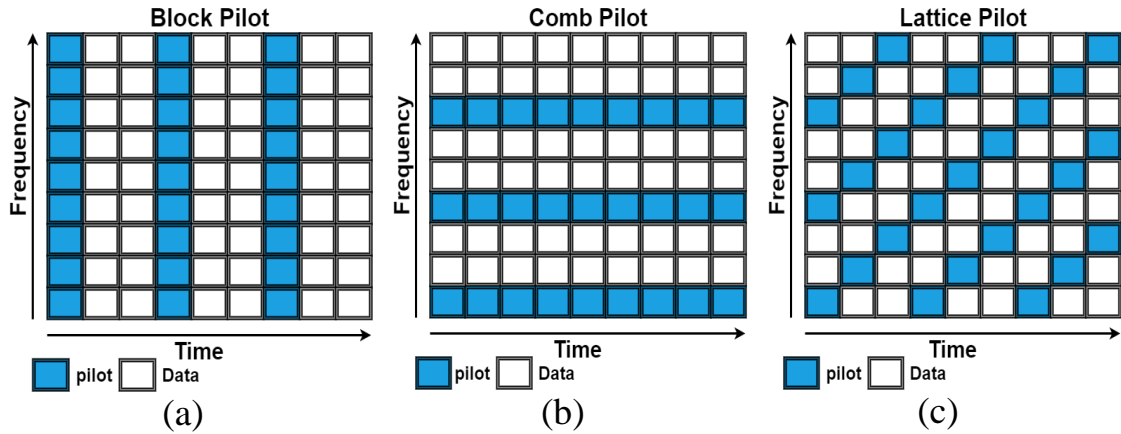


Figure (2.6) Pilots arrangement types: (a) Block pilot (b) Comb pilot (c) Lattice pilot.

2.5.4 Channel Estimation

In the OFDM technology, the transmitted signal is usually distorted due to the channel characteristics. In fact, the channel characteristics can be estimated using frequency domain channel estimation techniques with the assistance of pilot signals. Pilot Aided Channel Estimation (PACE) and Decision-Directed Channel Estimation (DDCE) are frequency-domain channel estimation methods. PACE used block or comb pilot tones to estimate the coefficients of the channel. In DDCE, the preliminary estimation depends on preambles/pilots, and tracking or prediction algorithms are used for predicting the channel characteristics for the next data symbols. Error propagation is the major problem of DDCE due to Doppler effects. In comparison to DDCE, PACE provides reliable channel estimation by proper design of pilot patterns [36]-[40].

A blind channel estimation is another technique that uses channel statistics without the need of a preamble or pilots. The estimation depends on receiving a large number of symbols for extraction channel properties. The performance of this type of estimation is usually worse than other techniques employed by the pilots [40].

2.5.5 Synchronization

Because of the multicarrier transmission over a multipath channel, both time and frequency synchronization between the transmitting and receiving sides is essential in the OFDM technology for proper detection. The two aspects of the timing synchronization error are symbol synchronization and sampling clock synchronization. The multipath channel causes the spread of the OFDM symbol, which results in an error in determining the beginning point of the symbol at the receiver. Due to sample clock offset, the OFDM symbol drifts away from the FFT window at the receiver. ISI and ICI are the result of these two issues [41].

A mismatch in the local oscillators between the transmitter and receiver causes CFO, which results in OFDM samples having a phase rotation with respect to the previous one. Furthermore, CFO shifts the spectrum of the received signal, causing ICI. The orthogonality between the subcarriers is still achieved when the offset is integer multiple subcarrier spacing, this yields increase the BER. When the offset of carrier frequency is fractional part of the spacing, ICI will occur, causing increasing the BER of the system and degrading the performance [41].

Phase noise, an issue related to synchronization errors in OFDM results from the instability of the transmitter/receiver clock, causing a random frequency shift to the OFDM symbols [28].

With the assistance of cyclic prefix, preambles, and pilot symbols, the synchronization in OFDM is performed in two stages; coarse and fine synchronization both in terms of time and frequency domains. A coarse synchronization algorithm is used to detect the beginning of the OFDM samples. Then the coarse algorithm output is used in the fine synchronization stage to equalize the signal due to the channel effect [41]-[42].

2.5.6 OFDM Implementation Issues

Practical implementation of the OFDM technology faces two significant challenges described below:

2.5.6.1 Peak-to-Average Power Ratio (PAPR)

PAPR is an implementation problem in the OFDM technology, and it is defined as the ratio of the maximum OFDM peak power to its average power. In the communication systems, the signal is amplified before it is transmitted over the channel using the Power Amplifier (PA). The signal to be amplified must be within the linear response of the PA to avoid distortion that leads to higher sidelobes. Designing PA with a higher linear response leads to an increase in the cost, power consumption, and larger size. OFDM signal due to subcarriers addition together resulted in larger peaks [28]. Furthermore, higher PAPR of a system makes DAC/ADC implementation at the transmitter and receiver extremely difficult [38]. Various techniques are employed with OFDM to reduce the PAPR, some of which are described below:

- A. **Clipping and Filtering:** This is the simplest way to reduce PAPR by clipping the signal to the desired level. Clipping causes in-band and out-band distortion that results in lost orthogonality among the subcarriers. Filtering process is used to reduce the OOB and hence improve the BER [43].
- B. **Selective Mapping (SLM):** In this method, the transmitted data symbols of length N are multiplied by a set of N different phase sequences. IFFT is used, and one of the minimum PAPRs is chosen to be transmitted. The different phase sequences are transmitted to the receiver for the ability to recover the original data.

- C. Partial Transmit Sequence (PTS): In this method, the N data symbols are partitioned into several sub-blocks. The IFFT is processed individually for each sub-block and then each sub-block is multiplied by the corresponding phase factor to minimize the PAPR. The complexity increases with larger partitioning when searching for the optimum phase factor.

Other PAPR reduction techniques based on coding category by assigning bits in a codeword to improve the BER are assigned for PAPR reduction. The codeword with the lowest PAPR must be selected for transmission. The complexity increased when optimizing the selection of codewords. The adaptive pre-distortion technique is also used to compensate for the distortion proposed by the PA due to the nonlinearity-induced by correcting of the input constellation with pilot signals [40].

2.5.6.2 Sidelobes

Due to the rectangular pulse shape in the time domain, the spectrum of the OFDM has larger sidelobes. The sidelobes cause interference with the adjacent frequency band systems. One of the techniques used for sidelobes suppression is to reserve some subcarriers and optimize them depending on the content of other subcarriers for sidelobe minimization. An alternative way is to reduce the power transmission level for the edge subcarriers. Time-domain windowing is another way of suppressing the sidelobes applied to the OFDM symbols [28].

2.6 Required Waveform Specifications for 5G

Flexible and adaptive design are required for the adopted 5G waveform. The new waveform should support the following different use cases: mMTC, eMBB, and URLLC for a wide range of frequencies. Furthermore, the newly waveform is capable of dealing with the MIMO system.

The variety of waveform numerology design (i.e., M-QAM, subcarriers spacing, CP, and transmission time interval) must be taken into account depending on the deployment options and the operation frequency. The new waveform allows scalable numerologies to be mixed on the used carrier frequency, where the subcarriers of a specified numerology interfere in the frequency domain with other subcarriers of another numerology as shown in figure (2.7). The subcarrier spacing is specified to be $\Delta f = 15 \times 2^c \text{ KHz}$, where $c = 1, 2, \dots$ for each sub-band.

There are certain conditions that the new waveform must satisfy in order to support the requirements in the 5G system, which are as follows:

1. Higher SE and lower PAPR.
2. Immunity to channel frequency selectivity.
3. Well-localized in time and frequency domain.
4. Protection against synchronization issues.
5. Lower transceiver complexity.
6. More flexible and scalable for various services.
7. Simple equalizer.
8. Forward and backward compatibility [44].

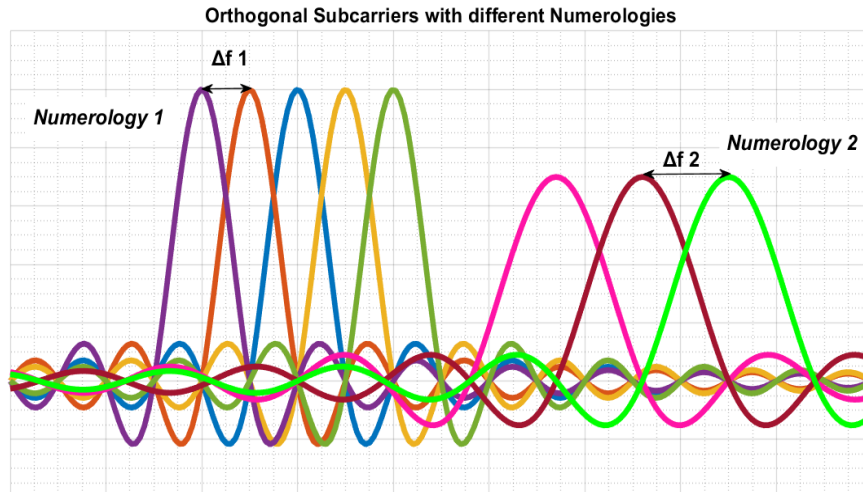


Figure (2.7) Mixed numerologies design [43].

2.7 Candidates 5G Waveforms

Due to the drawbacks of conventional OFDM, numerous new waveforms have been proposed for the 5G system:

1. Filter-OFDM (F-OFDM): This waveform is proposed to address some limitations of OFDM technology, in which the entire allocated spectrum is divided into smaller sub-bands, each with its own set of modulated subcarriers. Flexible filter designs are performed for every sub-band in order to attain perfect frequency domain localization. F-OFDM is quasi-orthogonal, meaning that the orthogonality between the subcarriers inside each sub-band is maintained but not between the sub-bands [7]-[8].
2. Universal Filter Multicarrier (UFMC): In this type of waveform, a group of orthogonal subcarriers are filtered using the same or different filter performance in each sub-band to minimize the OOB. A Zero prefix (ZP) is added to mitigate the effect of ISI. The filter length in UFMC must be within the ZP length. The main limitation of UFMC is that it is not recommended for applications that require higher data rates [7]-[45].

3. Filter Bank Multicarrier (FBMC): It is a non-orthogonal waveform, the filtering is performed per subcarrier, and thus a long filter length is used. The accomplished SE using FBMC is higher compared to other waveforms due to the advanced filter design, therefore, the CP can be omitted. Offset Quadrature Amplitude Modulation (OQAM) is used to preserve time-domain signals. FBMC is not preferred for 5G services because the length of the filter requires more processing and hence increases the latency. In addition, the complexity is increased with MIMO technology [38]-[46].
4. Generalized Frequency Division Multiplexing (GFDM): GFDM is a non-orthogonal waveform with block base transmission, in which the subcarriers are spaced with more flexibility and pulse shaping is performed on the subcarriers for eliminating ICI and providing spectral confinement. In addition, the CP insertion minimize the impact of ISI. GFDM is preferred for services with lower data rates. The more complex processing required at the receiver makes it inefficient for low latency applications in 5G [22]-[46].

2.8 Filtered-OFDM (F-OFDM)

F-OFDM is a new waveform that paid attention in the 5G system due to its performance and outperforming the limitations proposed in the conventional OFDM. The principle of operation is based on sub-band filtering contrary to the OFDM. The sub-band process can be performed in three different cases: based on users, based on services, and based on Resource Block (RB) as shown in figure (2.8). Each consecutive of the 12 subcarriers is considered an RB, and it is the smallest unit that can be assigned to the user. In sub-band filtering, synchronous between the devices can be dispensable, and the asynchronous transmission is boosted. In F-OFDM, using an optimal filter design can suppress the OOB and minimize the guard band between the sub-bands. Furthermore, different numerologies

are applied to each sub-band to be suitable for the multi-services requirements [22]-[47].

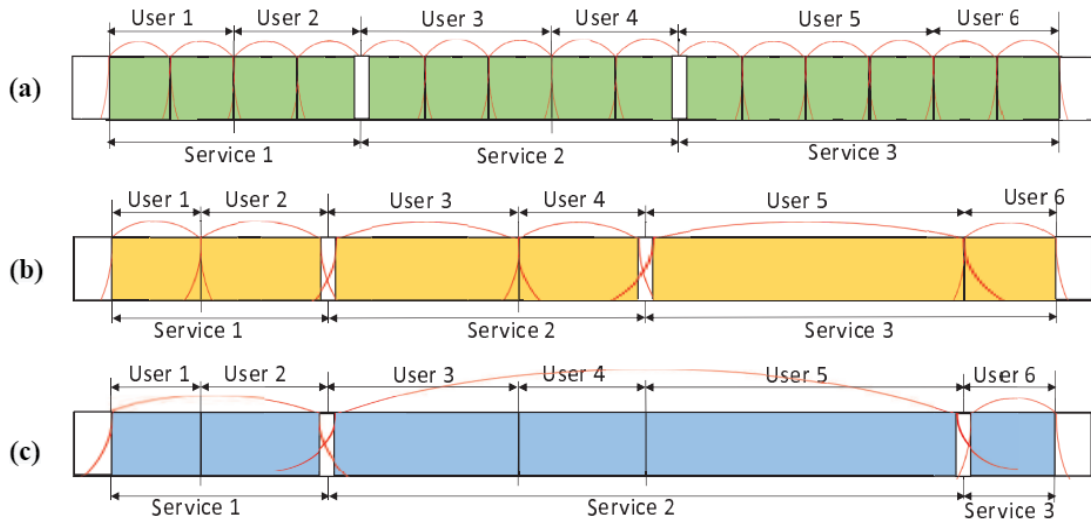


Figure (2.8) Methods of sub-band filtering: (a) Per RB (b) Per user (c) Per service [46].

2.8.1 F-OFDM Transceiver Scheme

On the transmitting side, the entire band is split into smaller sub-bands where the data in each sub-band is processed separately. The bitstreams for each sub-band are mapped to various QAM constellation symbols. The symbols are transformed from serial to parallel, and the time-domain signal is performed by N-IFFT at each sub-band to obtain the orthogonality in which the subcarrier is produced at the zero-crossing point of the other subcarrier to avoid interference. To mitigate the impact of multipath propagation, dissimilar lengths of CP are inserted for the sub-bands. The signal is then filtered by a digital prototype FIR filter to provide the isolation between numerology-based sub-bands. Finally, the F-OFDM signal of all sub-bands is combined to be transmitted over the channel. Figure (2.9-a) illustrates the F-OFDM transmitter as a block diagram.

The inverse processes of the transmitter are carried out on the receiving side. The signal is filtered to take the desired sub-band spectrum and attenuate the others with a filter designed as a similar version of the transmission filter. A simple equalization process necessitates canceling the effects of the channel and the used filter. CP is removed and N-FFT is performed on the desired sub-band to be able to demodulate the received data [9]-[19]. Figure (2.9-b) illustrates the block diagram of the F-OFDM receiver.

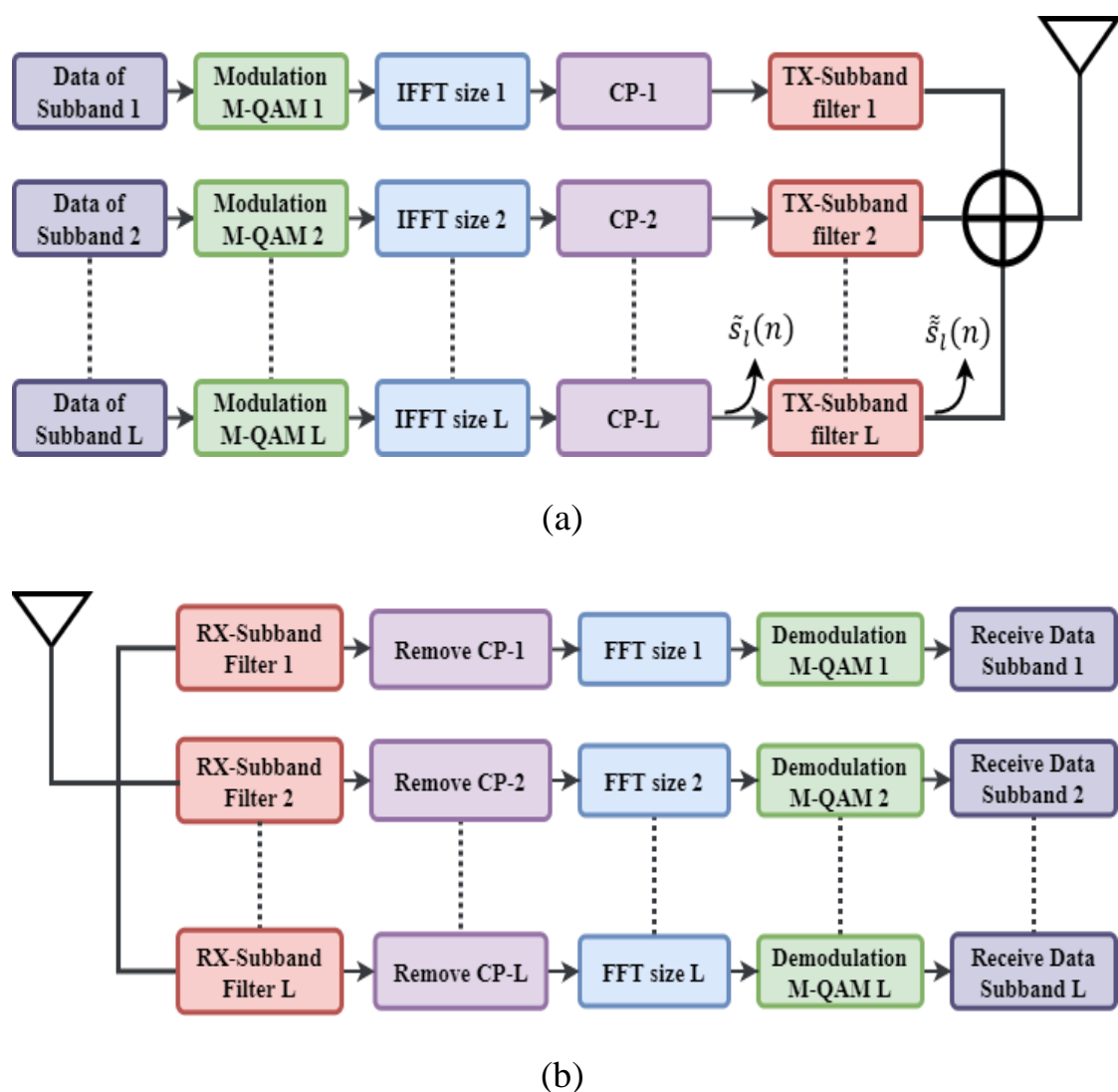


Figure (2.9) F-OFDM transceiver block diagram: (a) Transmit side (b) Receive side.

The F-OFDM signal for each sub-band ($\tilde{s}_l(n)$) is obtained by the linear convolution of the filter impulse response with the OFDM signal for that sub-band:

$$\tilde{s}_l(n) = \tilde{s}_l(n) * f_l(n) \quad (2.7)$$

where, $\tilde{s}_l(n)$ is the OFDM signal for the l th sub-band with the CP samples, $f_l(n)$ is the impulse response of the digital filter of the l th sub-band. The received signal is filtered with a filter has an impulse response given by $f_l^*(-n)$, which is a matched copy of the transmission filter [7].

2.8.2 Sub-band Filter Characteristics

The filter must meet certain criteria in order to accommodate the 5G waveform requirements. The passband of the designed filter should be as flat as possible to ensure that the distortion of the filter does not affect the subcarriers. The roll-off of the filter should begin at the edges of a passband with a very narrow transition band. This ensures that the system bandwidth is efficiently used with the minimum effort of guard band overhead. Furthermore, neighboring sub-band signals with various numerologies can be placed in frequency next to each other with a minimum number of guard bands. Higher-order filters will reduce the OOB by decreasing the sidelobes. Usually, the filter length exceeds the CP length for better localization in the frequency domain [48].

CHAPTER THREE

F-OFDM MODELING, SIMULATION, AND RESULTS

3.1 Introduction

In any wireless communication system, the choice of multicarrier waveform is an important factor in determining system performance. This chapter describes modeling, several simulations, and results with some comparisons for the F-OFDM downlink waveform with two design scenarios using two software simulator approaches, MATLAB-Simulink and LabVIEW NXG.

The adopted two scenarios are based on sub-banding the available spectrum into equal and unequal sizes. Digital FIR filters will be used to evaluate the performance of the proposed waveform.

3.2 Model Assumptions

In this work, several assumptions were adopted. Some of these parameters related to the limitations of the available tools, others are for the sake of models simplification. The model assumptions are:

1. Four sub-bands are taken to obtain the overlapping among the F-OFDM sub-bands without interference and also to evaluate the performance in terms of SE.
2. The total FFT/IFFT size is 1024 and the subcarrier spacing (Δf) is 15 kHz.
3. Based on the structure of the OFDM block mentioned in chapter 2 subsection (2.5.3), 78% of the subcarriers carry information, and 22% are allocated as a guard band in an equal sub-band scheme, while in an unequal sub-band scheme, 72% of subcarriers carry information, and 28% are allocated as a guard band to ensure the transmission without errors.
4. No pilot signals are added to the OFDM signal. These signals are used in studying the characteristics of the channel, channel estimation and

equalization algorithms, which are outside of the research scope (characteristics of the channel are supposed to be known).

5. The type of filter used is a Window-Sinc FIR filter with different time-domain window functions.
6. The Filter length is taken at half FFT size to achieve tradeoff between time and frequency domains localization [8].
7. Using QAM type with different orders (16, 64, 128, 256, and 512) for various sub-bands.
8. The CP is used to complete the structure of the F-OFDM signal, and the length is taken at (1/2, 1/4, or 1/8) rates to be able to sum the sub-bands samples in Simulink.
9. The number of data subcarriers from the total FFT length (1024) in equal sub-band sizes is 200 subcarriers, while the data subcarriers in unequal sub-band sizes (93, 186, and 372).
10. The average BER and PAPR calculation means the total BER and PAPR of the four combined designed sub-bands.
11. The utilized bandwidth (BW_u) per each sub-band depends on the number of used subcarriers, N_u taking into consideration the DC subcarrier in each sub-band, and can be defined as [39]:

$$BW_u = N_u \Delta f \quad (3.1)$$

12. The SE is calculated using the following equation [15]:

$$SE = \frac{\sum_{sub=1}^{SUB} \sum_{n=n_u-1}^{N_u+n_u-1} C_{sub,n}}{\sum_{sub=1}^{SUB} BW_u + \sum_{i=1}^{SUB-1} BW_{g,i}} \quad (3.2)$$

where, SUB is the total number of sub-bands, sub is the sub-band index, n_u is the location of the active subcarrier for each sub-band, and $C_{sub,n}$ the capacity of each sub-band measured in (bit/s), and calculated based on the properly received bits per simulation time. BW_u represent the utilized bandwidth for each sub-band. $BW_{g,i}$ is the minimum guard band between the sub-bands. The minimum guard

band between the sub-bands is obtained based on the flowchart process in figure (3.1).

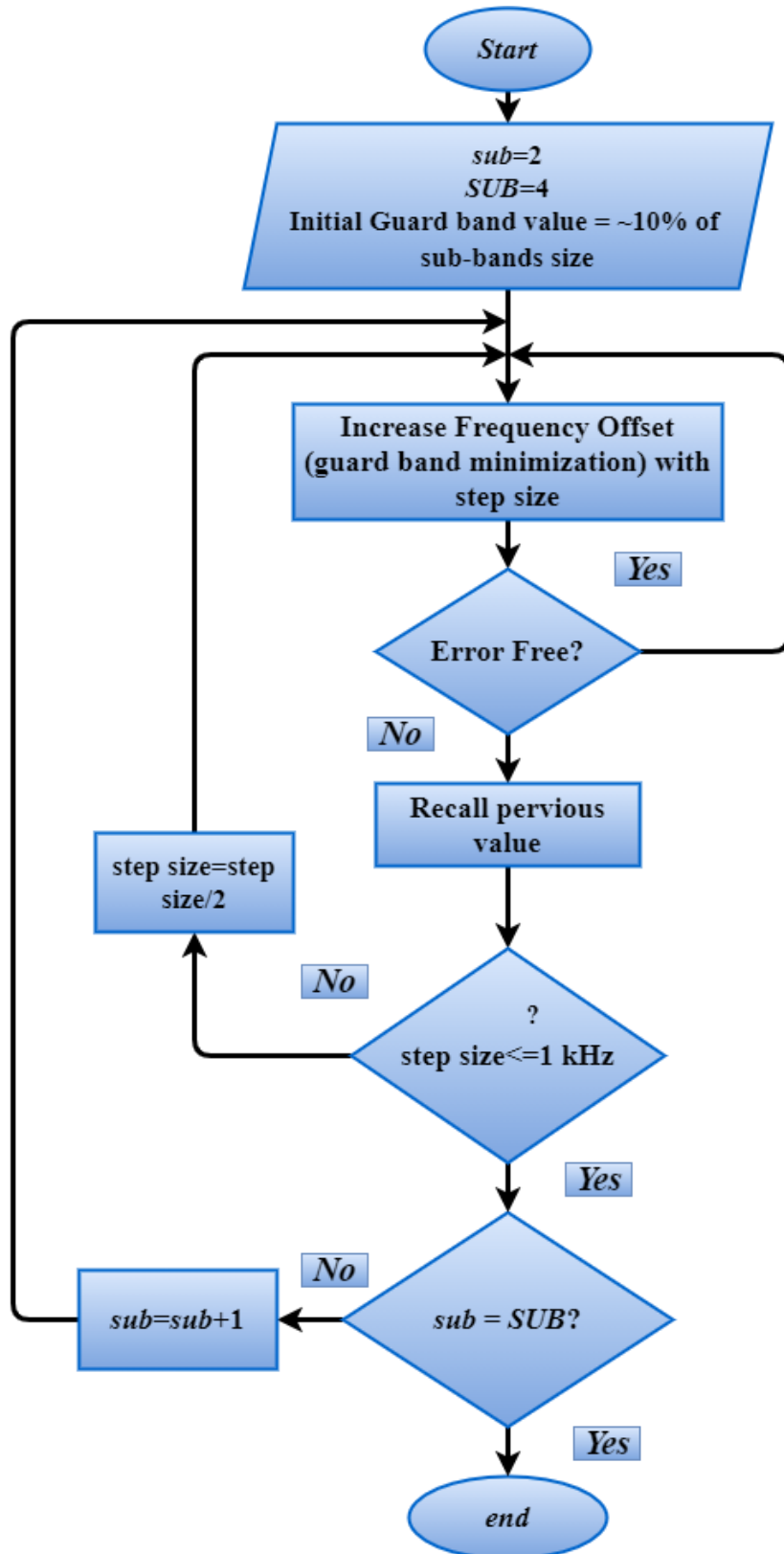


Figure (3.1) Flowchart of minimizing the guard band between the sub-bands.

3.3 First Approach MATLAB-Simulink F-OFDM Methodology

This section explains the modeling and simulation of the OFDM, F-OFDM, and F-OFDM sub-banding, as well as the results obtained using the Matlab-Simulink software.

3.3.1 OFDM System Model (Simulink)

In this simulation part, the OFDM block was designed according to equation (2.3), which describes the orthogonal subcarriers of the OFDM technology. The MATLAB-Simulink system block is shown in figure (3.2).

At the transmitter, the data generated by a random integer block is used with 372 samples per frame. The Rectangular-QAM modulator is used as a second process to modulate the input bits using various modulation orders (16, 64, 128, 256, and 512) to obtain QAM symbols. The constellation diagrams for various QAM orders obtained from the simulation is shown in figure (3.3) for a one time unit. The IFFT process subsystem is shown in figure (3.4), where the input symbols are divided into two parallel groups by multiport selector block. Matrix concatenates block used to create a continuous signal vertically consisting of the modulated symbols, zeros, and DC input. Applying IFFT to the signal formed by the previous block to obtain the OFDM block of orthogonal subcarriers. CP added to the beginning of the OFDM signal with a length of 64 samples. The complete OFDM signal is sent through the AWGN channel.

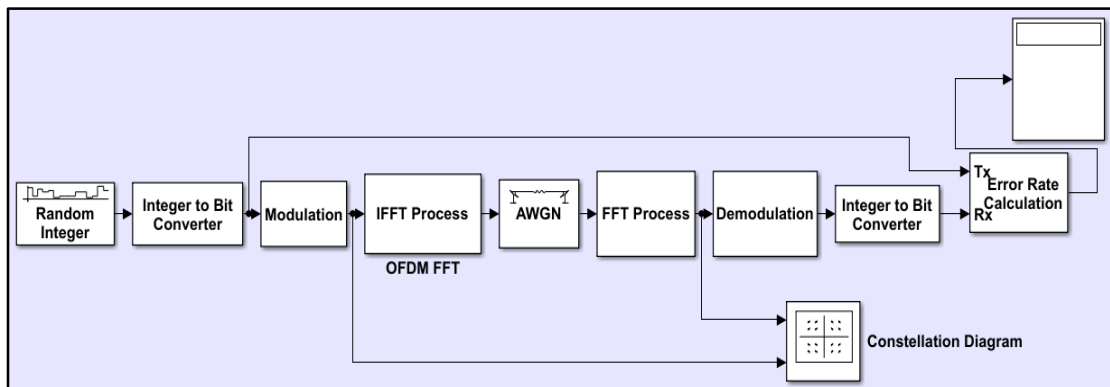


Figure (3.2) OFDM block (Simulink).

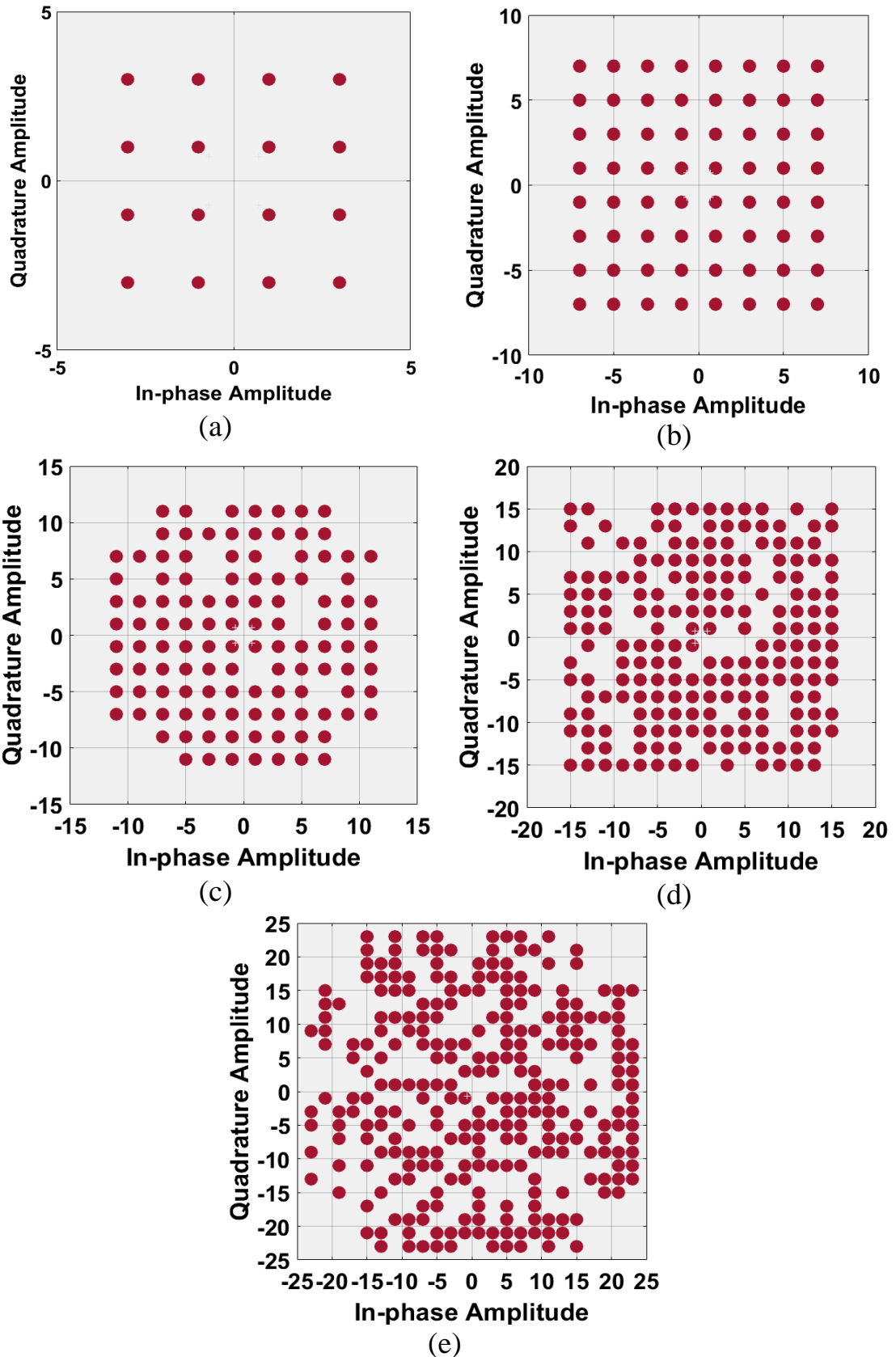


Figure (3.3) A snapshot constellation diagrams of various modulation orders in Simulink: (a) 16-QAM, (b) 64-QAM, (c) 128-QAM, (d) 256-QAM, (e) 512-QAM.

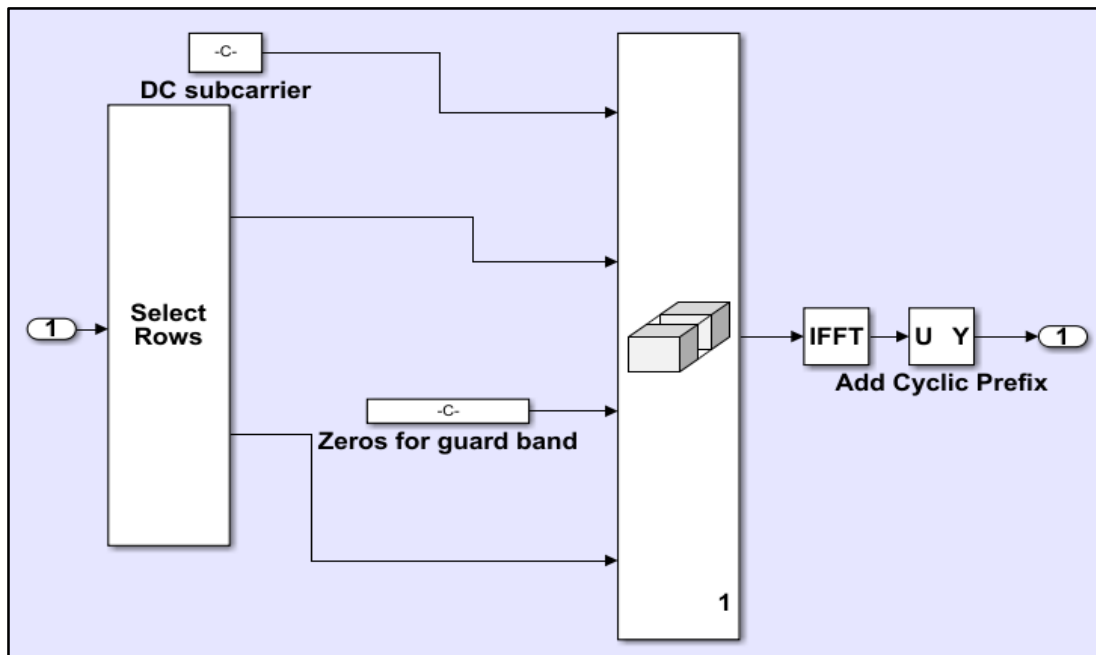


Figure (3.4) IFFT process subsystem.

At the receiver, the inverse process was performed. The CP was removed from the complete symbol and the FFT was applied to the OFDM signal. Removing the zeros and DC signal from the output of the FFT block using a selector block, the remainder is the modulated data. The subsystem of these processes is shown in figure (3.5). The Rectangular-QAM Demodulator block is used to demodulate the signal.

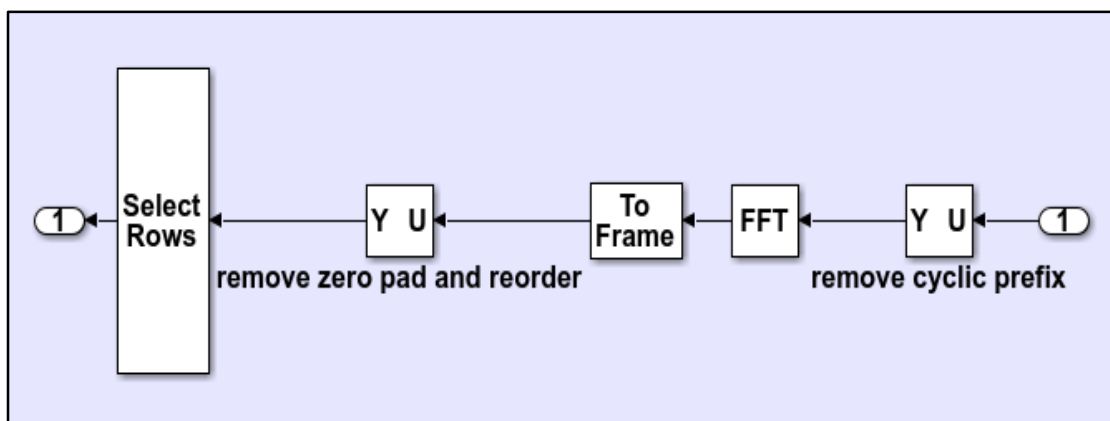


Figure (3.5) FFT process subsystem.

3.3.2 F-OFDM System Model (Simulink)

The aims of this simulation part is to study the filter effects on the performance of the OFDM system. Using MATLAB codes, FIR filters were designed by multiplying the infinite impulse response of sinc function with finite time-domain window functions creating Window-Sinc FIR filters. Five types of time-domain window functions were applied (Gaussian, Hanning, Nuttall, Blackman, and BlackmanHarris), and two new window functions were proposed. The first proposed window created by combining the Hanning window with the Blackman window, and the second proposed window created by combining the first proposed window with the BlackmanHarris window. The representation of the utilized window functions in the time and frequency domain is shown in figure (3.6) based on the equations presented in Appendix-A [49]-[50]-[51]-[52].

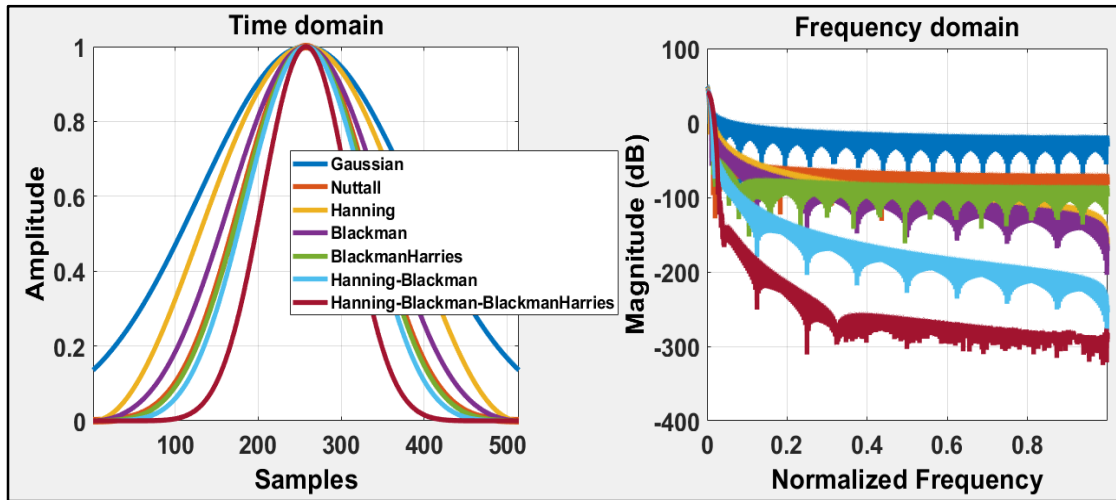


Figure (3.6) Time-Frequency domain representation of the utilized window functions.

The normalized Sinc function prototype filter ($f_d(n)$) is represented in the equation below [53]:

$$f_d(n) = \text{Sinc}[(N_u + 2 \times \text{toneoffset}) \times n / \text{FFTsize}] \quad (3.3)$$

where, *toneoffset* is the excess bandwidth (in subcarrier), used to protect the information at the edges subcarriers from loss.

The FIR Sinc truncation filter for the l th-Sub-bands is obtained after multiplying the Sinc function by a time-domain window function $w(n)$ as follows:

$$f_l(n) = f_d(n).w(n) \quad (3.4)$$

On the transmitting side, the designed FIR filter of linear phase linear convolved with the complete OFDM signal, and on the receiving side, a matched version of the transmitted filter is applied to the received signal. After the filtering process is performed, the signal is modified by removing samples that have the length of the utilized filter and adjusting the power of the signal to the desired level. The frequency response and the phase response of the designed digital filters are shown in figures (3.7), (3.8), (3.9), (3.10), (3.11), (3.12), and (3.13), see Appendix-B. It can be noticed that, based on the utilized window functions, the filters provide various attenuation to the sidelobes with linear phase variation. The impulse response of the 513 tap filter length is shown in figure (3.14), and the complete F-OFDM of one sub-band is shown in figure (3.15).

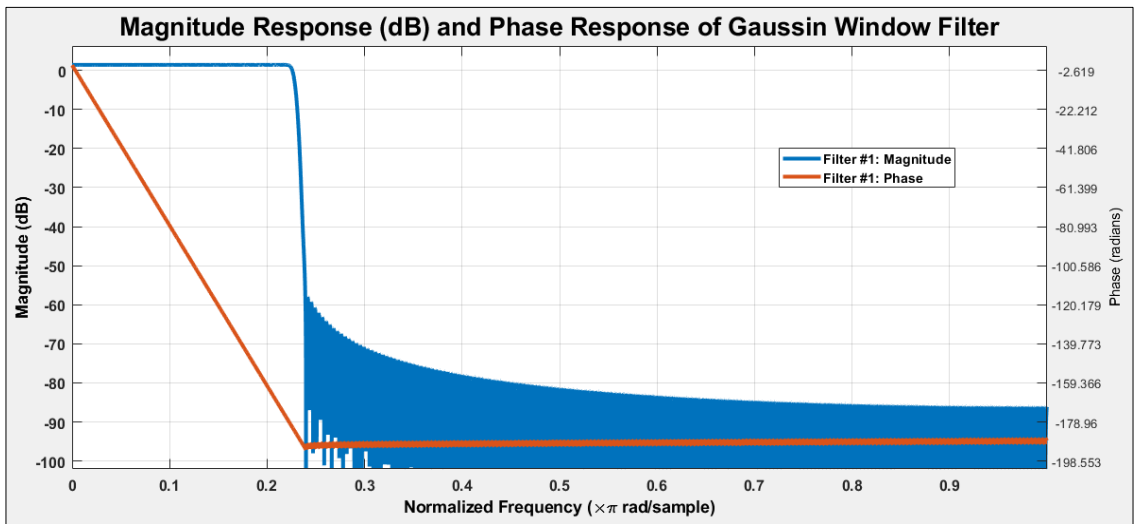


Figure (3.7) Magnitude and phase response of the Gaussian window filter.

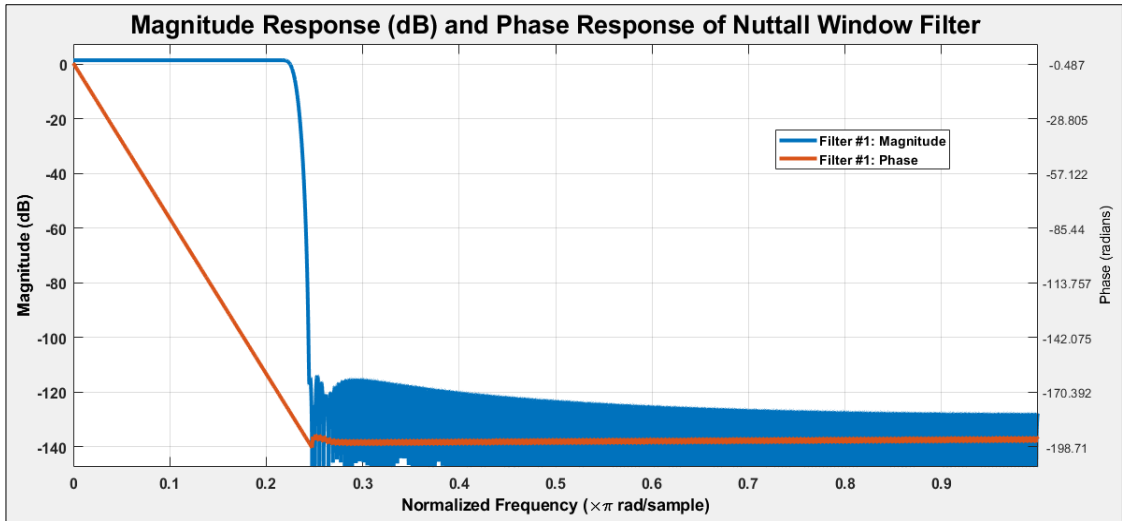


Figure (3.8) Magnitude and phase response of the Nuttall window filter.

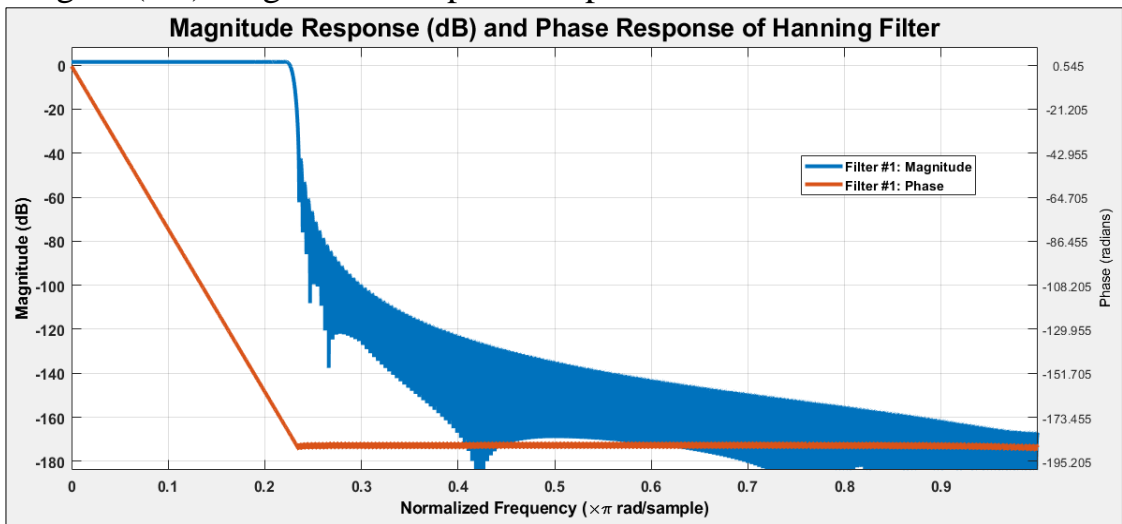


Figure (3.9) Magnitude and phase response of the Hanning window filter.

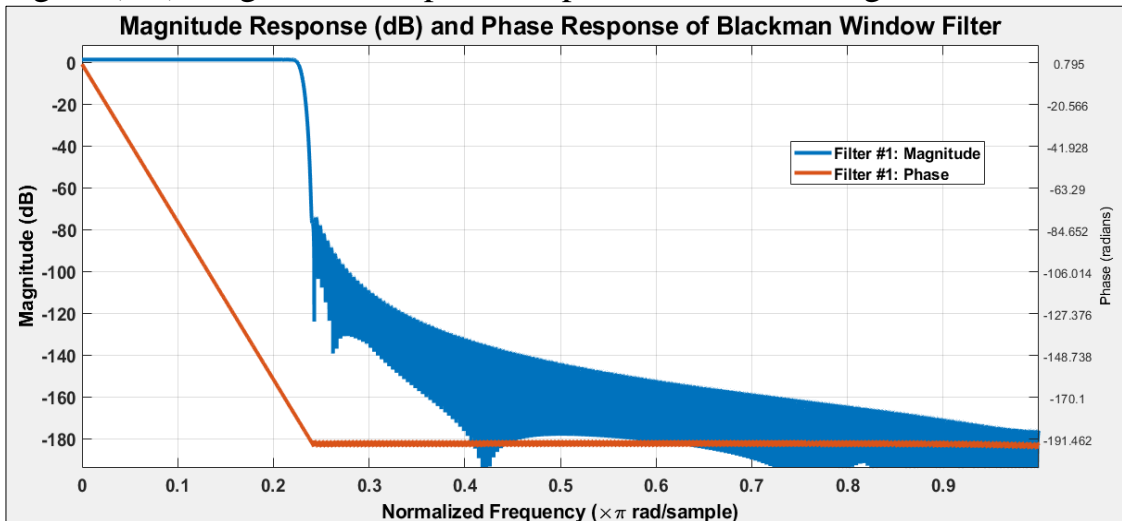


Figure (3.10) Magnitude and phase response of the Blackman window filter.

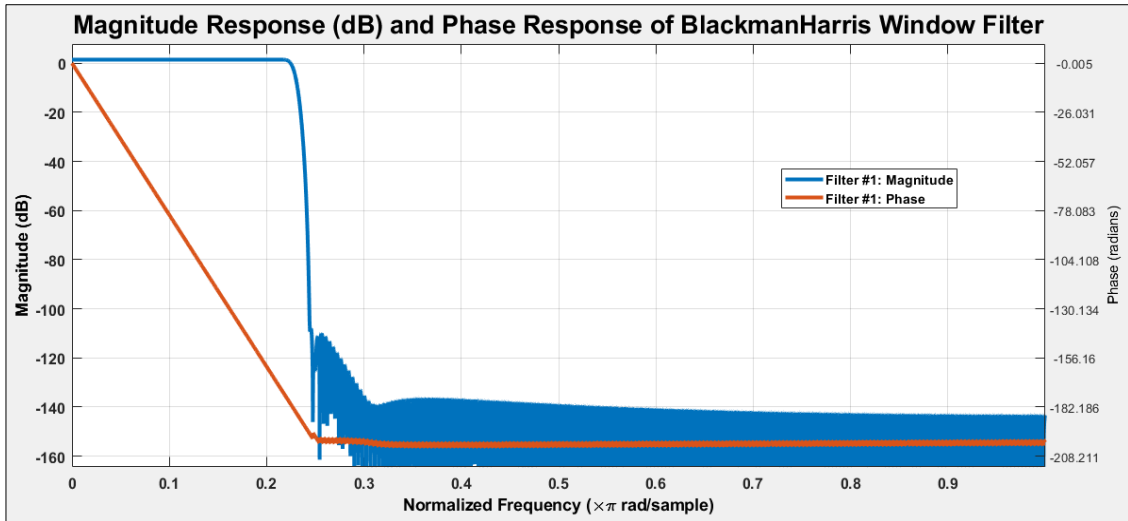


Figure (3.11) Magnitude and phase response of the BlackmanHarris window filter.

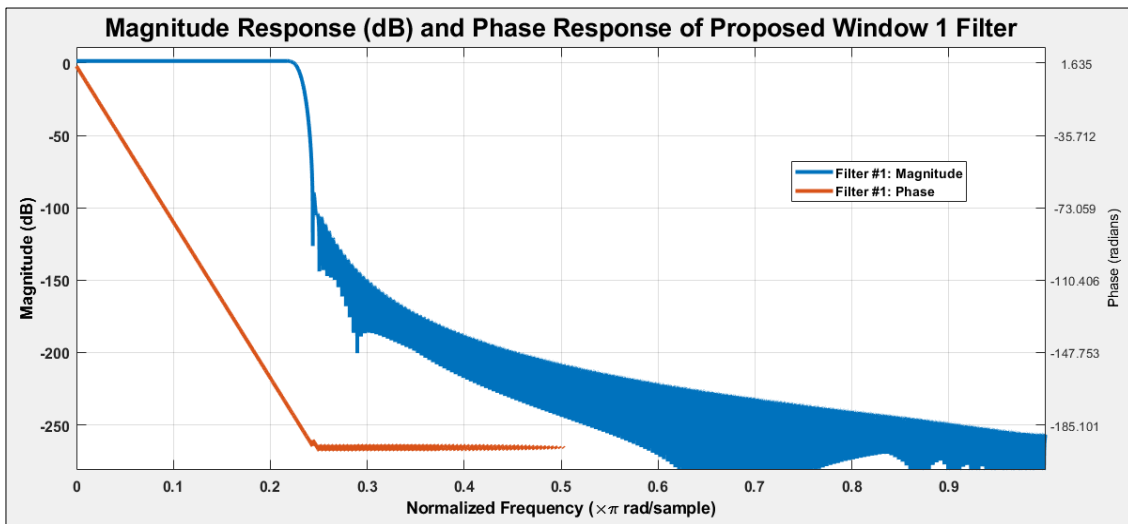


Figure (3.12) Magnitude and phase response of the Proposed window 1 filter.

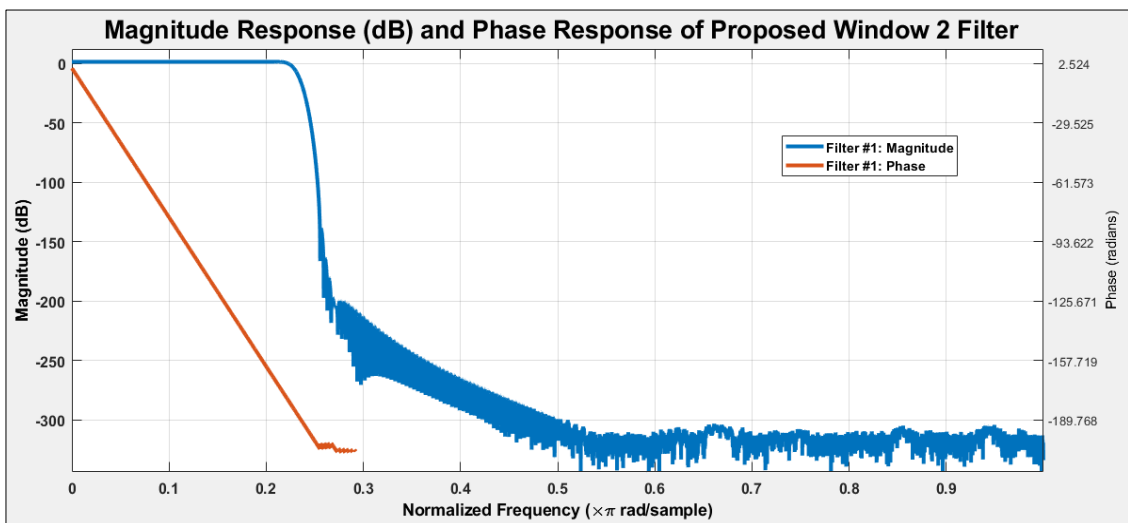


Figure (3.13) Magnitude and phase response of the Proposed window 2 filter.

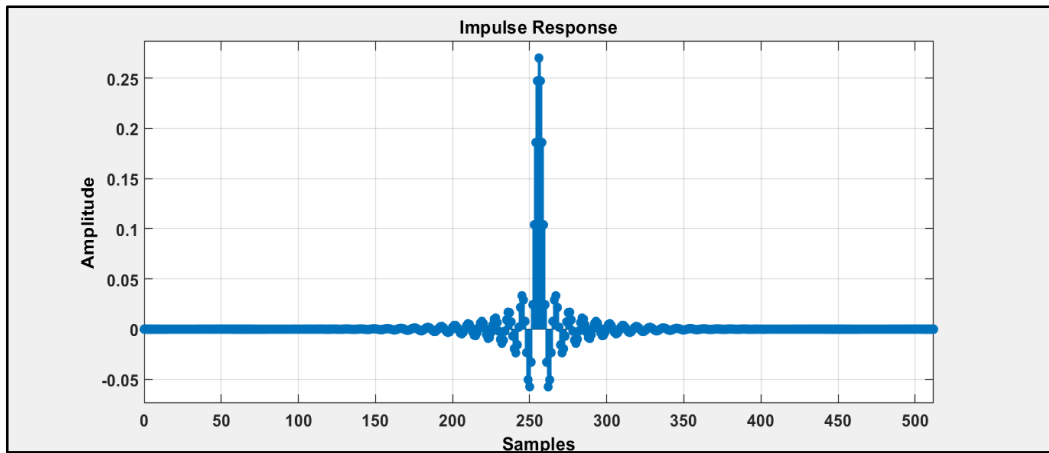


Figure (3.14) Impulse response of 513 samples length of the utilized digital filter.

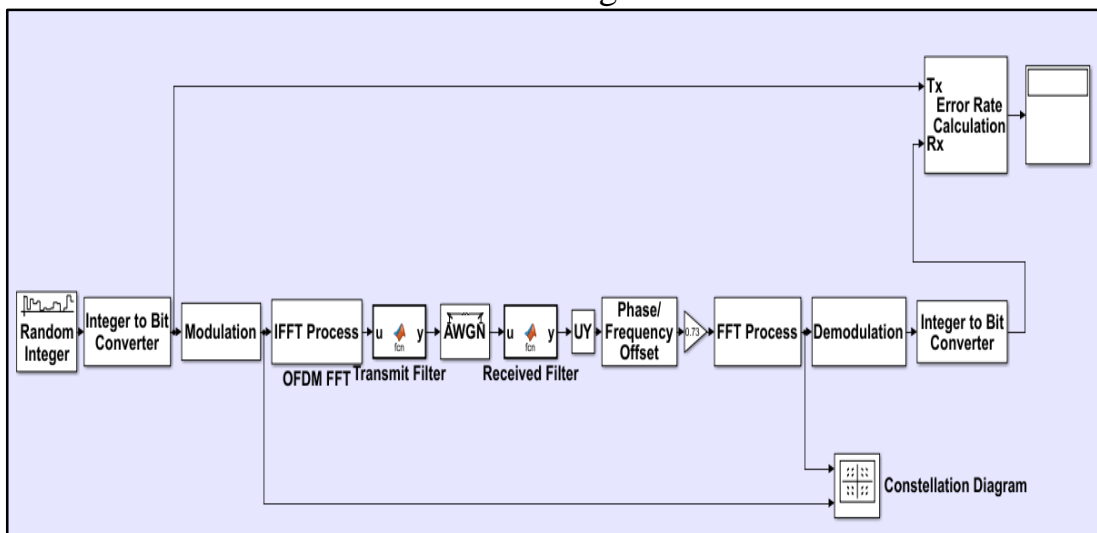


Figure (3.15) MATLAB-Simulink block diagram of one sub-band F-OFDM.

3.3.3 F-OFDM and OFDM Results and Comparisons (Simulink)

The performance of F-OFDM was analyzed based on two parameters: spectrum confinement (OOBE) and BER, which were compared to the performance of OFDM as follows:

Figure (3.16) shows the power spectrum of the F-OFDM waveform with different window filters and is compared to the conventional OFDM spectrum. The simulation was performed on five orders of QAM modulation, and the obtained spectrum has a slight effect on OOBE in all orders.

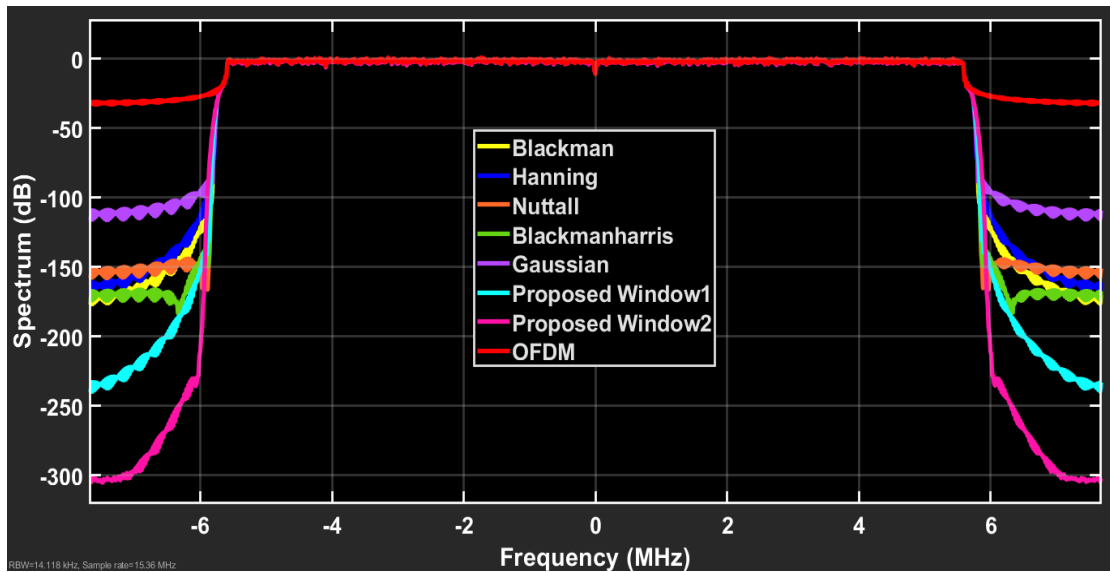


Figure (3.16) F-OFDM power spectrum compared with OFDM spectrum using different Window-Sinc filters (MATLAB-Simulink).

It can be noticed that higher sidelobes attenuation were achieved with different window filters compared to OFDM. The Blackman window filter achieves lower OOB than others as an individual window function. Higher suppression of the sidelobes is achieved at the proposed window 1 filter and proposed window 2 filter because the multiplication of two and three window functions with different characteristics made the main beam narrower.

The Gaussian window filter gives 80 dB lower sidelobes compared with OFDM, which produced -30 dB. The Nuttall window filter produces -120 dB OOB, the Hanning window filter produces -130 dB OOB, while BlackmanHarris and Blackman give approximately 137 dB and 140 dB respectively lower than OFDM. More enhancement appears at combination criteria, where the results obtained are 202 dB and 270 dB lower than OFDM at proposed window 1 and proposed window 2 respectively.

The performance of F-OFDM evaluated and compared with OFDM over AWGN at various Signal-to-Noise Ratio (SNR). The BER was measured due to the effects of filtering with various utilized window filters and constellation mapping as shown in figures (3.17), (3.18), (3.19), (3.20),

and (3.21). It is evident from the obtained BER curves of F-OFDM and OFDM approximately have the same behavior at lower values of SNR, while at higher SNR, the performance worsens than OFDM over different modulation orders.

The performance of all utilized filters offers approximately the same BER performance and is worsened in comparison with traditional OFDM. Furthermore, proposed window functions have a slightly worse case than the individual window function at higher orders of QAM.

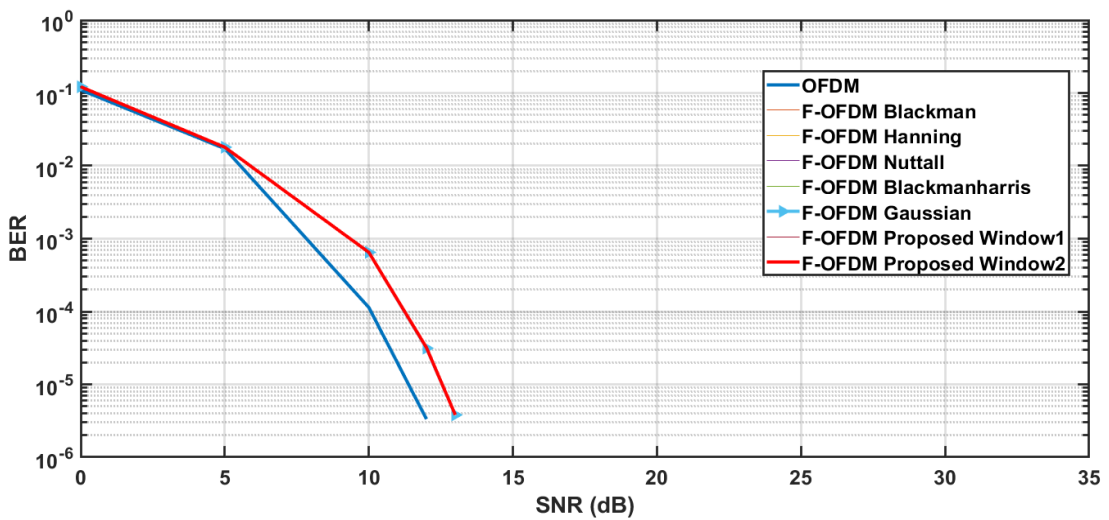


Figure (3.17) BER performance of F-OFDM compared with OFDM using 16-QAM Simulink results.

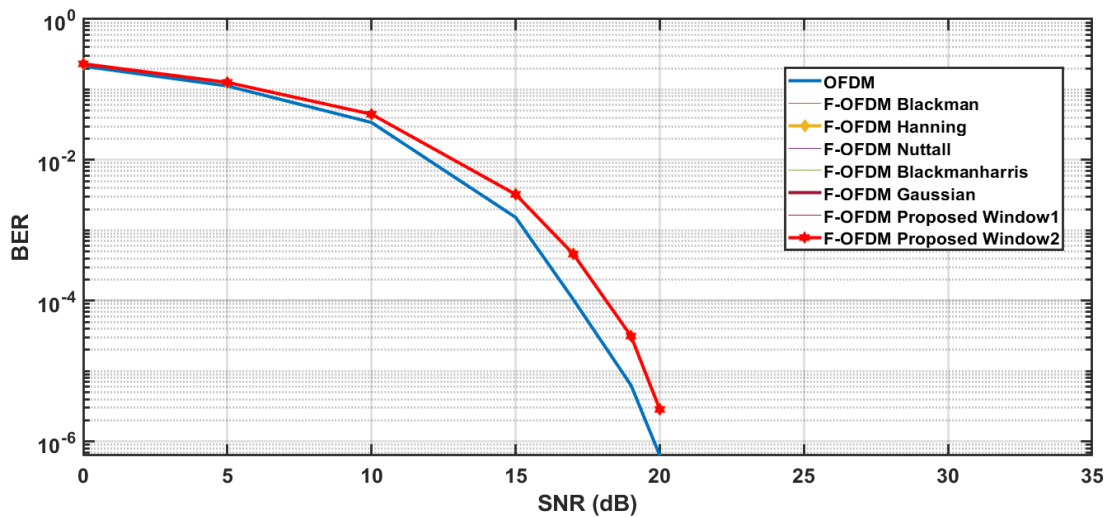


Figure (3.18) BER performance of F-OFDM compared with OFDM using 64-QAM Simulink results.

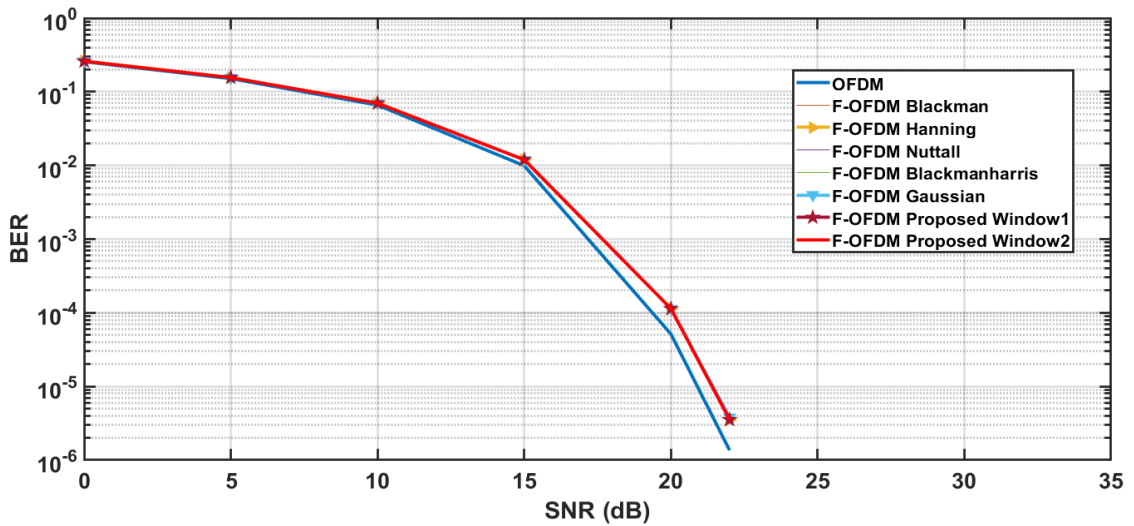


Figure (3.19) BER performance of F-OFDM compared with OFDM using 128-QAM Simulink results.

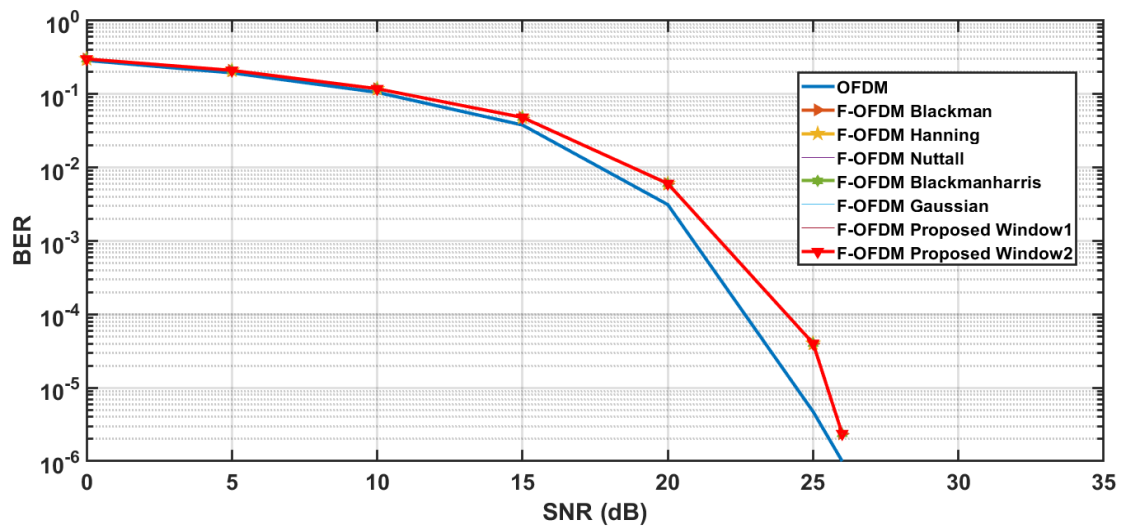


Figure (3.20) BER performance of F-OFDM compared with OFDM using 256-QAM Simulink results.

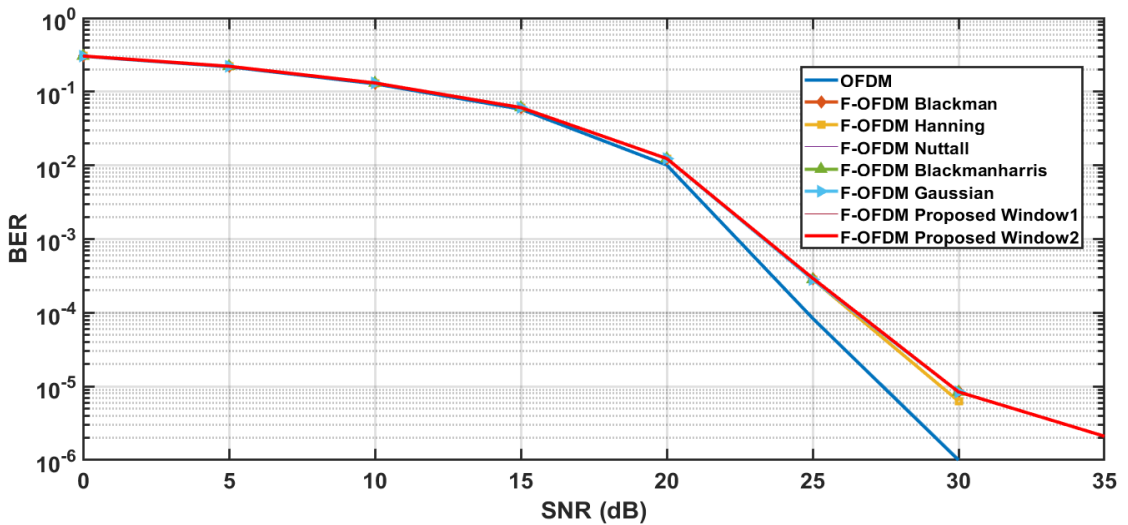


Figure (3.21) BER performance of F-OFDM compared with OFDM using 512-QAM Simulink results.

3.3.4 F-OFDM Sub-banding (Simulink)

The section of the simulation adopted two scenarios of sub-band scheme. The first scenario split the utilized spectrum into four sub-bands of equal size, while the second scenario split the utilized spectrum into four sub-bands of unequal size. The two scenarios have different specifications in terms of the number of utilized subcarriers, filter design bandwidth, and modulation orders per sub-band.

3.3.4.1 Equal-Sized Sub-bands F-OFDM (Simulink)

The entire Simulink block for equal sub-bands sizes F-OFDM is shown in figure (3.22) which is modeled according to the transceiver block diagram of F-OFDM in chapter two sub-section (2.8.1). The F-OFDM waveform is constructed by dividing the utilized bandwidth into four equal-sized sub-bands. In each sub-band, the Random Integer blocks contain various initial seed values to generate varied data. Different modulation orders are applied to the sub-bands. Before the orthogonal subcarriers are executed, a shift of the sub-band to the desired location is necessary. The shifting process is performed by injection of a zero pad before, after, or both into the modulated data, IFFT then used to achieve orthogonality. To complete the system, CP added. The frequency response of the transmit filter moved to the desired sub-band using MATLAB code for the utilized filter, see Appendix-B. The signals from the sub-bands are combined, and delivered over the channel.

On the receive side, an equivalent version of the transmit filters is applied to the received signal to separate the intended signal from the various sub-band signals and minimize interference. Distortion occurs as a result of adding the filter, and the shifting property is treated by applying a phase rotation to the constellation points using a Phase/Frequency Offset block to modify the phase distortion. Furthermore, zero samples of the same length as the filter must be removed and the power level must be adjusted. The FFT

process is performed, and demodulation of the received symbols obtains the desired information for each sub-band.

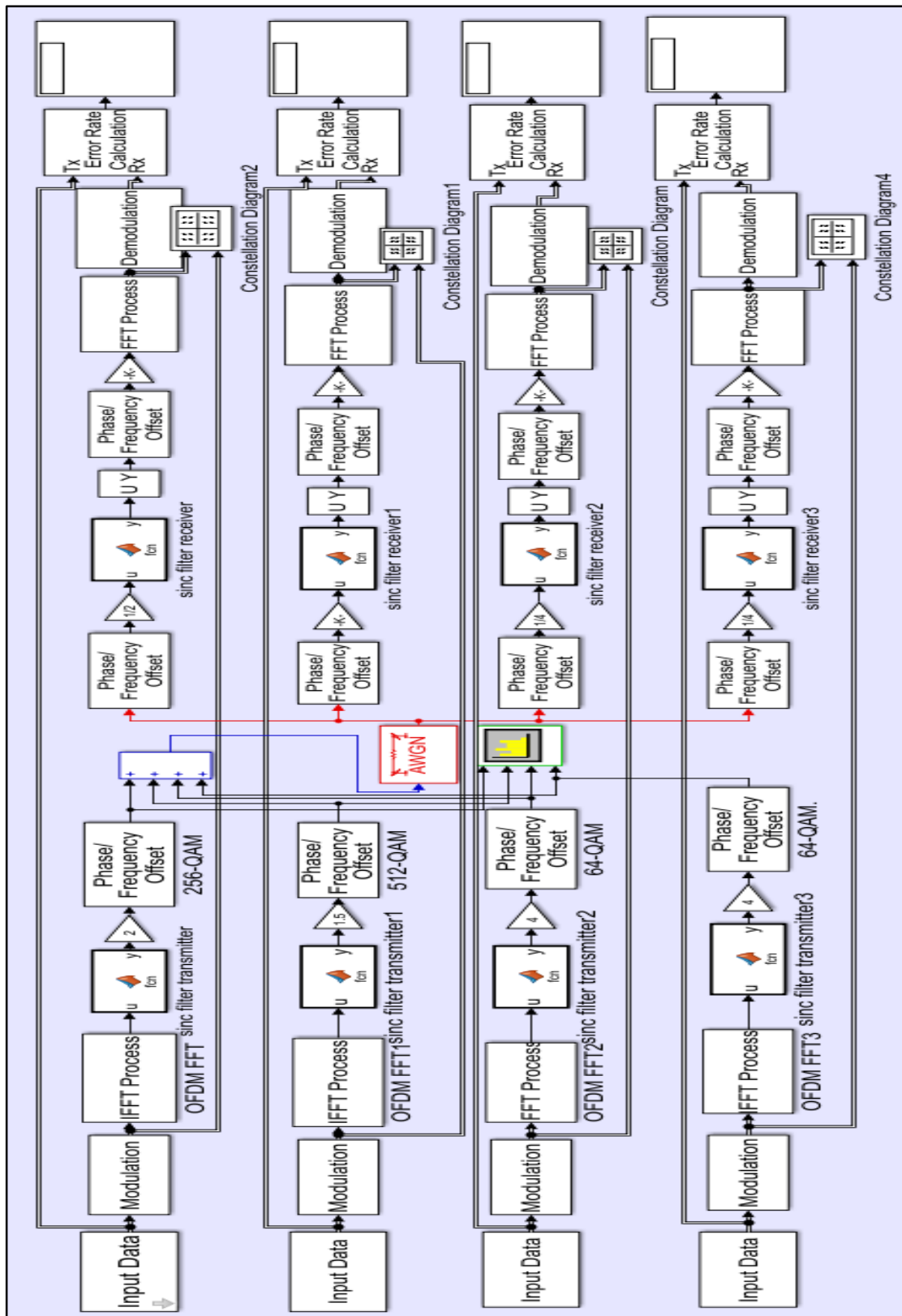


Figure (3.22) Sub-bands F-OFDM waveform in MATLAB-Simulink.

3.3.4.2 Equal-Sized Sub-bands Results and Comparisons (Simulink)

Evaluating the performance of equal-sized sub-bands F-OFDM waveform is based on achieved OOB, average BER, SE measurement, and finally the PAPR values.

A. Achieved OOB

The OFDM mechanism based filtering helps to reduce the sidelobes, resulting in lower OOB. The reduction of sidelobes leads to minimizing the guard band between the sub-bands, and without any interference. Three types of window filters are used in this step: Blackman window, proposed window 1 and proposed window 2 filters. The reasons of utilizing the Blackman window are: good time-frequency localization, acceptable BER, and lower passband, while the two proposed window filters gave minimum sidelobes attenuation.

Figure (3.23) illustrates four OFDM sub-bands power spectrum in equal sizes, which provides larger OOB (-29 dB) compared to figures (3.24), (3.25), and (3.26), which illustrate the transmit power spectrum of the equal sub-bands sizes F-OFDM of three kinds of utilized filters. The summation of the sub-bands power spectra (at the sidelobes region) achieves approximately -160 dB, -212 dB, and -213 dB OOB for Blackman, proposed window 1 and proposed window 2 filters respectively.

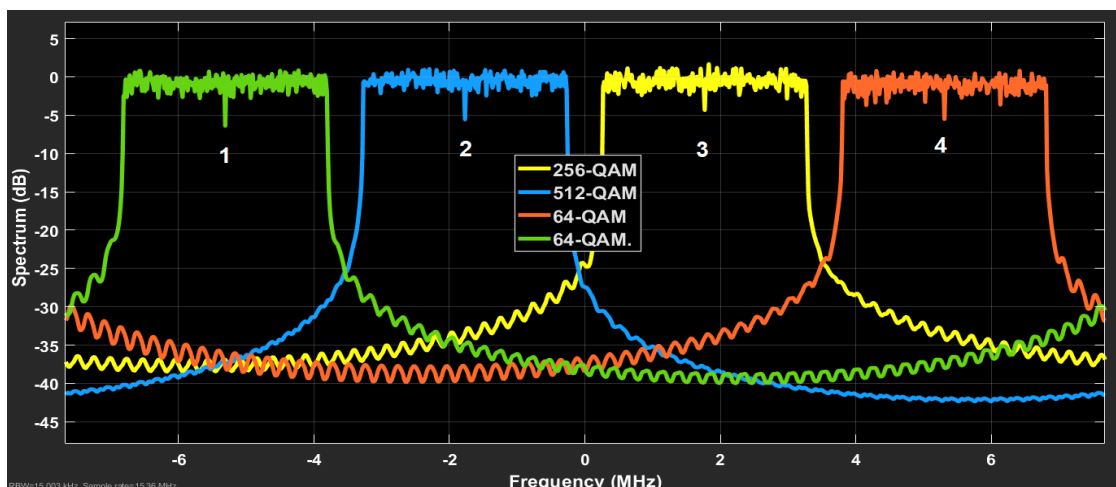


Figure (3.23) Power spectrum of equal-sized sub-bands OFDM (Simulink).

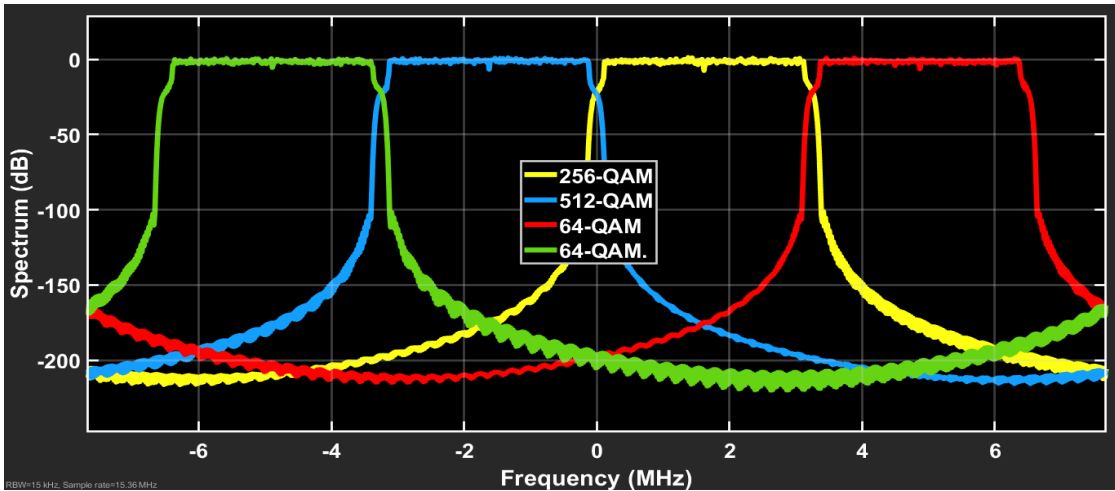


Figure (3.24) Power spectrum of equal-sized sub-bands F-OFDM using Blackman window filter (Simulink).

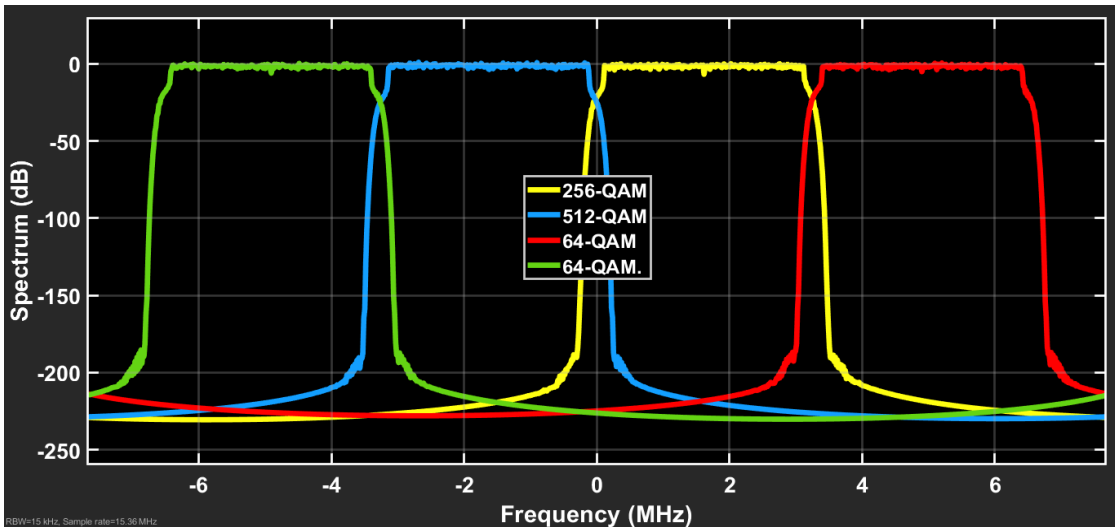


Figure (3.25) Power spectrum of equal-sized sub-bands F-OFDM using proposed window 1 filter (Simulink).

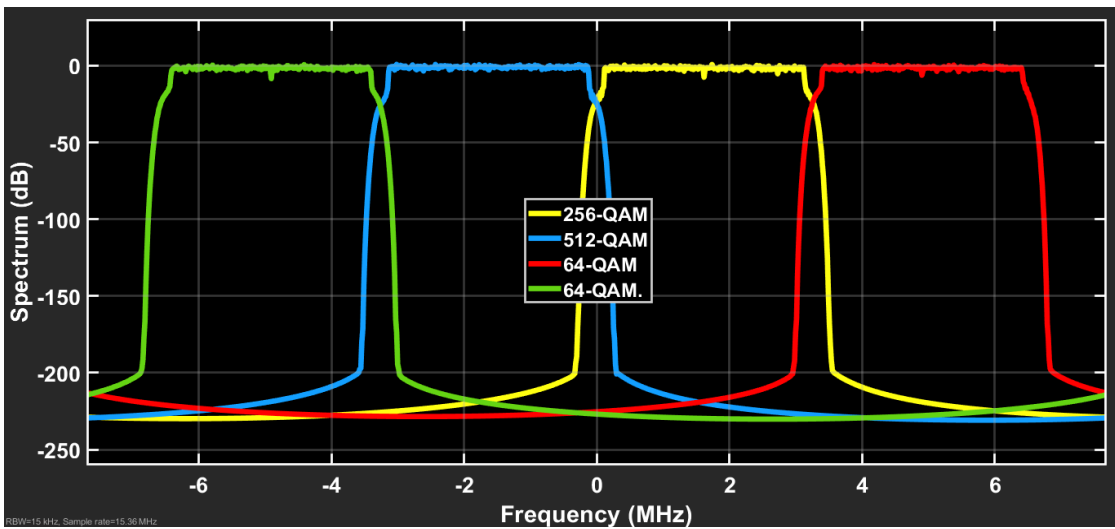


Figure (3.26) Power spectrum of equal-sized sub-bands F-OFDM using proposed window 2 filter (Simulink).

B. Average BER Performance

The performance of average BER of the equal sub-bands with the three adopted filters are illustrated in figure (3.27). It is worth noting that at the lower values of SNR, the BER of F-OFDM has the same performance as OFDM. At higher values of SNR, the BER of F-OFDM curves degrades, where at 37 dB of SNR the BER is 1.6×10^{-6} , 1.5×10^{-5} , 9.1×10^{-6} and 6×10^{-6} for OFDM, Blackman, proposed window 1 and 2 F-OFDM respectively.

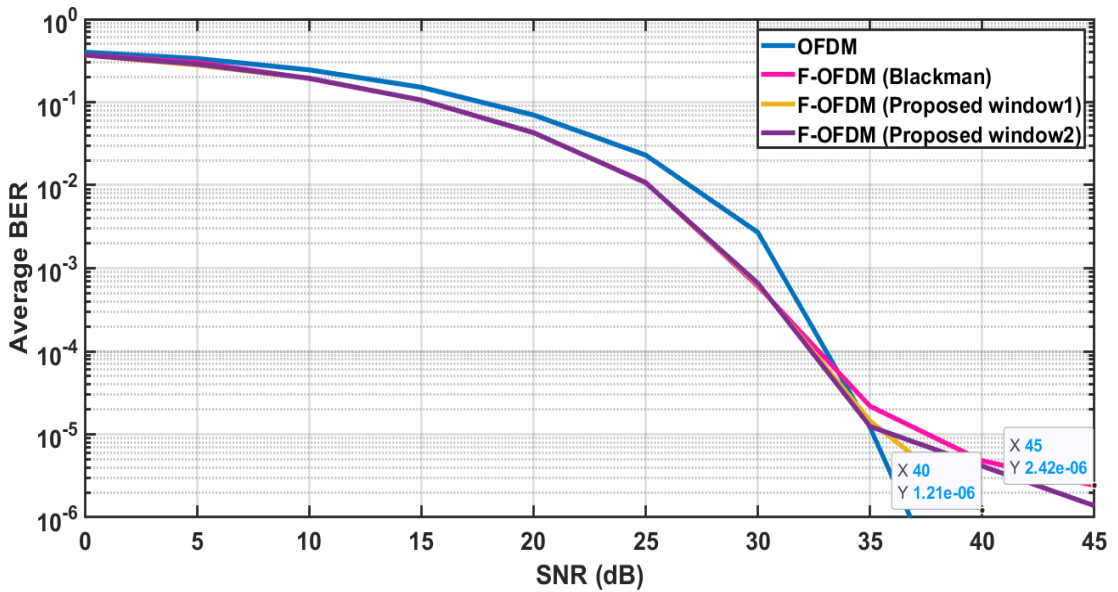


Figure (3.27) Average BER of equal-sized sub-bands (Simulink).

At 40 dB of SNR, the BER of Blackman, proposed window 1 and 2 are 4.8×10^{-6} , 1.21×10^{-6} , and 4.14×10^{-6} , respectively. The minimum BER value of the Blackman window filter at 45 dB SNR is 2.42×10^{-6} , while for the proposed window 2 filter the minimum BER value is approximately 1.38×10^{-6} .

C. Spectrum Efficiency Enhancement

The SE of the equal-sized sub-band waveform was calculated based on the reduction of the guard band between the sub-bands to a minimum value according to the flowchart in figure (3.1) and equation (3.2). It can be shown from figure (3.28) that the four sub-bands waveform using filters,

achieve higher SEs than that of OFDM, where at lower values of SNR the SE enhancement for Blackman window filter is approximately 4.8%, while at higher values of SNR the SE achieved is approximately 4.9%. In comparison to OFDM, the maximum SE enhancement at the proposed window 1 and 2 filters is 5.1% and 5.2%, respectively.

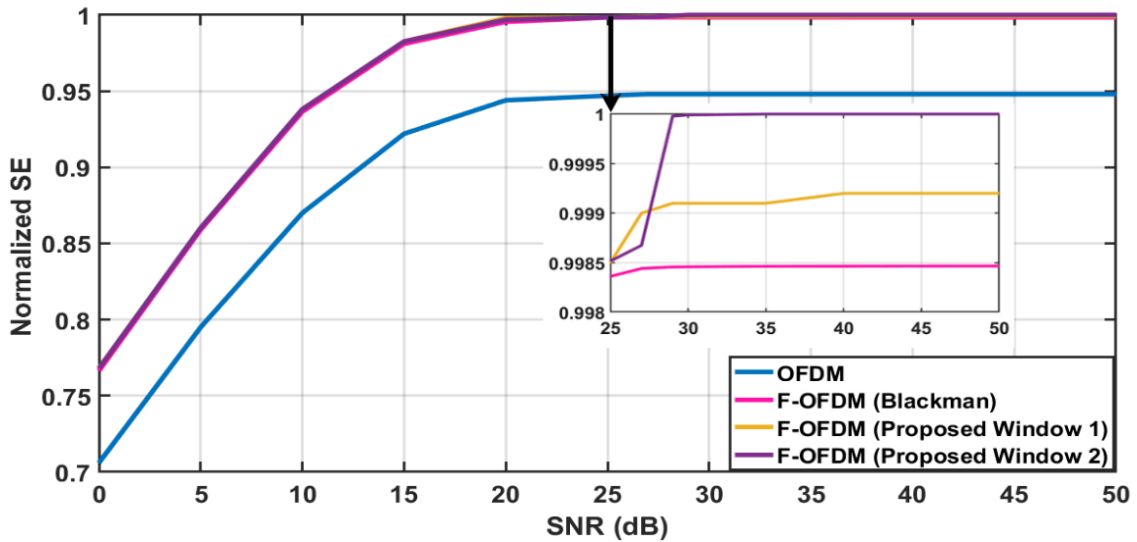


Figure (3.28) Normalized SE of equal-sized sub-band F-OFDM compared to OFDM (Simulink).

D. Average PAPR Comparison

PAPR is an important implementation issue related to the performance of F-OFDM. Figure (3.29) compares the average PAPR performance of the equal-sized sub-band waveform at the three filters used to that of OFDM. F-OFDM with equal sub-bands has a higher PAPR than OFDM.

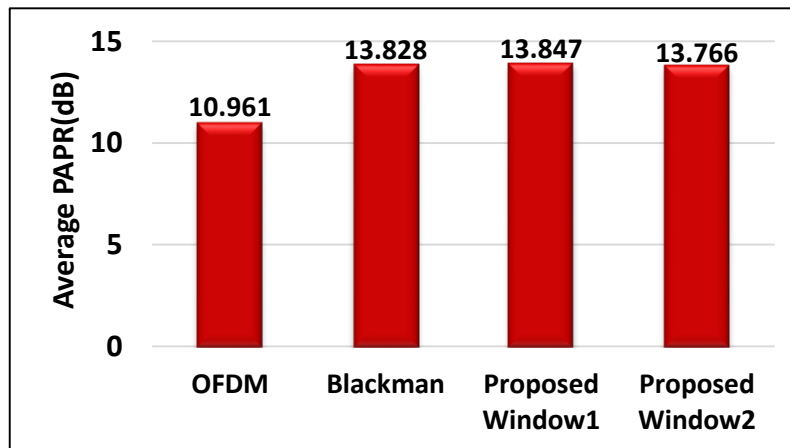


Figure (3.29) Average PAPR of equal-sized sub-bands F-OFDM (Simulink).

3.3.4.3 Unequal-Sized Sub-bands F-OFDM (Simulink)

Based on the requirements of the 5G system for supporting multi-services, the F-OFDM waveform is configured by dividing the spectrum into different sizes of sub-bands. Four sub-bands support varying numbers of data subcarriers and various orders of modulation. The Simulink block is created in the same manner as the equal sub-banding that is illustrated in figure (3.22), the difference is the allocated subcarriers per each sub-band which support (16, 64, 128 and 256) QAM.

3.3.4.4 Unequal-Sized Sub-bands Results and Comparisons (Simulink)

The evaluation of unequal-sized sub-band waveform performance is based on the same four factors as for equal-sized waveform: achieved OOBE, average BER, SE measurement, and PAPR.

A. Achieved OOBE

Due to the different sizes of the sub-bands, the guard band is a variant. The small band requires the smallest guard, while at the large band size, the guard is increased. The optimum guard band obtained is related to the OOBE of the sub-bands by shifting the sub-bands to a minimal guard to ensure that no errors appear. Blackman and the two proposed window filters were adopted for the same reasons listed in section (3.3.4.2). Figure (3.30) illustrates four OFDM sub-bands power spectrum in unequal sizes, which provides a larger OOBE (-29 dB). Figures (3.31), (3.32), and (3.33) illustrate the power spectrum of the F-OFDM waveform using Blackman, proposed window 1, and proposed window 2 filters, respectively. The summation of the sub-band power spectrum (at the sidelobes region) achieves approximately -164 dB, -208 dB, and -212 dB OOBE for Blackman, proposed window 1 and proposed window 2 filters, respectively.

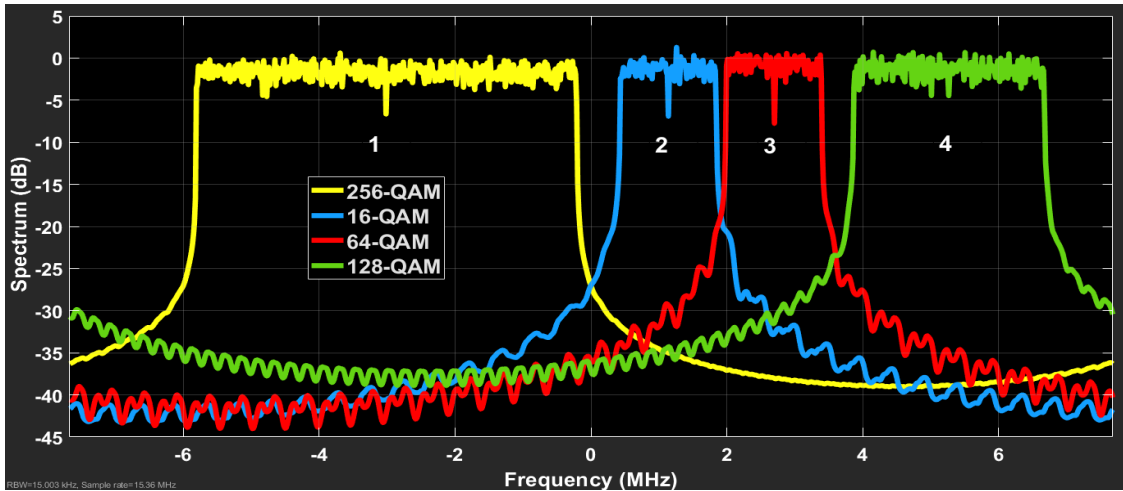


Figure (3.30) Power spectrum of unequal-sized sub-bands OFDM (Simulink).

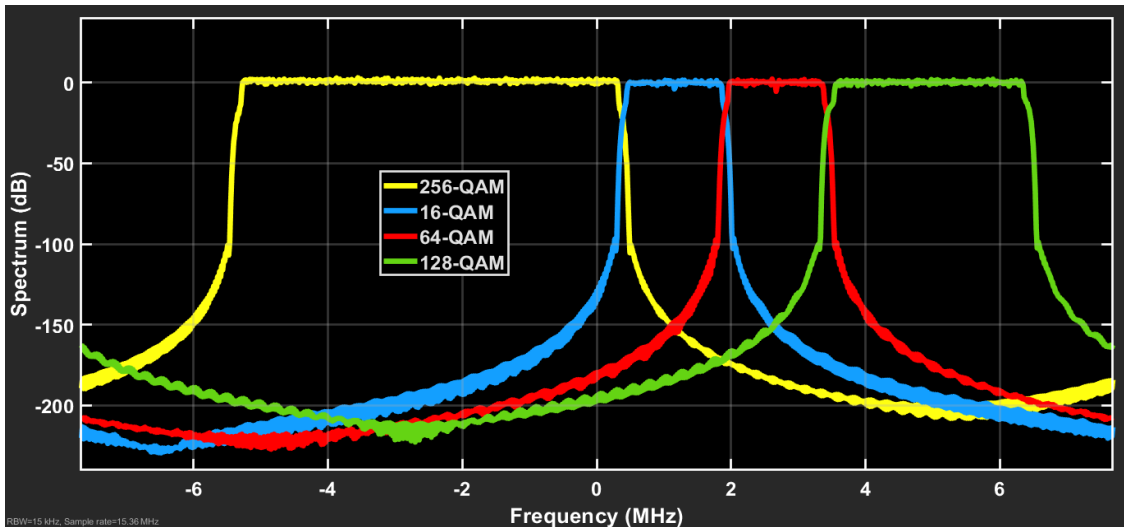


Figure (3.31) Power spectrum of unequal-sized sub-bands F-OFDM using Blackman window filter (Simulink).

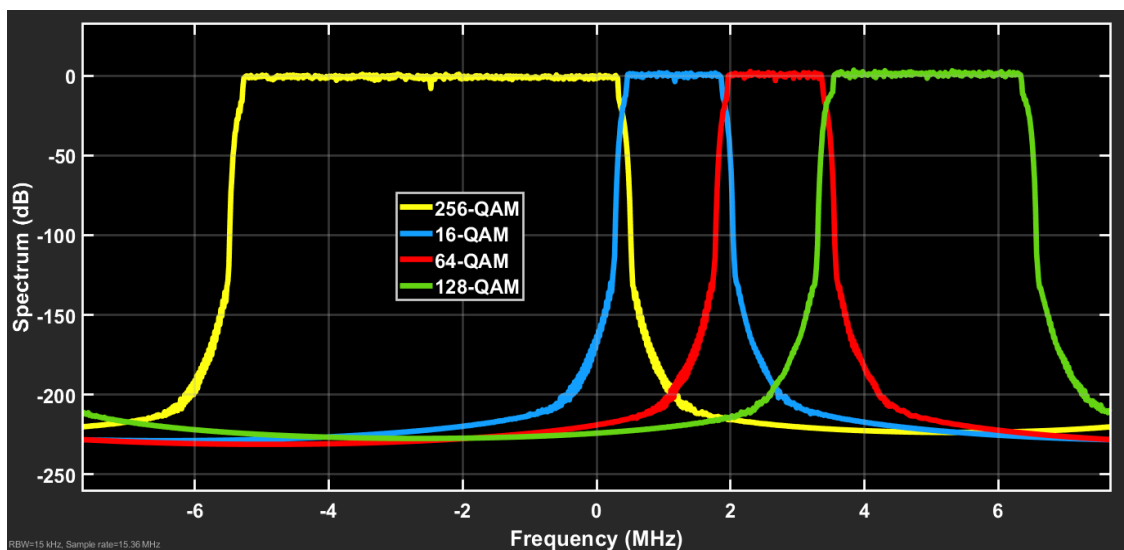


Figure (3.32) Power spectrum of unequal-sized sub-bands F-OFDM using proposed window 1 filter (Simulink).

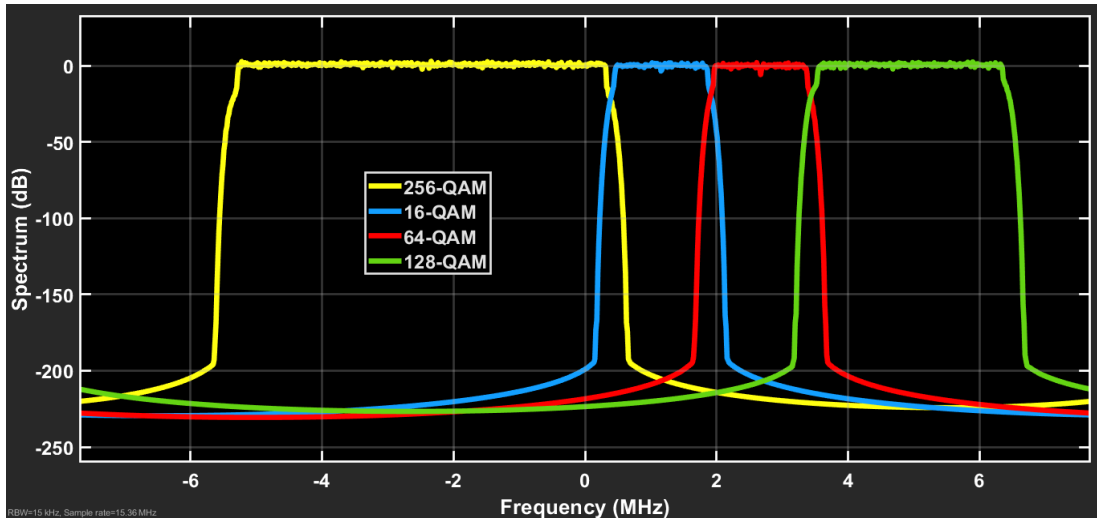


Figure (3.33) Power spectrum of unequal-sized sub-bands F-OFDM using proposed window 2 filter (Simulink).

B. Average BER Performance

The performance of the average BER of the unequal sub-bands with the three adopted filters is illustrated in figure (3.34). It can be noticed that at the lower values of SNR, the BER of F-OFDM has the same performance as OFDM. At higher values of SNR, the performance is differ and get to worse. At 40 dB SNR, the BERs are 1.35×10^{-6} , 1.78×10^{-6} , 6.79×10^{-6} and 2.7×10^{-6} for OFDM, Blackman, proposed window 1 and 2 filters, F-OFDM respectively.

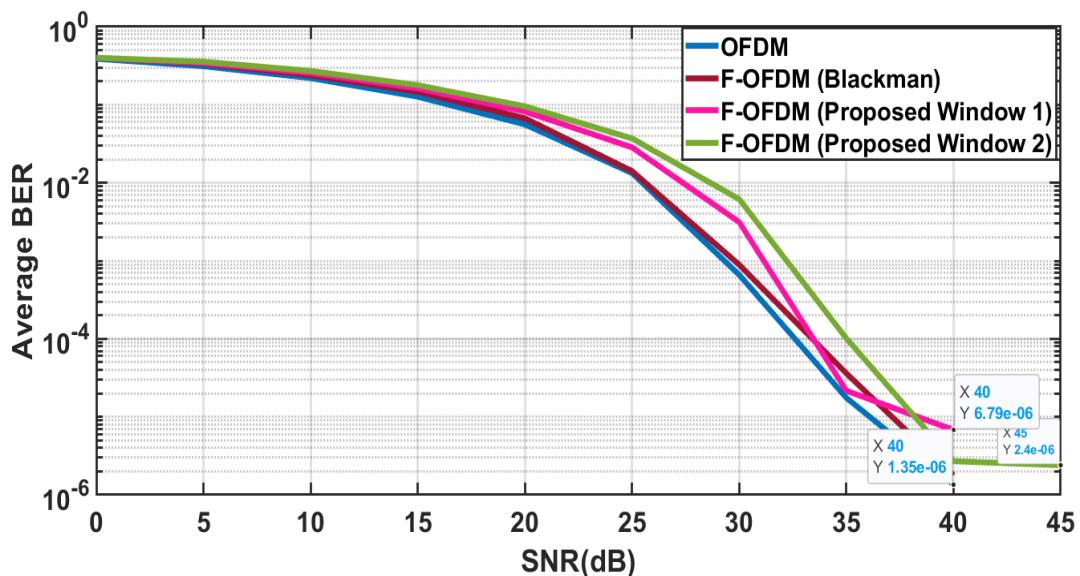


Figure (3.34) Average BER of unequal-sized sub-bands sizes (Simulink).

C. Spectrum Efficiency Enhancement

The same method used to calculate the performance of equal sub-band sizes in terms of SE is also adopted for unequal sub-band sizes. The optimized guard band between the sub-bands achieves higher SE compared to OFDM. It can be noticed from figure (3.35) that the improvement SE at lower values of SNR is 6 %, 5.5%, and 4.6% for Blackman window, proposed window 1, and 2 filters, respectively. At higher values of SNR, the achievement SE for each of Blackman, proposed window 1 and 2 filters is 5.25%, 5.3%, and 5.7%, respectively.

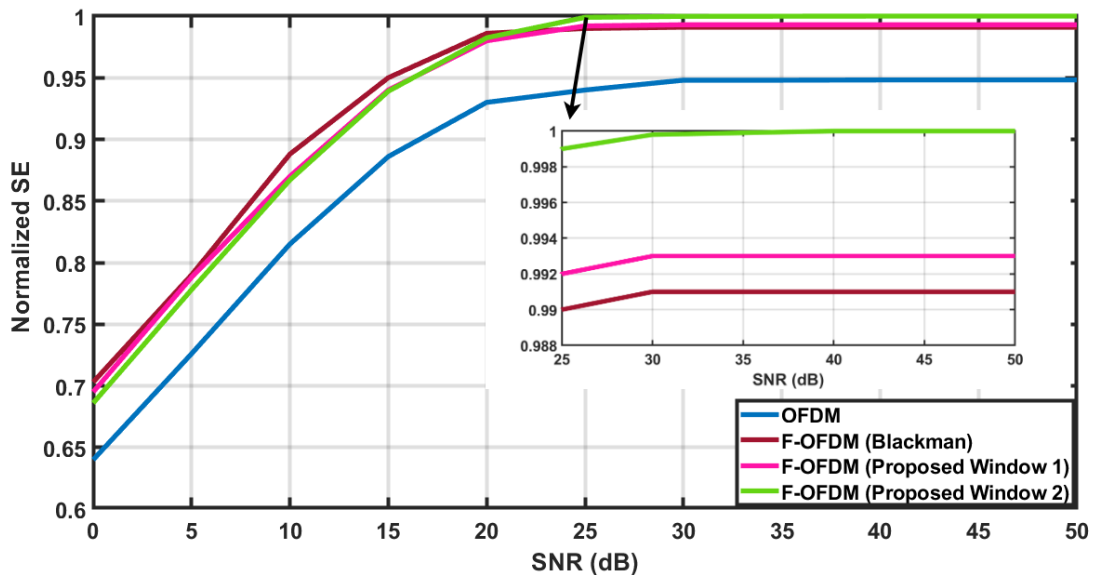


Figure (3.35) Normalized SE of unequal-sized sub-bands F-OFDM compared to OFDM (Simulink).

D. Average PAPR Comparison

Figure (3.36) illustrates the average PAPR performance of the unequal sub-banding waveform at the three utilized filters and is compared to that of OFDM. It can be noticed that the PAPR values of the unequal sub-bands F-OFDM are higher than in OFDM, which may deteriorate system performance.

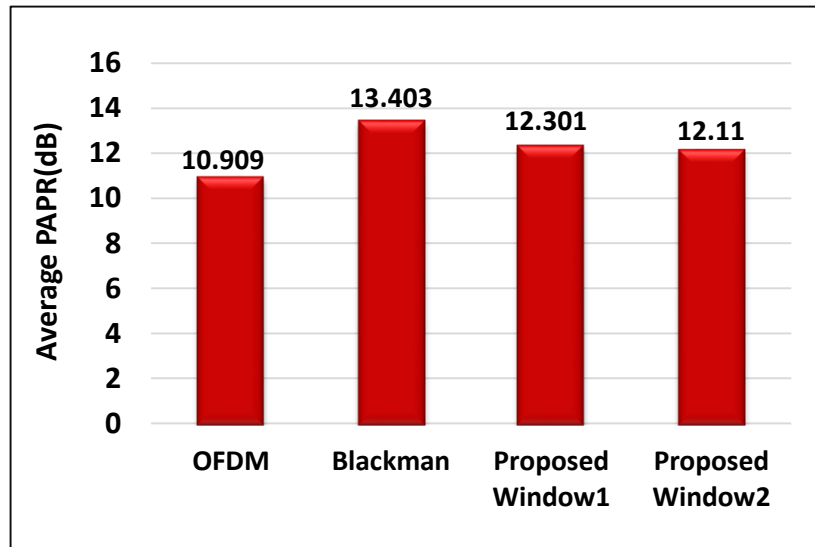


Figure (3.36) Average PAPR of unequal-sized sub-bands F-OFDM (Simulink).

3.4 Second Approach LabVIEW NXG F-OFDM Methodology

The second alternative approaches for modeling and simulation the proposed waveform is accomplished using the LabVIEW NXG, which is a graphical programming environment used for test and measurement. NXG is the next generation of LabVIEW for communication from National Instruments. The new platform was developed in 2017 to enhance the user experience, and it is more advanced for designing wireless communication systems [54]. The simulation steps include OFDM, F-OFDM, and F-OFDM sub-banding designs with their results.

3.4.1 OFDM System Model (LabVIEW)

Figure (3.37) illustrates the OFDM transceiver model block diagram designed in LabVIEW. The first step at the transmitter is to generate a bit sequence using the MT Generate Bits (Galois, PN Order) node. Maps the incoming bits to obtain complex-valued QAM using the MT Map Bits to QAM Symbols node, which depends on the order specified by MT Generate QAM System Parameters (M) node and the number of bits generated. The constellation diagrams for various QAM orders obtained from the simulation is shown in figure (3.38). Construction of the parallel form of an OFDM block consists of modulated data symbols, DC subcarrier, and null subcarriers as a guard band. To maintain the orthogonality, Inverse complex FFT is applied, and the CP inserted. Finally, the complete signal is transmitted over the AWGN channel.

On the receive side, first the CP is removed, then the complex FFT is applied to the sequence symbols. The DC and null subcarrier then removed to get the modulated data. Finally, demodulate the received symbols using MT Map QAM symbols to Bits node.

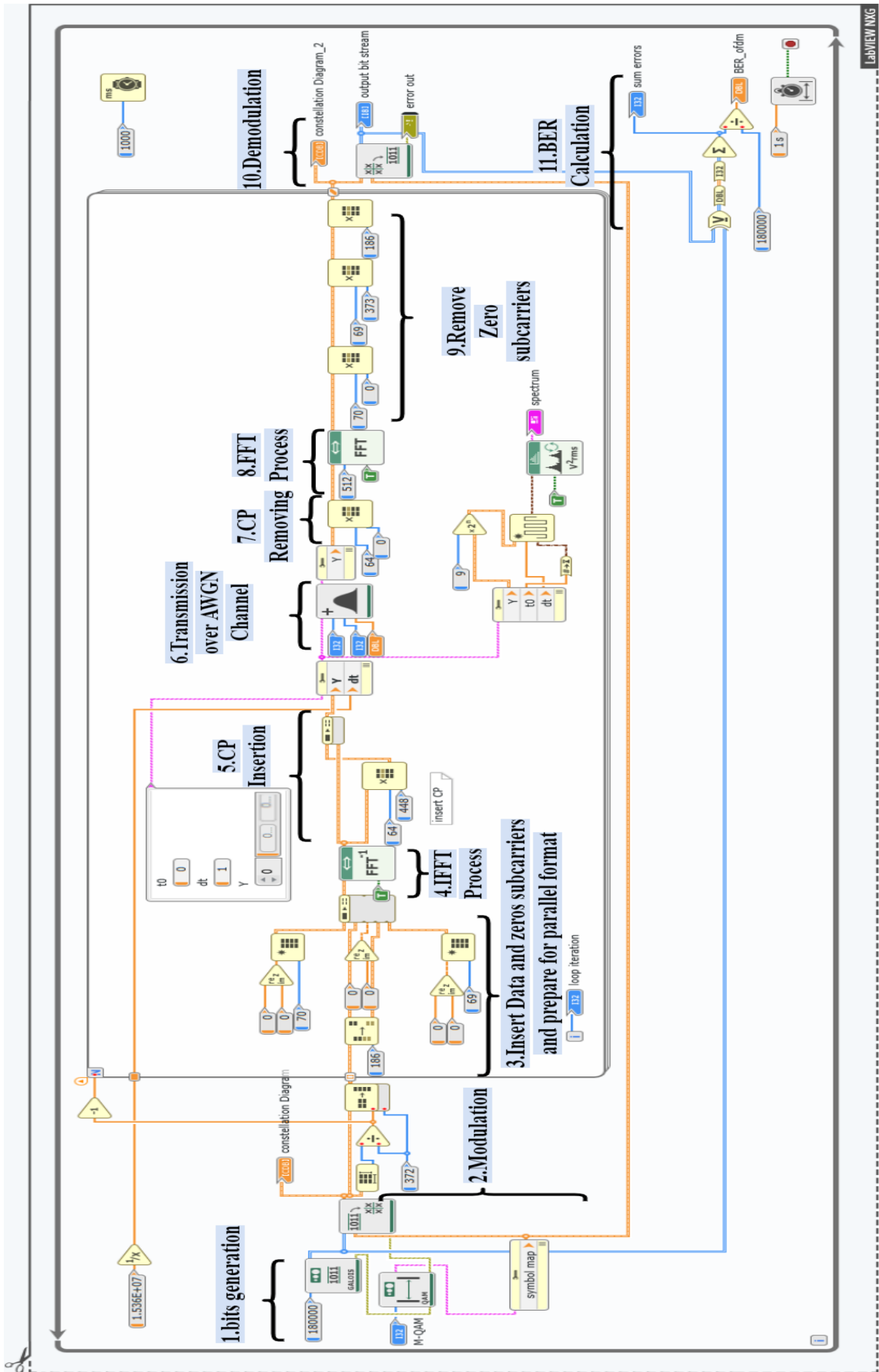


Figure (3.37) OFDM diagram window in LabVIEW NXG.

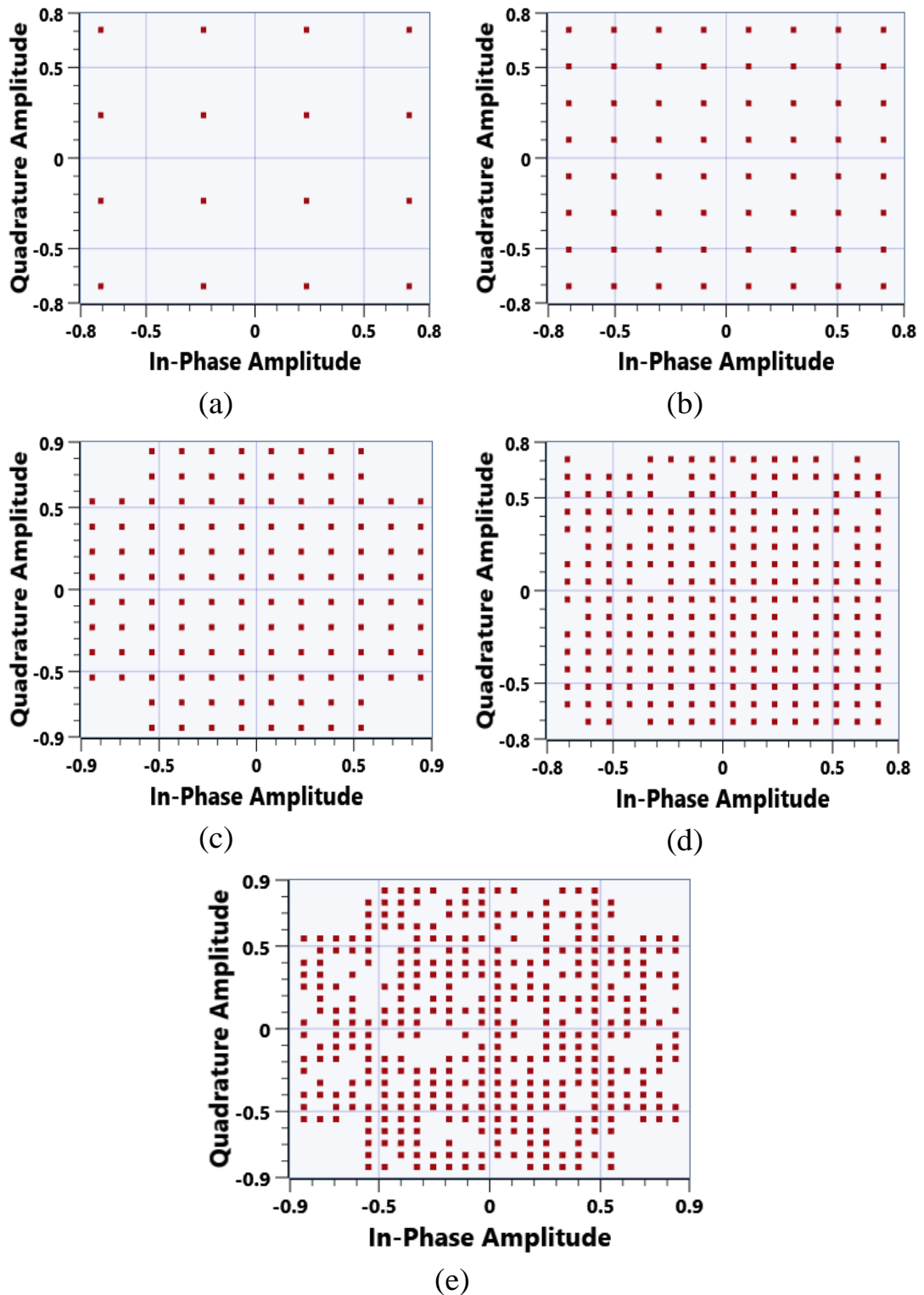


Figure (3.38) A snapshot constellation diagrams of various modulation orders in LabVIEW: (a) 16-QAM, (b) 64-QAM, (c) 128-QAM, (d) 256-QAM, (e) 512-QAM.

3.4.2 F-OFDM System Model (LabVIEW)

After the OFDM model is completed, various Window-Sinc filter forms are applied to evaluate the system performance. The same set of filters used in Simulink are reused in LabVIEW by establishing an interface to MATLAB to call MATLAB filter functions inside LabVIEW NXG. The interfacing process is illustrated in figure (3.39) and the entire system of F-OFDM is illustrated in figure (3.40). At the transmitter side, the filter is inserted after CP insertion, while it is inserted directly into the received signal to pick the desired sub-band and eliminate the distortion caused by the utilized filters.



Figure (3.39) Interfacing process between MATLAB function and LabVIEW NXG.

3.4.3 F-OFDM and OFDM Results and Comparisons (LabVIEW)

The F-OFDM and OFDM performance evaluation is based on two parameters: spectrum confinement and BER as follows:

Figure (3.41) shows the power spectrum comparison of F-OFDM and OFDM using the same filter types utilized in Simulink. It is obvious that the F-OFDM outperforms the OFDM in terms of sidelobes suppression. The achieved OOBE for the Gaussian window filter was -80 dB better than that of OFDM. The Nuttall window filter has a -127 dB OOBE enhancement, the Hanning window filter has a -136 dB OOBE enhancement, while BlackmanHarris and Blackman have an improvement of -144 dB and -151 dB, respectively. More enhancement was realized for the proposed filters, where the results obtained 208 dB, and 286 dB lower than OFDM for proposed window 1 and proposed window 2, respectively.

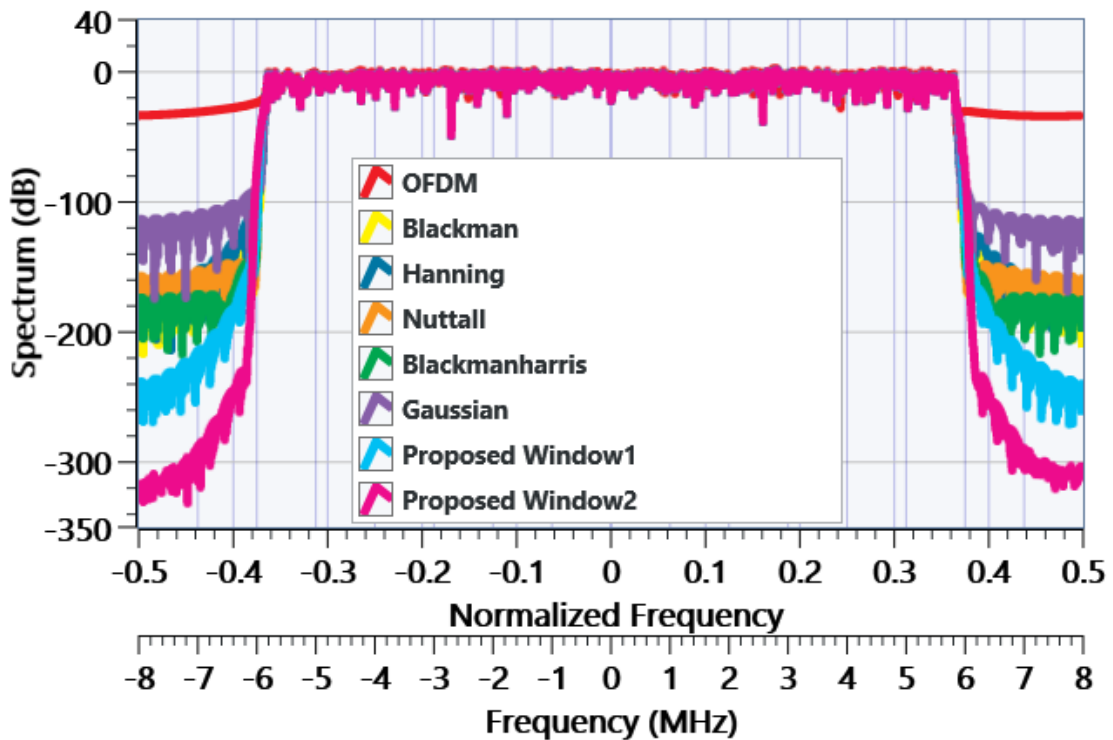


Figure (3.41) F-OFDM power spectrum compared with OFDM spectrum using different Window-Sinc filters (LabVIEW).

The BER performance of the F-OFDM was assessed for the five orders of QAM and compared to that of OFDM. As shown in figures (3.42), (3.43), (3.44), (3.45), and (3.46) the types of the filters used in this section do not affect the BER for various modulation orders. At lower values of SNR, the BER of F-OFDM gives approximately the same results as OFDM, while at higher values of SNR, the BER performance deteriorates.

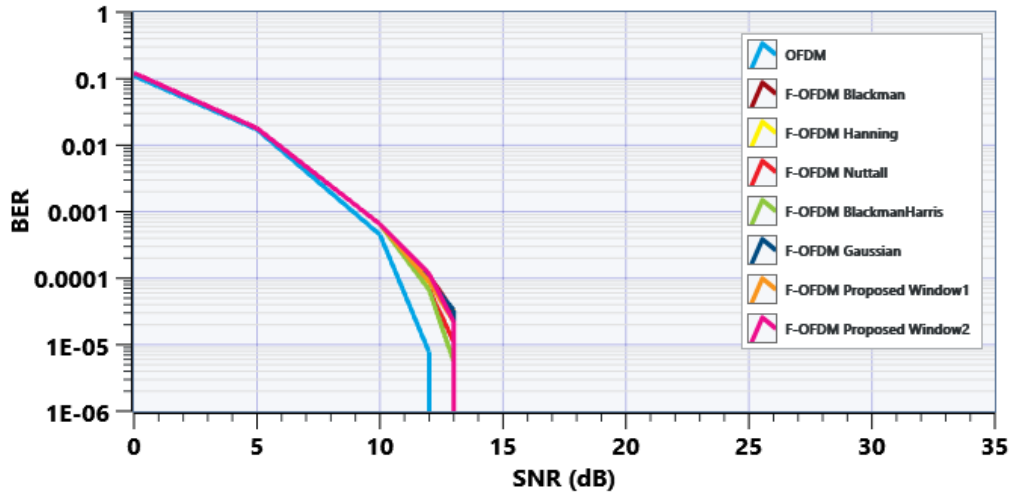


Figure (3.42) BER performance of F-OFDM compared with OFDM using 16-QAM LabVIEW results.

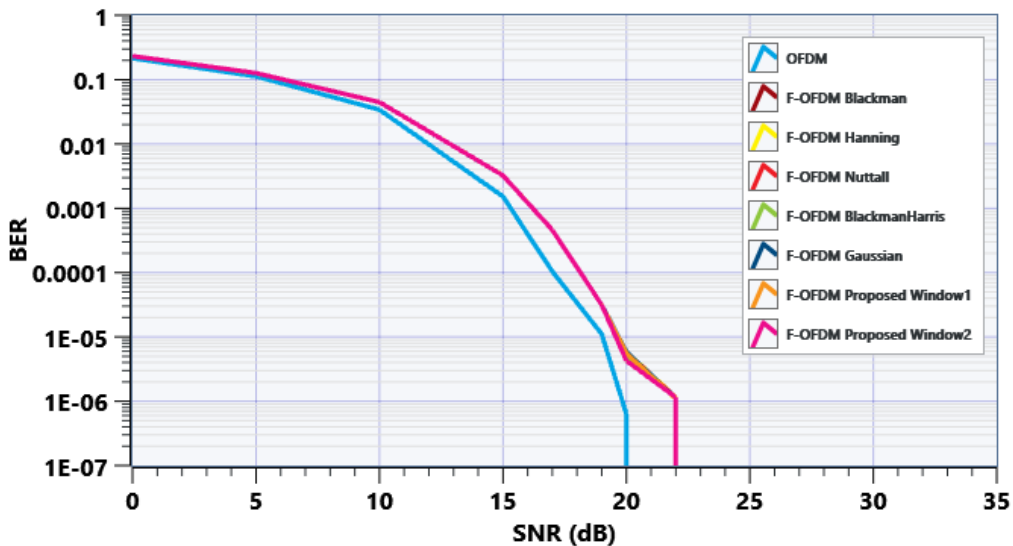


Figure (3.43) BER performance of F-OFDM compared with OFDM using 64-QAM LabVIEW results.

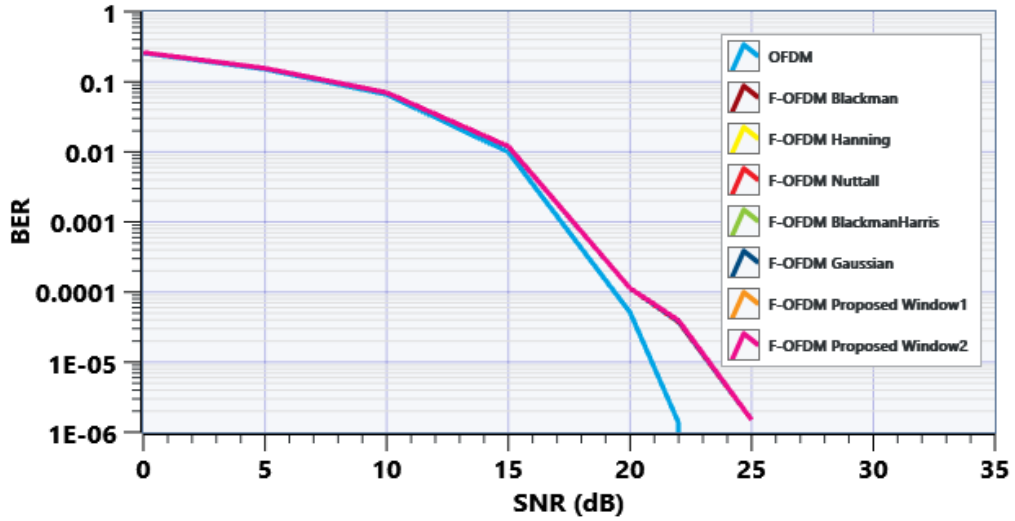


Figure (3.44) BER performance of F-OFDM compared with OFDM using 128-QAM LabVIEW results.

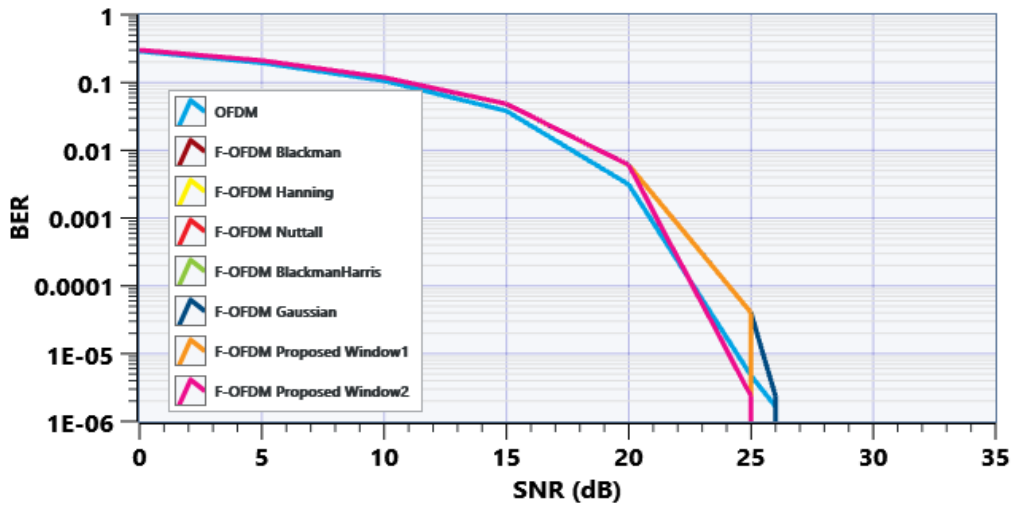


Figure (3.45) BER performance of F-OFDM compared with OFDM using 256-QAM LabVIEW results.

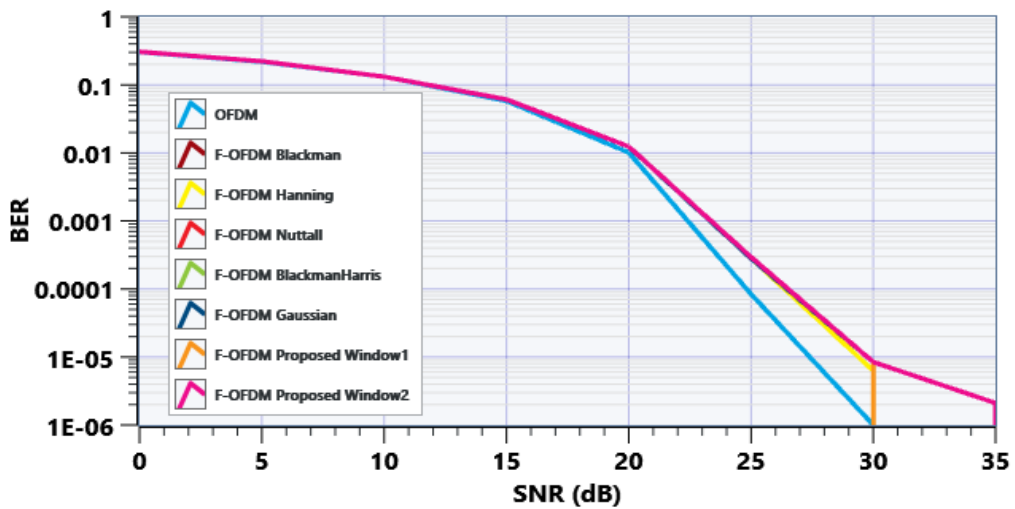


Figure (3.46) BER performance of F-OFDM compared with OFDM using 512-QAM LabVIEW results.

3.4.4 F-OFDM Sub-banding (LabVIEW)

In this subsection, the simulation is based on the same two scenarios modeled in MATLAB-Simulink. The first scenario splits the allocated bandwidth into four equal sub-band sizes, while the second scenario splits it into four unequal-sized sub-bands.

3.4.4.1 Equal-Sized Sub-bands F-OFDM (LabVIEW)

In this part, the constructed four equal sub-band sizes are based on the same Simulink model specifications and assumptions in sub-section (3.3.4.1). On the transmitter side, the designed waveform generates different bit sequences per each sub-band using different seed values for the MT Generate Bits (Galois, PN Order) node. The resulted sequences are modulated using four different orders of QAM specified by the supported services. The OFDM signal per each sub-band is constructed and shifted to the desired location. Applying complex IFFT to maintain the orthogonality principle and the CP inserted to complete the OFDM signal. The designed filters with the property of shifting used in Simulink are reused in LabVIEW by creating an interface to MATLAB to call MATLAB filters functions inside LabVIEW and are performed on the sub-bands. In the last stage, the complete signals from the sub-bands are combined and transmitted via the AWGN channel.

At the receiver, the identical received filters with the same properties used in MATLAB were reused in LabVIEW. The filters are capable of isolating and reducing interference between the sub-bands. The rest of the receiving process is the same as in Simulink, including eliminating the samples that are the length of the filter, addressing distortion caused by the used filters, and power level modification. Additionally, removing the CP, complex FFT implementation, and finally demodulation to obtain the received data. Figure (3.47) represents the four sub-banding system of F-OFDM in LabVIEW NXG.

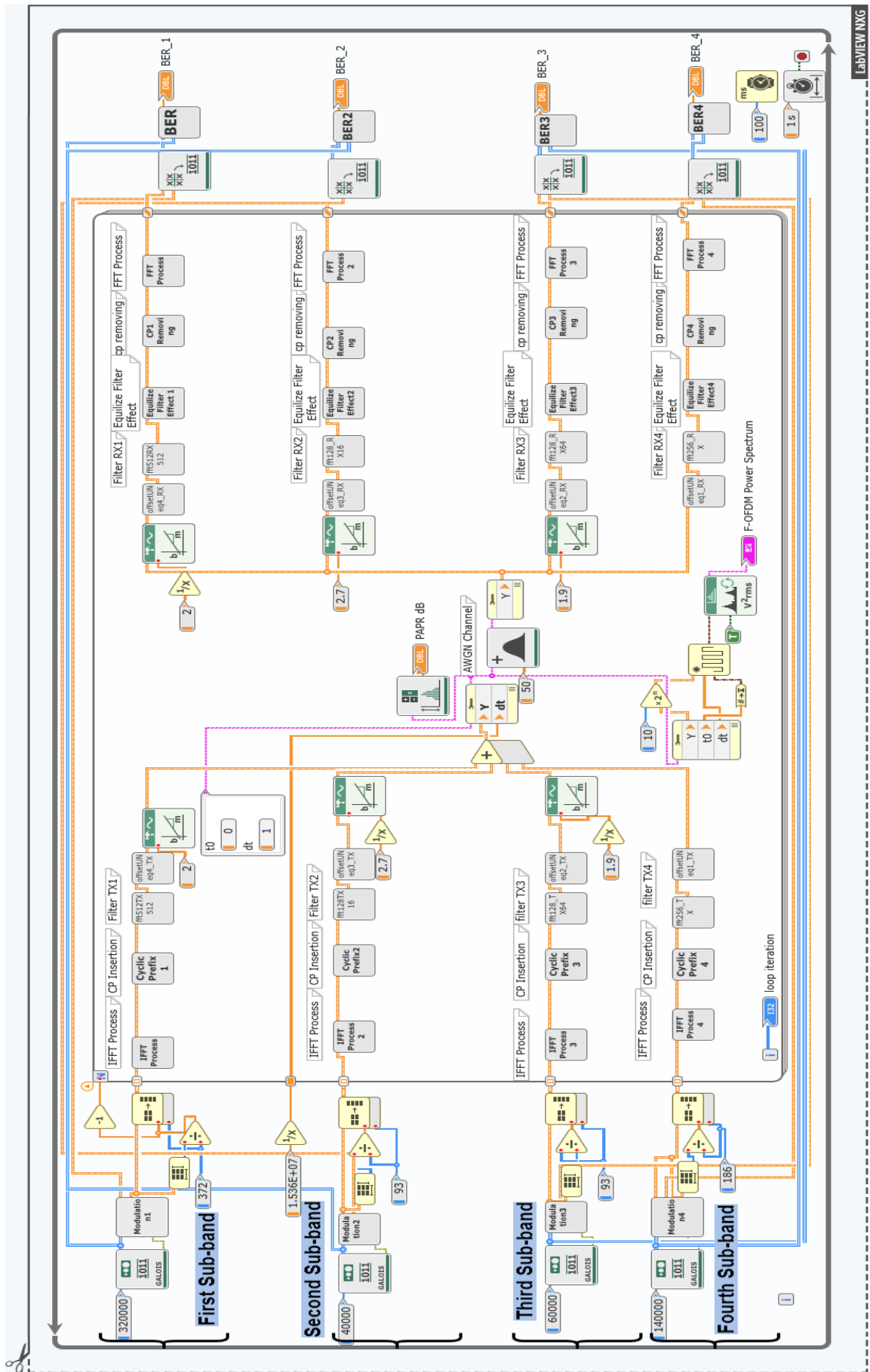


Figure (3.47) Sub-bands F-OFDM waveform in LabVIEW NXG.

3.4.4.2 Equal-Sized Sub-bands Results and Comparisons (LabVIEW)

This sub-section discusses the performance of four equal sub-band sizes based on the achieved OOB, average BER behavior, SE measurement, and PAPR compared to OFDM.

A. Achieved OOB

The main advantages of reducing OOB is the minimization the guard bands, interference reduction, and hence improving the SE. The same filters used in MATLAB-Simulink were reused in LabVIEW for the same reasons mentioned before. Figure (3.48) illustrates four equal sizes OFDM sub-bands power spectrum where the OOB was -30 dB compared to figures (3.49), (3.50), and (3.51), the OOB enhancement of the three utilized filters were -160 dB, -243 dB and -285 dB for Blackman window filter, proposed window 1 and 2 filters, respectively.

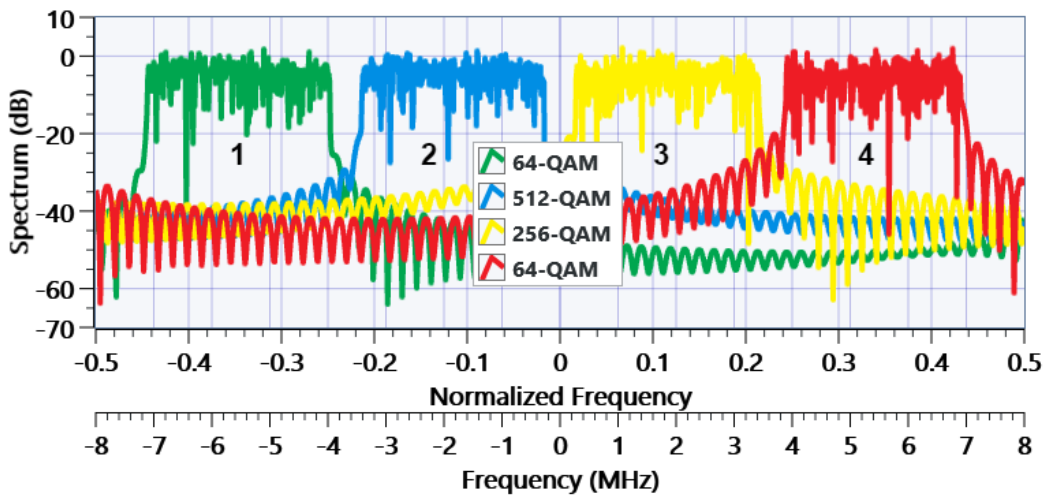


Figure (3.48) Power spectrum of equal-sized sub-bands OFDM (LabVIEW).

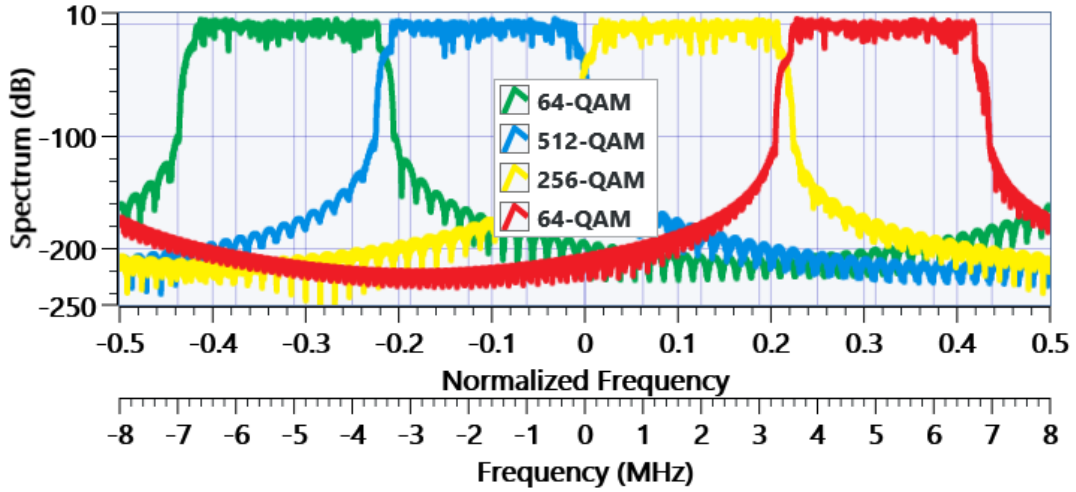


Figure (3.49) Power spectrum of equal-sized sub-bands F-OFDM using Blackman window filter (LabVIEW).

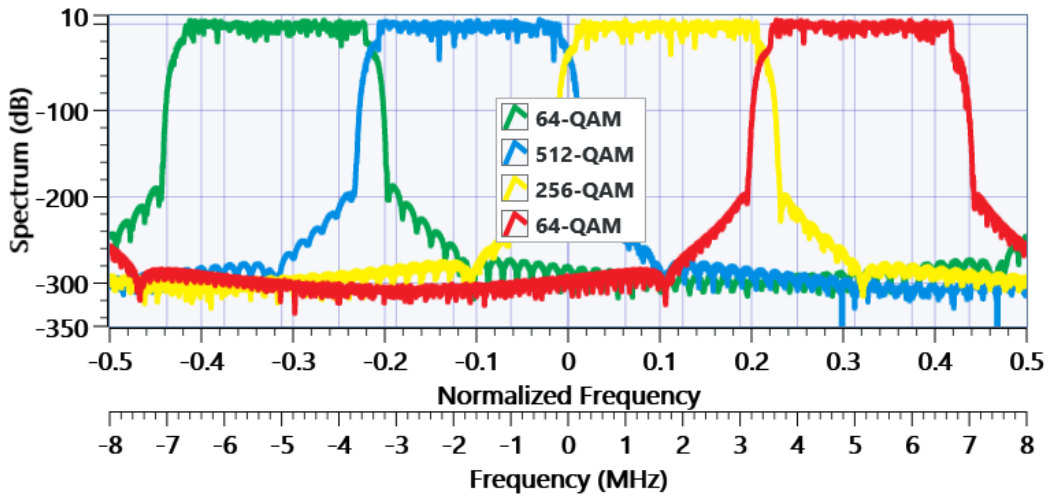


Figure (3.50) Power spectrum of equal-sized sub-bands F-OFDM using proposed window 1 filter (LabVIEW).

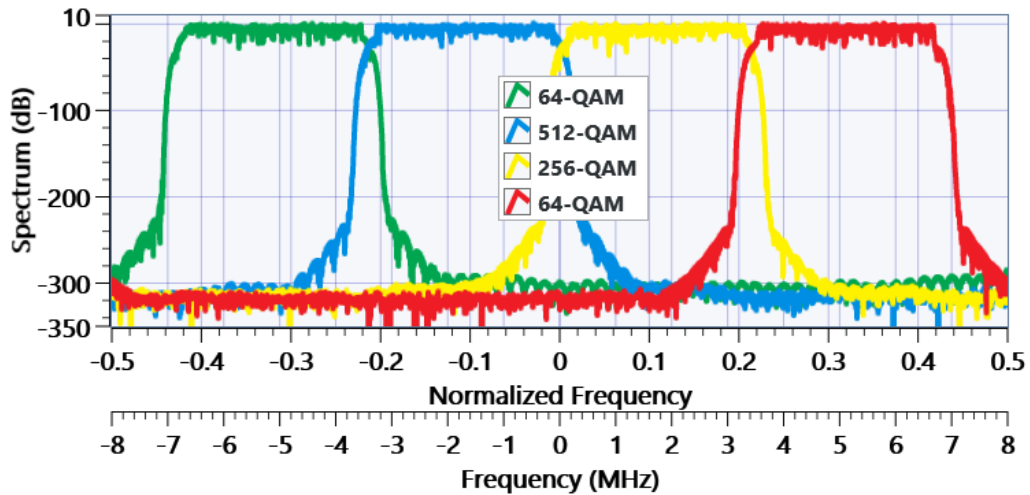


Figure (3.51) Power spectrum of equal-sized sub-bands F-OFDM using proposed window 2 filter (LabVIEW).

B. Average BER Performance

The average BER was evaluated for each of the three utilized filters of the equal sub-banding and compared to OFDM as shown in figure (3.52). The F-OFDM sub-bands have almost the same BER performance as OFDM at lower values of SNR, while different behaviors are obtained at higher values of SNR. The performance is degraded compared to OFDM, where at 35 dB, the OFDM BER is 1.7×10^{-6} , while at the Blackman, proposed window filter1 and 2 the BER are 1.36×10^{-4} , 2.4×10^{-5} and 7.06×10^{-5} , respectively. At 45 dB SNR, the BER for the Blackman filter is 1.2×10^{-5} , while the BER for the proposed window 1 and 2 filter are same and equal to 1.72×10^{-6} .

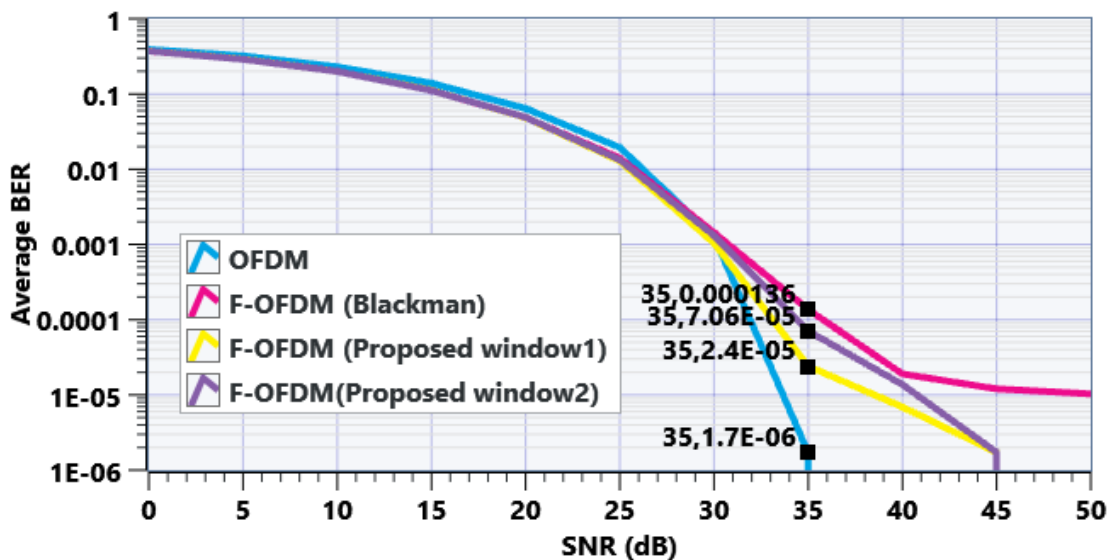


Figure (3.52) Average BER of equal-sized sub-bands (LabVIEW).

C. Spectrum Efficiency Enhancement

The normalized SE of the equal sized sub-bands was calculated in LabVIEW for the three filters and compared to OFDM. The three filters can obviously contribute to increasing the SE as compared to OFDM as shown in figure (3.53). The improvement of SE after optimizing the guard band obtained at lower values of SNR is about 3.9% for F-OFDM and 4% identical for proposed window 1 and 2 filters. At the higher values of SNR the

maximum enhancement is about 4.43%, 5.1% and 5.2% for Blackman, proposed window 1 filter, and proposed window 2 filter respectively.

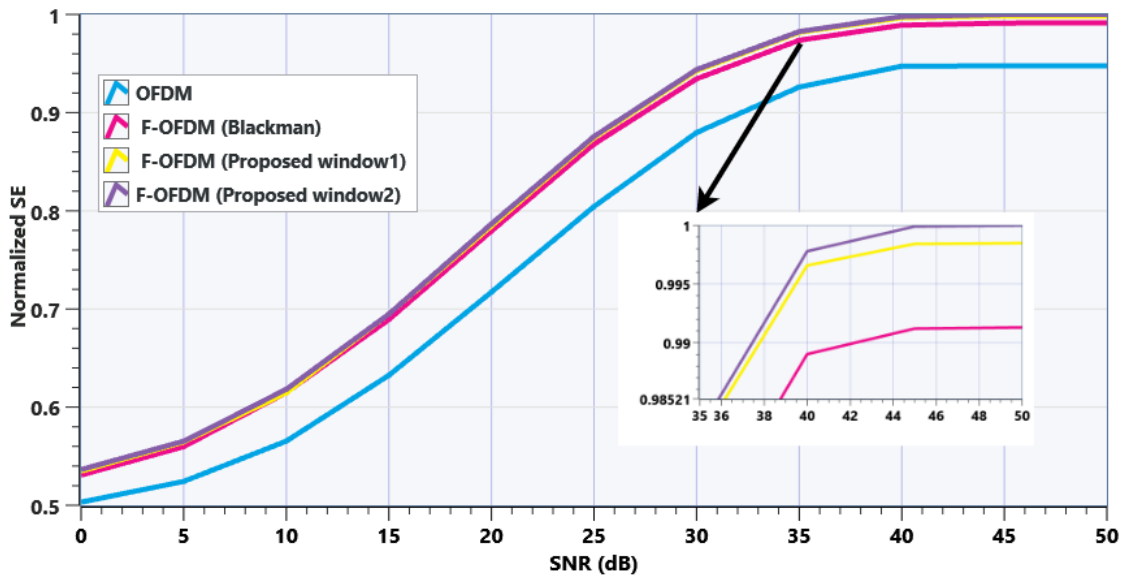


Figure (3.53) Normalized SE of equal-sized sub-bands F-OFDM compared to OFDM (LabVIEW).

D. Average PAPR Comparison

Figure (3.54) compares the average PAPR values for the three utilized filters with the average OFDM PAPR. It can be seen that the equal-sized F-OFDM sub-bands waveform has higher PAPR than OFDM, which may degrade the performance.

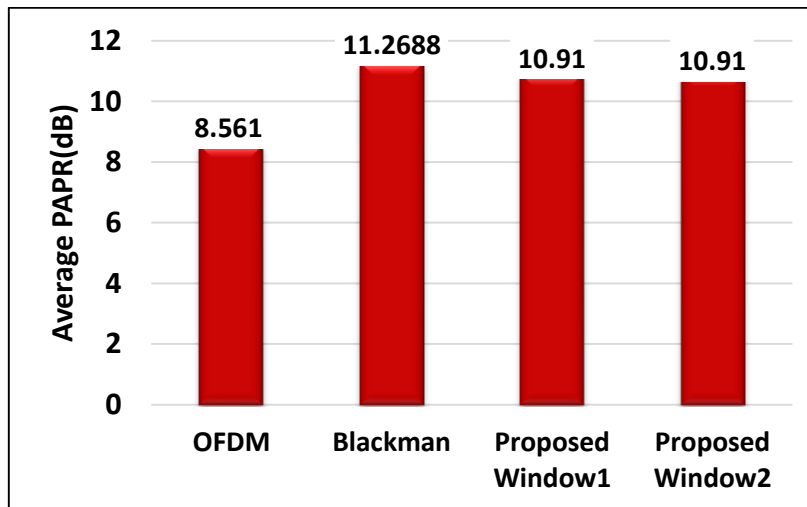


Figure (3.54) Average PAPR of equal-sized sub-bands F-OFDM (LabVIEW).

3.4.4.3 Unequal-Sized Sub-bands F-OFDM (LabVIEW)

The sub-bands with different sizes modeled in LabVIEW NXG with the same specifications and assumptions have been used in Simulink. The identical diagram of the equal splitting reused in the unequal splitting is shown in figure (3.47) with the exception of the amount of utilized data subcarriers given to each sub-band, the order of modulation per sub-band and optimal filter design specifications suitable for the sub-bands.

3.4.4.4 Unequal-Sized Sub-bands Results and Comparisons (LabVIEW)

This sub-section discusses the performance of four unequal sub-band sizes based on the achieved OOB, average BER behavior, SE measurement, and PAPR compared to OFDM.

A. Achieved OOB

Figure (3.55) illustrates four OFDM sub-bands power spectrum in unequal sizes with an OOB of -30 dB compared to figures (3.56), (3.57), and (3.58). The F-OFDM waveform reaches -174dB, -230dB and -300 dB OOB at the Blackman window filter, proposed window 1 and 2 filters, respectively. The minimum guard band exists between the two sub-bands that support 16 and 64 QAM orders, while the guard is enlarged to avoid interference at the other sub-bands.

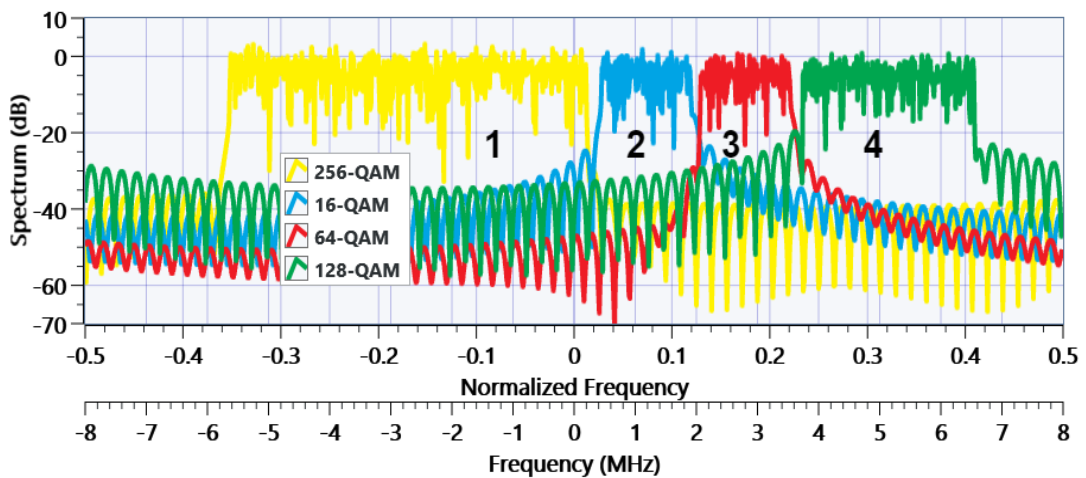


Figure (3.55) Power spectrum of unequal-sized sub-bands OFDM (LabVIEW).

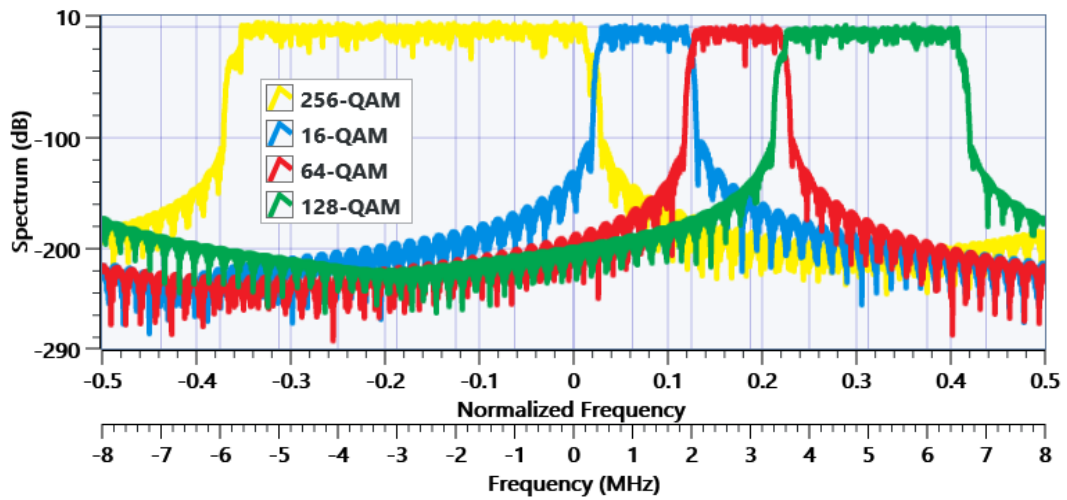


Figure (3.56) Power spectrum of unequal-sized sub-bands F-OFDM using Blackman window filter (LabVIEW).

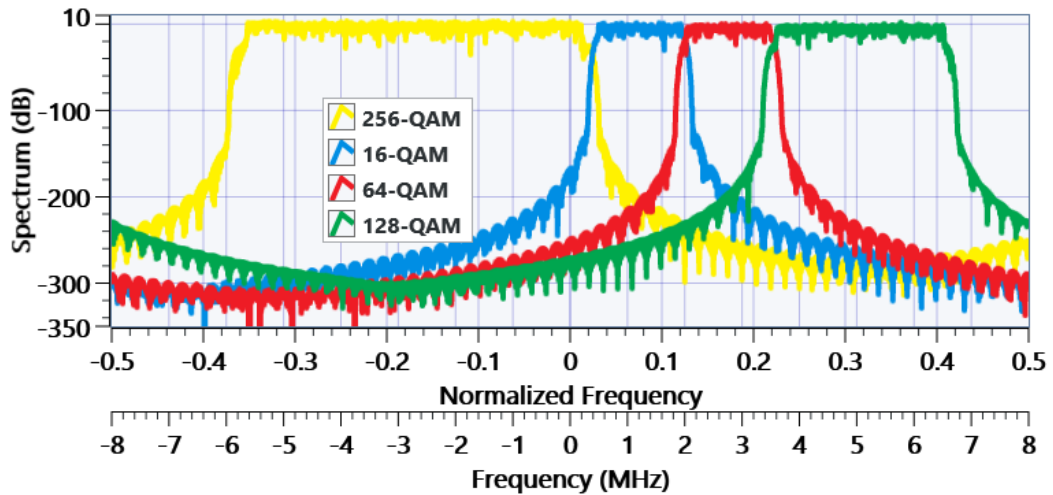


Figure (3.57) Power spectrum of unequal-sized sub-bands F-OFDM using proposed window 1 filter (LabVIEW).

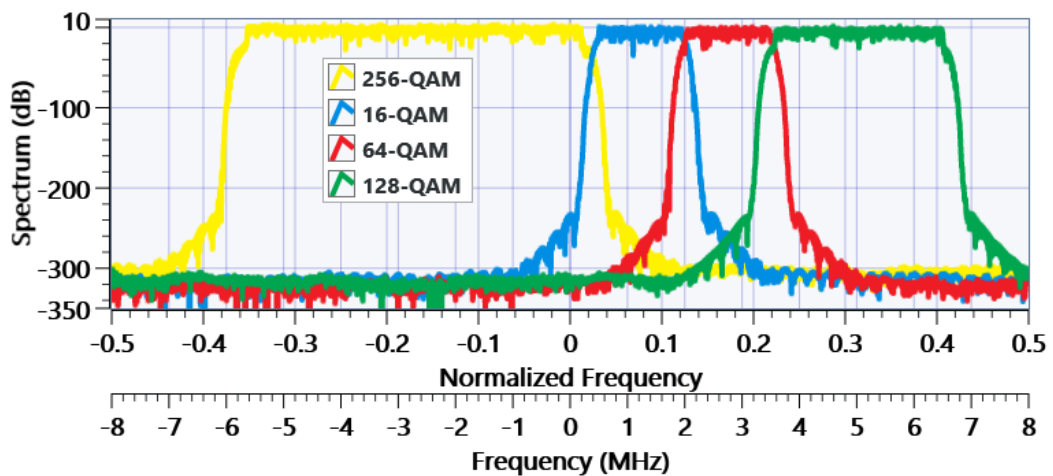


Figure (3.58) Power spectrum of unequal-sized sub-bands F-OFDM using proposed window 2 filter (LabVIEW).

B. Average BER Performance

The average BER curves of unequal sub-banding F-OFDM are shown in figure (3.59). It is obvious at lower values of SNR the BERs behave similarly to that in OFDM, while at higher SNR values the performance differs and gets worse. At 40 dB of SNR, the BER of OFDM, Blackman, proposed window 1 and 2 filters are 1.78×10^{-6} , 2.7×10^{-6} , 7.142×10^{-6} , and 2.142×10^{-5} , respectively, while at 45 dB the BER of proposed window 1 and 2 are 7.142×10^{-6} and 1.7×10^{-5} respectively.

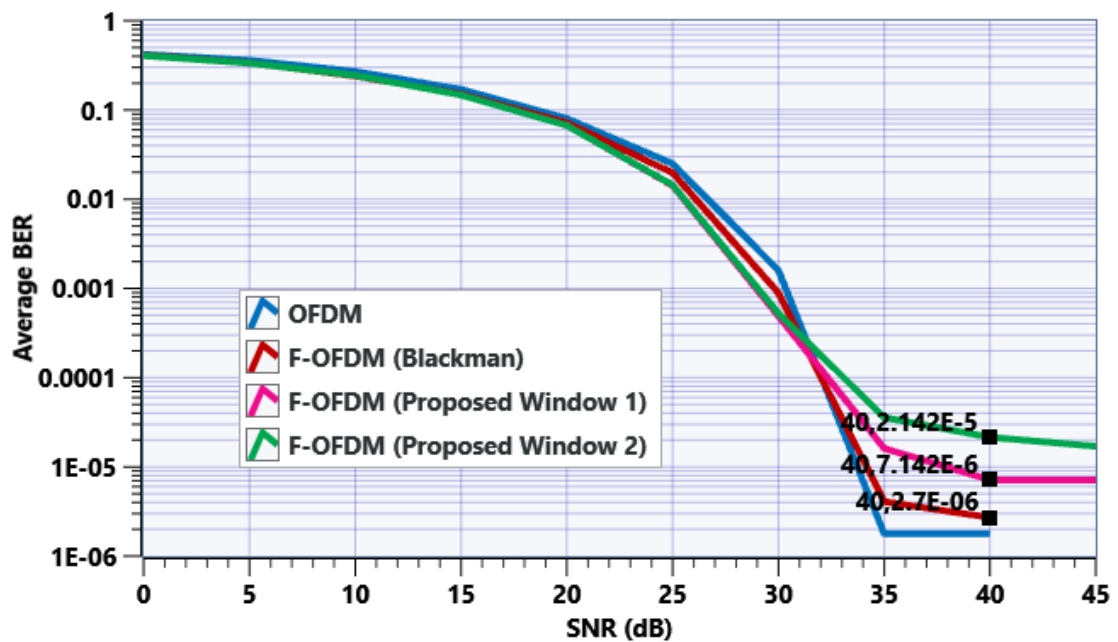


Figure (3.59) Average BER of unequal-sized sub-bands sizes (LabVIEW).

C. Spectrum Efficiency Enhancement

The normalized SE of the unequal sized sub-bands was calculated for the three filters and compared to OFDM. The attained SE over OFDM using the three utilized filters is illustrated in figure (3.60). At lower values of SNR, the SE achieved 4.6%, 4.7, and 5% enhancement for Blackman, proposed window 1 and proposed window 2 filters respectively. At higher SNR values, the enhancement is around 5.3%, 5.6%, and 5.8% for Blackman, proposed window 1 and proposed window 2 filters respectively.

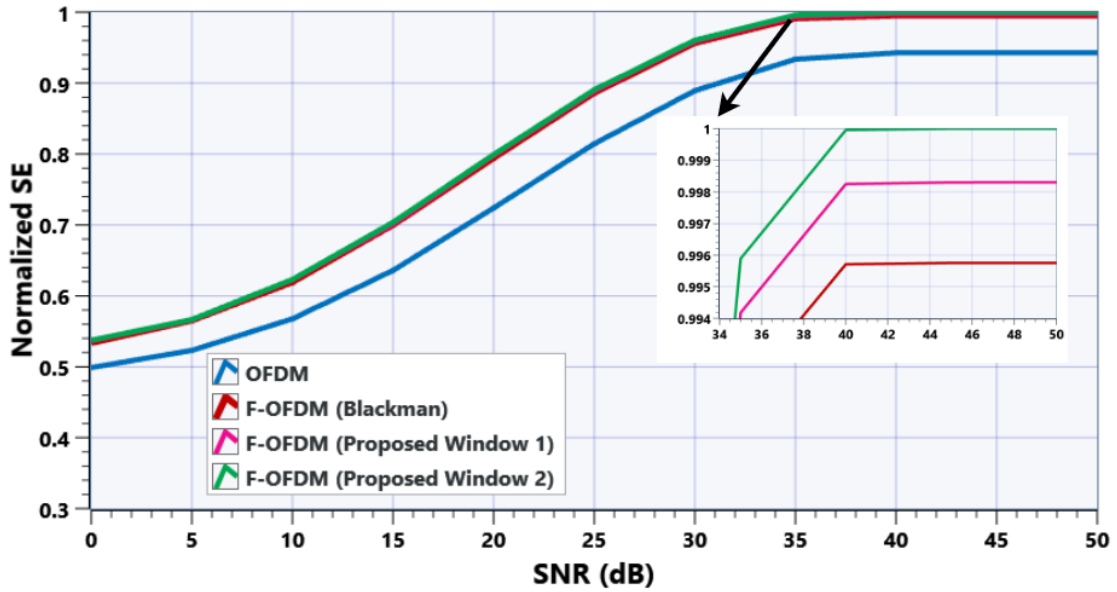


Figure (3.60) Normalized SE of unequal-sized sub-bands F-OFDM compared to OFDM (LabVIEW).

D. Average PAPR Comparison

Figure (3.61) compared the performance of the proposed waveform to that of OFDM in terms of average PAPR. It can be seen that the proposed unequal sub-bands sized waveform with the designed three filters has higher PAPR values than OFDM, which may limit the system performance.

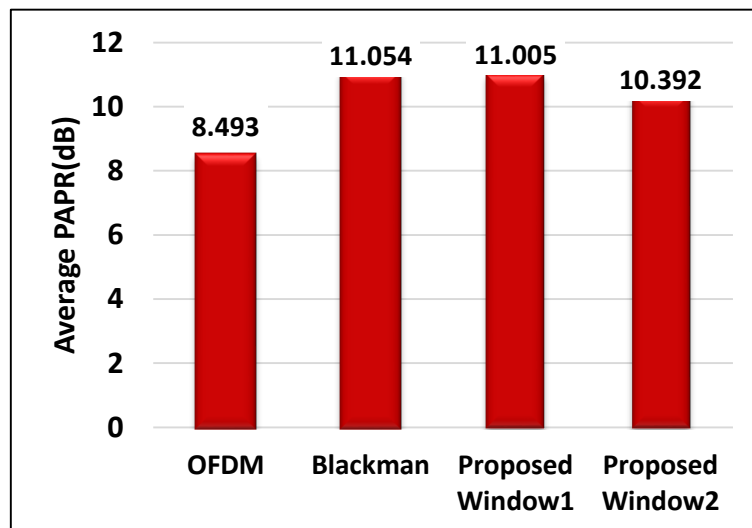


Figure (3.61) Average PAPR of unequal-sized sub-bands F-OFDM (LabVIEW).

3.5 Results Discussion and Comparisons

This section discusses the simulation results obtained and their comparisons with other works as below:

A. Regarding to the Sidelobes Levels (OOBE)

In comparison between the two approaches (Matlab and LabVIEW), each of the utilized Window-Sinc filters achieved approximated equal reduction in sidelobes level compared to traditional OFDM as shown in figures (3.16), and (3.41).

Figure (3.62) illustrates the OOBE comparison among UFMC, conventional OFDM, and F-OFDM. For the UFMC waveforms, following parameters were adopted: Chebyshev filter with a sidelobe level equal to -100 dB, and ZP instead of CP. It is obvious that F-OFDM exhibits lower sidelobes levels than the others.

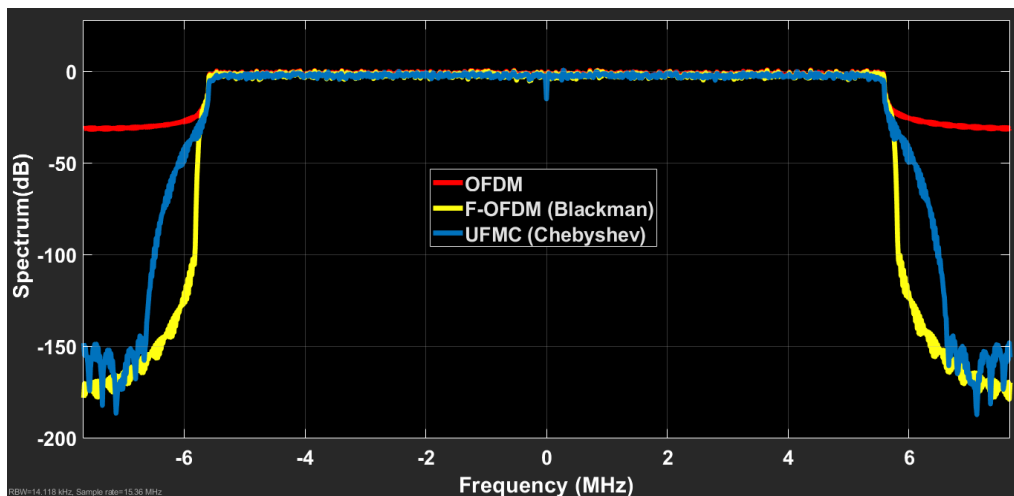


Figure (3.62) The power spectrum comparison among OFDM, F-OFDM and UFMC waveforms.

B. Regarding to the BER (Single Band)

The BER performance in the two approaches indicates that the F-OFDM has the same OFDM behavior at lower values of SNR and the worst case at higher values of SNR, as shown in figures (3.17), (3.18), (3.19), (3.20), (3.21), (3.42), (3.43), (3.44), (3.45), and (3.46). Furthermore, higher QAM orders for both OFDM and F-OFDM need higher SNR for better BER performance.

C. Regarding to the BER (Multiband)

In the two scenarios of sub-bands, the average F-OFDM BER performance indicates that at lower values of SNR (20 dB and below), the curves approximately have the same attitude to OFDM. At higher values of SNR (25 dB and above) the BER curves degrade for the two approaches as shown in figures (3.27), (3.34), (3.52) and (3.59). The reason for the difference is that when the filter passband is close to the sub-band size, this will destroy the edge subcarriers and increase the BER. For the purpose of comparison between the results of the two approaches, figure (3.63) illustrates the average BER curves for the two scenarios of sub-banding, OFDM and F-OFDM. As can be seen, the two approaches have roughly comparable performance.

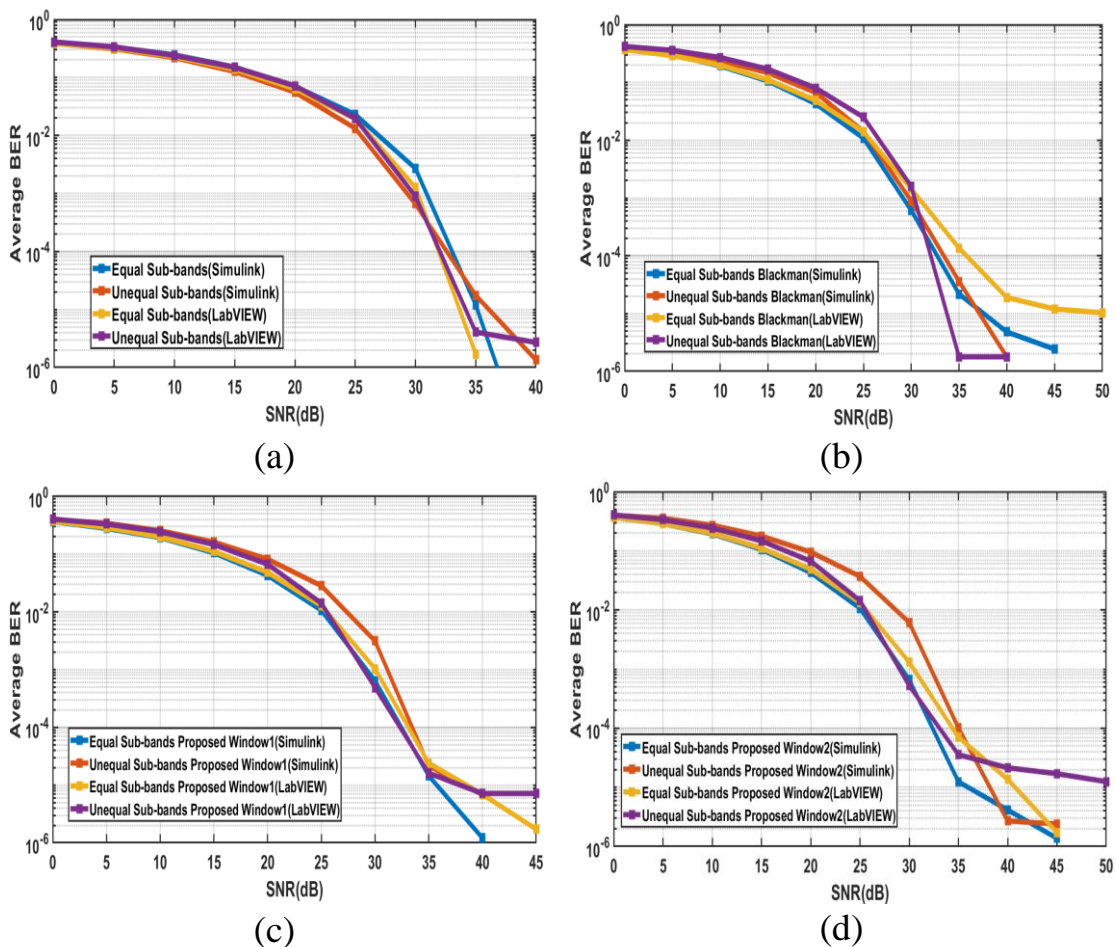


Figure (3.63) Average BER comparison for: (a) OFDM, (b) F-OFDM (Blackman), (c) F-OFDM (Proposed Window1), (d) F-OFDM (Proposed Window2).

D. Regarding to the Spectrum Efficiency

The accomplished SE enhancement in the two scenarios of sub-bands is almost the same in the two approaches as shown in figures (3.28), (3.35), (3.53) and (3.60). It should be noted that unequal sub-banding accomplishes higher SE compared with equal sub-banding. Table (3.1) compares the maximum SE obtained using the two approaches.

Table (3.1) SE enhancements for F-OFDM using a variety of used window functions

| Waveform Model | SE Enhancement Using Blackman Window | | SE Enhancement Using Proposed Window 1 | | SE Enhancement Using Proposed Window 2 | |
|-----------------|--------------------------------------|---------|--|---------|--|---------|
| | Simulink | LabVIEW | Simulink | LabVIEW | Simulink | LabVIEW |
| First scenario | 4.9% | 4.43% | 5.1% | 5.1% | 5.2% | 5.2% |
| Second scenario | 5.25% | 5.3% | 5.3% | 5.6% | 5.7% | 5.8% |

The minimum guard band between the sub-bands obtained for the two approaches is illustrated in Tables (3.2) and (3.3) for equal-sized and unequal-sized sub-bands, respectively.

For the sake of discussion, it should be noted that the guard band size between the equal-sized sub-bands are somewhat equal, with a slight difference due to the order of modulation for each sub-band. Concerning the unequal sub-bands, there is a slight difference in the guard band size due to the size of each sub-band and the order of QAM, (large sub-band requires a slightly larger guard band than the smaller sub-band).

Table (3.2) Minimum guard band between the equal-sized sub-bands

| Waveform | Minimum Guard Band Between Sub-band 1 and 2 (KHz) | Minimum Guard Band Between Sub-band 2 and 3 (KHz) | Minimum Guard Band Between Sub-band 3 and 4 (KHz) |
|---|---|---|---|
| Initial present guard band for OFDM and FOFDM | 825 | 825 | 825 |
| OFDM | 525 | 525 | 525 |
| F-OFDM (Blackman) | 225 | 345 | 225 |
| F-OFDM (Proposed window 1) | 235 | 305 | 235 |
| F-OFDM (Proposed window 2) | 260 | 275 | 230 |

Table (3.3) Minimum guard band between the unequal-sized sub-bands

| Waveform | Minimum Guard Band Between Sub-band 1 and 2 (KHz) | Minimum Guard Band Between Sub-band 2 and 3 (KHz) | Minimum Guard Band Between Sub-band 3 and 4 (KHz) |
|---|---|---|---|
| Initial present guard band for OFDM and FOFDM | 1305 | 510 | 765 |
| OFDM | 658 | 144 | 458 |
| F-OFDM (Blackman) | 140 | 90 | 170 |
| F-OFDM (Proposed window 1) | 120 | 84 | 150 |
| F-OFDM (Proposed window 2) | 110 | 80 | 120 |

E. Regarding to the PAPR

The PAPR of the F-OFDM was measured for the two scenarios and in both approaches (Matlab and LabVIEW). The average PAPR of the F-OFDM sub-bands signal is higher than that of OFDM by approximately 2.86 dB and 2.7 dB for equal-sized sub-bands in the first and second approaches, respectively, as shown in figures (3.29) and (3.54). For unequal-sized sub-bands, the difference is approximately equal to 2.5 dB and 2.561 dB for the first and second approaches, respectively, as shown in figures (3.36) and (3.61). This gap is resulting from convolving the OFDM signal with the filter yielding more samples than the original OFDM signal. Consequently, the power will be distributed over more samples, which results in decreasing the mean value. This in return will increase the PAPR value of the resulting F-OFDM signal.

F. Regarding to Other Relevant Works

Table (3.4) illustrate the performance comparison between the proposed waveform and some of relevant works in terms of filter type, number of sub-bands, achieved BER, SE enhancement, and the used filter type.

Table (3.4) Comparison the performance of the proposed waveform to some relevant works.

| Waveform Reference | Applied Filter | Number of Sub-bands or RBs Filtered | BER (Compared to that of OFDM) | SE Enhancement (Compared to that of OFDM) | Used Filter Type |
|------------------------|----------------|-------------------------------------|--|---|---------------------------------------|
| [6] | Per RB | 25 | Worse when there is no ACI and better when ACI present | Same | Equal ripple |
| [7] | Per user | 3 | Worse | Not specified | Soft Truncation |
| [8] | Per sub-band | 3 | Same | Not specified | Soft - Truncated Sinc and Equi-ripple |
| [9] | Per sub-band | 1 | Same | Not specified | Window-Sinc |
| [5] | Per sub-band | 3 | Not specified | 7.47% higher | Window-Sinc |
| [11] | Per sub-band | 2 | Same | Same | Phydyas |
| [13] | Per sub-band | 2 | Same | Not specified | Window-Sinc |
| [15] | Per user | 2 | Better | Higher (percentage not specified) | Window-Sinc |
| [17] | Per sub-band | 1 | Not specified | Not specified | Interpolated Band-Pass Method |
| [18] | Per sub-band | 2 | Better | Not specified | Window-Sinc |
| [19] | Per sub-band | 1 | Same | Not specified | Window-Sinc |
| Proposed thesis models | Per sub-band | 4 | Worse | (5.2% in the first scenario and 5.8% in the second scenario) higher | Window-Sinc |

CHAPTER FOUR

F-OFDM IMPLEMENTATION BASED SOFTWARE DEFINED RADIO

4.1 Introduction

Most radio systems were previously designed to receive, process specific signals, and generally perform a single function, as well as operate in a known and stable environment. For example, the first generation of cellular phone systems relied on the transmission of sound in an analogous way. With the rapid development of the second and subsequent generations, mobile devices became more flexible and supported multiple carrier frequencies. As a result, the importance of communication systems that support more than one frequency band has become clear. Flexible testbeds with a wide range of reconfigurable parameters are required for the analysis and evaluation of information theoretic concept for wireless resource management in real environments. One of the most important technologies that offers this feature is the SDR.

This chapter explains the fundamentals of SDR and one of the USRP hardware products of SDR platforms. In addition, practical implementation of the proposed waveform is performed using USRP with the help of the LabVIEW NXG simulator.

4.2 Software Defined Radio Fundamentals

The SDR is a revolutionary wireless communication system that enables the system to be completely reprogrammed and reconfigured via software modules, with the exception of the RF stage. The SDR was defined as, “*a radio in which some or all of the physical layer functions are software-defined*” [54]. The first visualization of SDR was proposed by Joseph Mitola in the 1990s [55]. Mitola described the concept of an ideal SDR whose

physical components are the receive antenna and the ADC for the receiver, while the DAC and the transmit antenna for the transmitter.

SDR platforms can transmit and receive while the physical components (Filters, Amplifiers, Modulators, Coders, Detectors, and others) are implemented in software, unlike what is in traditional radio, which implements most of these functions in hardware, and for limited functionality. Based on the type of utilized signal processing, SDRs can be split into two groups: a general-purpose processor (in a computer, for example), whereas an on-board embedded processor is the second [56]. Ettus ResearchTM, which is a National Instruments (NI) joint company since 2010 developed the USRP as a follow-up to the first SDRs category [57].

For the first time in the real world, USRP assists in the design, development, and prototyping of the next generation of wireless system technologies in a high-quality and timely manner. In general, the USRP has two partitions: a fixed motherboard and a plug-in daughterboard. An ADC and DAC are included on the motherboard. In addition, a Field Programmable Gate Array (FPGA) for Digital Down Conversion (DDC) with a programmable decimation rate, and a host Personal Computer (PC) interface have been included. The daughterboard is in charge of basic RF frontend functionality. SDRs are well-suited for a variety of applications due to their wide bandwidths and adaptable RF front ends [56].

The USRP platforms are designed for RF applications including spectrum monitoring, cognitive radio, mobile phones, satellite navigation, and intelligent radios. Users can use the USRP products in commercial, academic, and military applications with flexible and reusable field deployments.

All USRP-SDR products are supported by the USRP Hardware DriverTM (UHD) software Application Programming Interface (API) that runs on the General Purpose Processor (GPP). UHD offers the essential

control for transporting user waveform samples to and from USRP hardware. The code for the UHD GPP driver and firmware is written in C/C++, while the FPGA code is written in Verilog. A C/C++ API is available for interacting with different software frameworks, including GNU Radio, LabVIEW, Matlab/Simulink, and RFNoC. UHD is available for Linux, Windows, and Mac [58].

Generally, the block diagram of the SDR transmitter depicted in figure (4.1), the major parts are detailed as follows [59]:

1. The Digital Signal Processing (DSP) block process the baseband signal contains coding, modulation, and others.
2. The Digital Up Converter (DUC) which consists of: (1) Interpolation filter, (2) Digital Mixer, and (3) Digital Local Oscillator, transfers the baseband signal processed by DSP to the IF stage.
3. The DAC transforms the samples into the analog form.
4. The RF Converter transforms the signals to the higher propagation frequencies.
5. The antenna transmits the signals after amplification to the communication channel as electromagnetic waves.

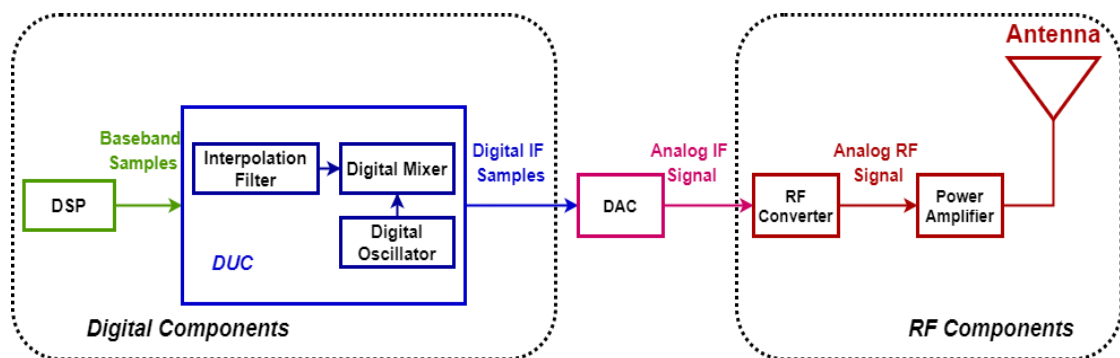


Figure (4.1) SDR transmitter block diagram.

Receiving schemes are also part of SDR technology. In the receiver block diagram depicted in figure (4.2), the construction of the receiver is as follows [59]:

1. The antenna and its function is to receive the electromagnetic waves propagating over a wireless communication channel.
2. The RF Tuner transforms the analog RF signals to the IF stage.
3. The ADC changes the signals domain, providing digital samples at its output.
4. A DDC is typically a monolithic chip that serves as a primary component of the SDR. It is made up of three main parts in digital form: (1) Digital Mixer, (2) Digital Local Oscillator, and (3) FIR Low Pass Filter.
5. The DSP block is where tasks like demodulating and decoding are carried out.

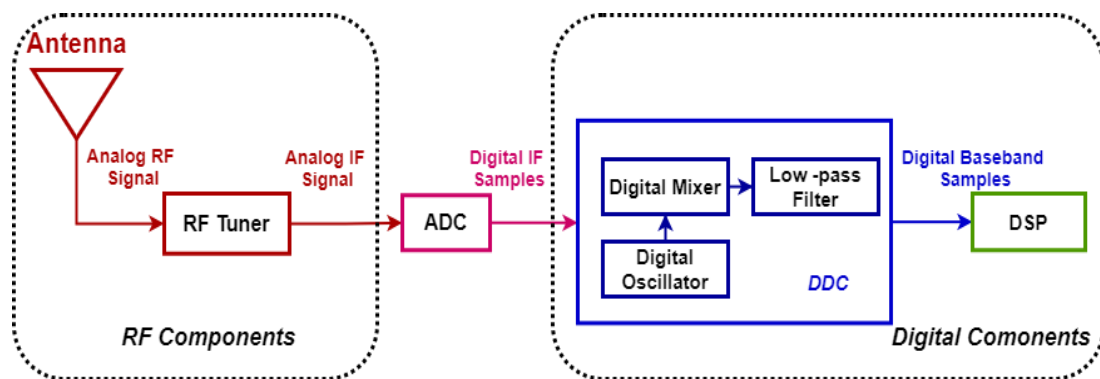


Figure (4.2) SDR receiver block diagram.

4.2.1 SDR Advantages

Like all new technologies that need time to emerge from research centers and development to practical reality, SDR is considered a new technology in the world of communications. Therefore, the following is a set of the features:

1. SDR compatibility: SDR is capable of working with different signals, and it is considered a link between technologies that use different signals.
2. Effective use of resources: The SDR can adapt the waveform that is used to obtain the best performance.

3. Reuse of the available frequencies: SDR can use the unutilized spectrum where the flexibility of these systems can be used for technologies like cognitive radio to increase SE.
4. Coexistence: SDR allows promotion of the current communication systems to support a modern communication standard. This feature is important for radios designed to last for a long time. This reduces in one way or another the cost of maintenance and training for these devices.
5. Ease of use in research and development: It is possible to use an SDR to perform different waveforms to analyze the performance in real time, which allows the implementation of many studies that would otherwise be only by simulation [60].

4.2.2 SDR Disadvantages

Since each technology has some defects and challenges, which limit its use. So the followings are some of the summarized challenges:

1. The cost: Since radio is designed to perform more than one function, its cost is greater than that which is designed to serve a single purpose.
2. High power consumption: Two reasons lead to increased power consumption in the devices that use the technology of SDR. The first is the complexity of the DSP unit, and the second is the utilization of wideband spectrum for these systems.
3. The complications: Complications due to the specifications and requirements, the SDR design to support specific waveforms, and waveforms that are expected to appear in the future [60].

4.3 Ettus Research™ USRP-X310

USRP-X310 is the third generation of the USRP devices that offer a high-performance, expandable SDR platforms for modelling and prototyping the next generation of wireless communication systems. The device combines multiple RF daughterboard slots with the high-bandwidth

that cover DC-6 GHz range of frequencies and the baseband bandwidth of 160 MHz supplied with the ultra-high-speed interfaces PCIe and dual 10/1 Gigabit Ethernet (GigE). The device has the largest customizable kintex-7 FPGA. USRP-X310 can be used for advanced wireless system prototyping in Wi-Fi, cellular applications, multiple antennas (MIMO) testbeds, passive Radar, and some intelligence signals [58]. Figure (4.3) is the photograph of USRP-X310 and a detailed view of the front and back panels. The internal components of the USRP X310 are shown in figure (4.4).

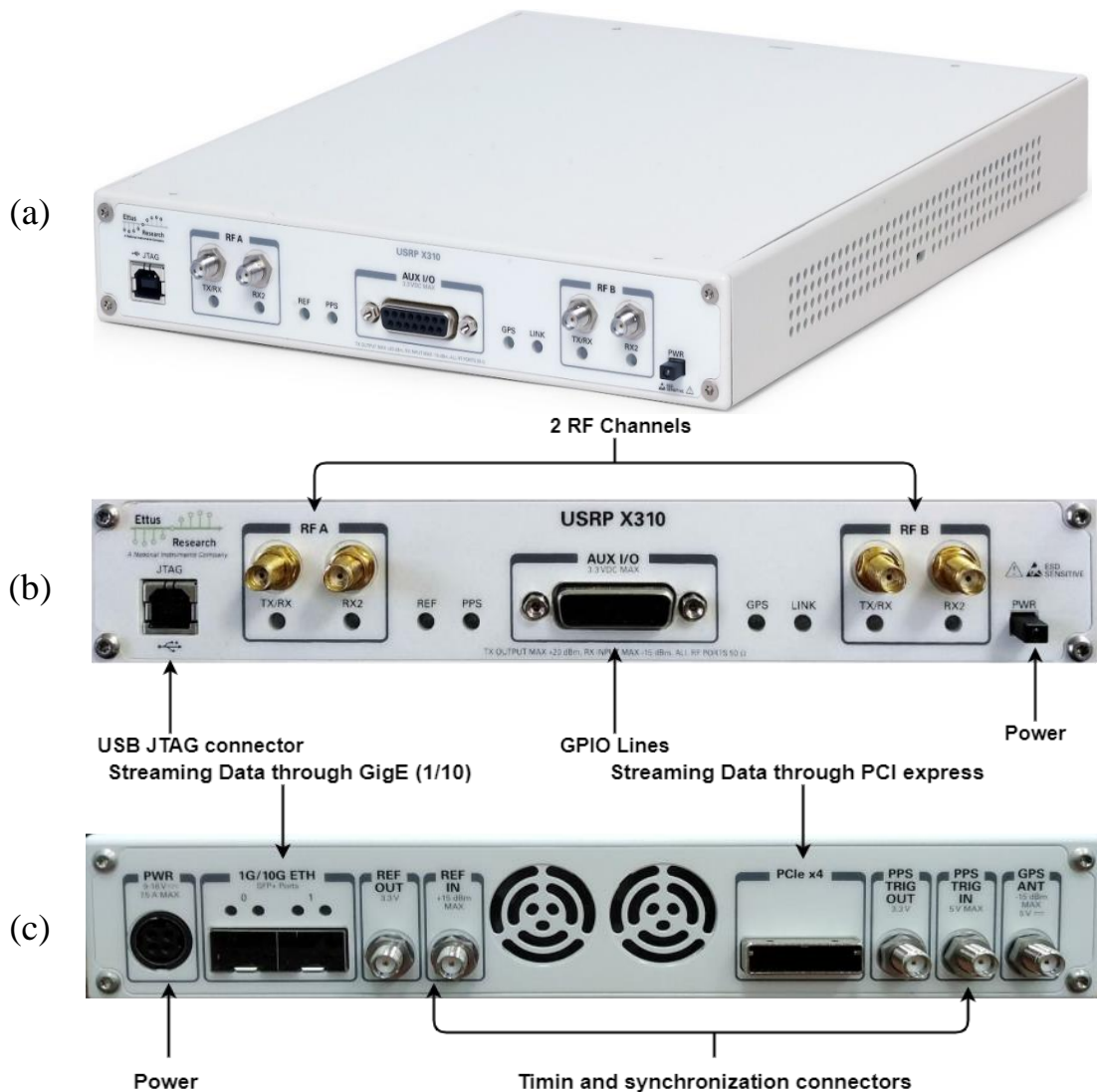


Figure (4.3) USRP-X310: (a) photograph (b) Front panel (c) Back panel.

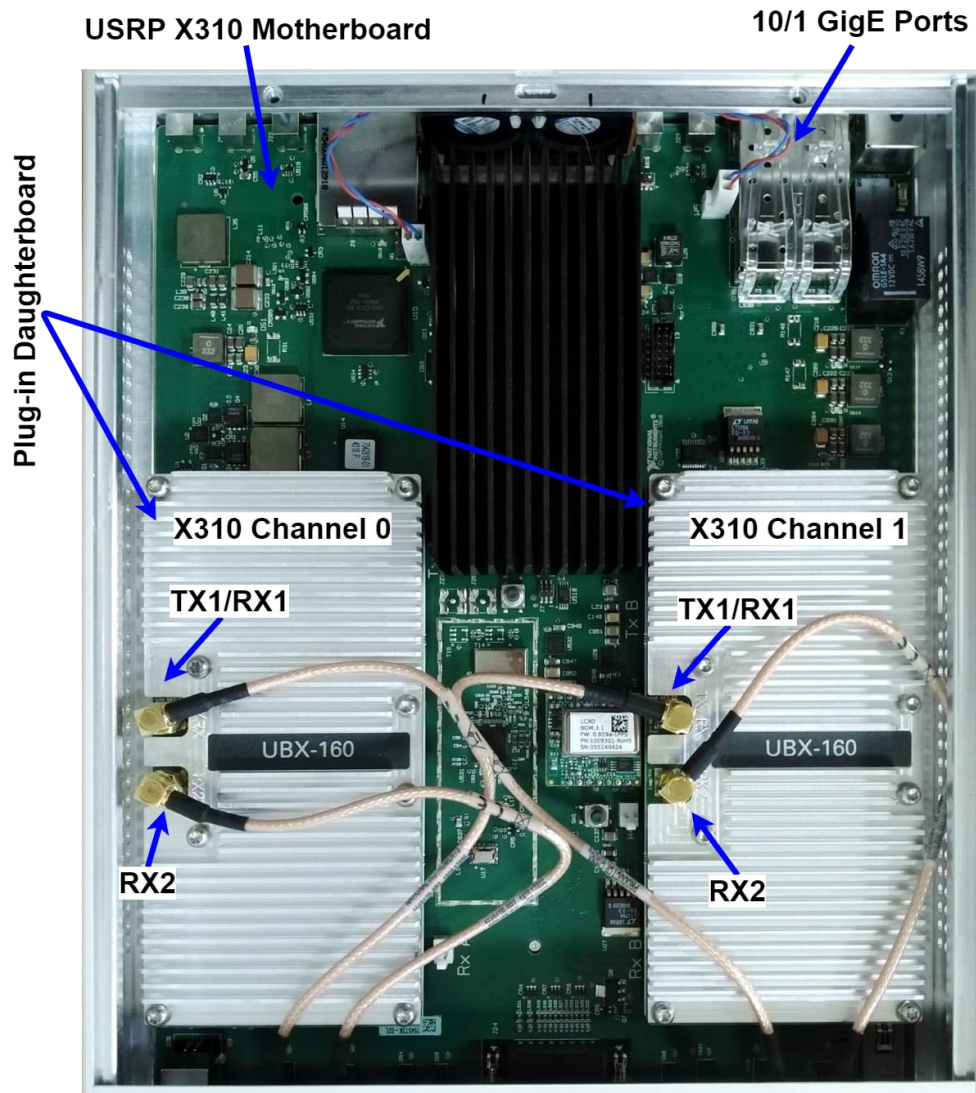


Figure (4.4) USRP X310 components.

4.3.1 USRP X310 Specifications

1. Large, customizable Xilinx Kintex-7 XC7K410T FPGA.
2. 2x2 transceiver channels or 4 receiver channels.
3. ADC with 14 bits resolution, 200 MS/s max sample rate.
4. DAC with 16 bits resolution, 800 MS/s max sample rate.
5. The selection frequencies covers 10 MHz to 6 GHz with a suitable daughterboard.
6. Two wideband RF daughterboard slots.
7. Daughterboard (UBX-160 MHz baseband bandwidth).
8. Optional GPS-disciplined oscillator option.
9. Configurable sample clock [58].

4.3.2 USRP Signal Workflow

USRP techniques are used to implement the radio functions by running the software modules on a hardware platform. Ettus Research™ USRP with LabVIEW NXG software, is used to perform the physical layer functions with high flexibility and scalability. In a network connection, the USRP connects to the host PC through an Ethernet cable as shown in figure (4.5).

On the transmitting side, the baseband In-phase and Quadrature components (IQ) signal samples from the host PC are fed to the USRP through the 1GigE port. The USRP hardware uses a DUC to interpolate the input signal to 800 MS/s before converting it to analog with a dual-channel 16 bit DAC. After that, the analog signal is mixed to the desired carrier frequency.

On the receiving side, the incoming receive signals are attached to the standard SubMiniature version A (SMA) connector and mixed down to baseband IQ, which is sampled at 200 MS/s, 14 bit ADC. The digitized IQ signal takes parallel pathways through DDC to process the 200 MS/s signal to user signal rate conversion. The down-converted samples either delivered to the host computer through the 1GigE connection directly or via DSP subsystem [58].

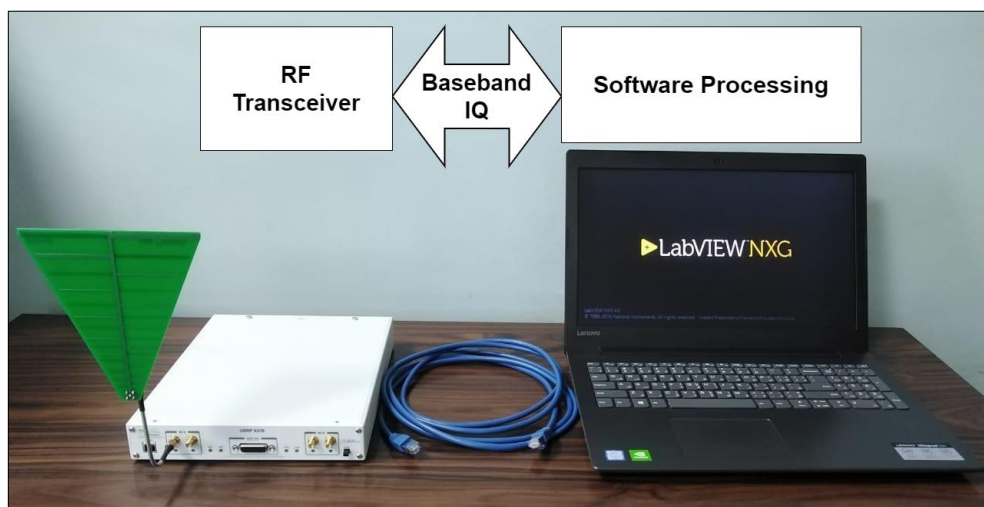


Figure (4.5) USRP network connection.

4.3.3 USRP Configuration in LabVIEW NXG

To enable the LabVIEW NXG software for interacting with USRP hardware, USRP nodes are configured for the transmitter and receiver in a Virtual Instrument (VI) function.

A. USRP Transmitter VI

The diagram of the transmitter VI function file (shown in figure (4.6-a)) has the following USRP components:

- NI USRP Open TX Session: It establishes a transmit session with the device, and returns the session handle as output. The device name is added to the input as the IP address of the device.
- NI USRP Configure Signal: Configures signal parameters of TX or RX, including IQ rate, the carrier frequency of the RF signal, TX gain applied, and Active antenna that specifies the port of the channel used.
- NI USRP Write TX Data: Writes four types of data specified in the input.
- NI Close Session: Closes the device session handle.

B. USRP Receiver VI

The diagram of the receiver VI (shown in figure (4.6-a)) has the following USRP components:

- NI Open RX Session: It establishes a receiver session with the device, and returns the session handle as output. The device name is added to the input as the IP address of the device.
- NI USRP Initiate: Starts the acquisition of the waveform in the RX session.
- NI USRP Fetch RX Data: Fetch data specified on the channel.
- NI USRP Abort: Stops a previously started acquisition [54].

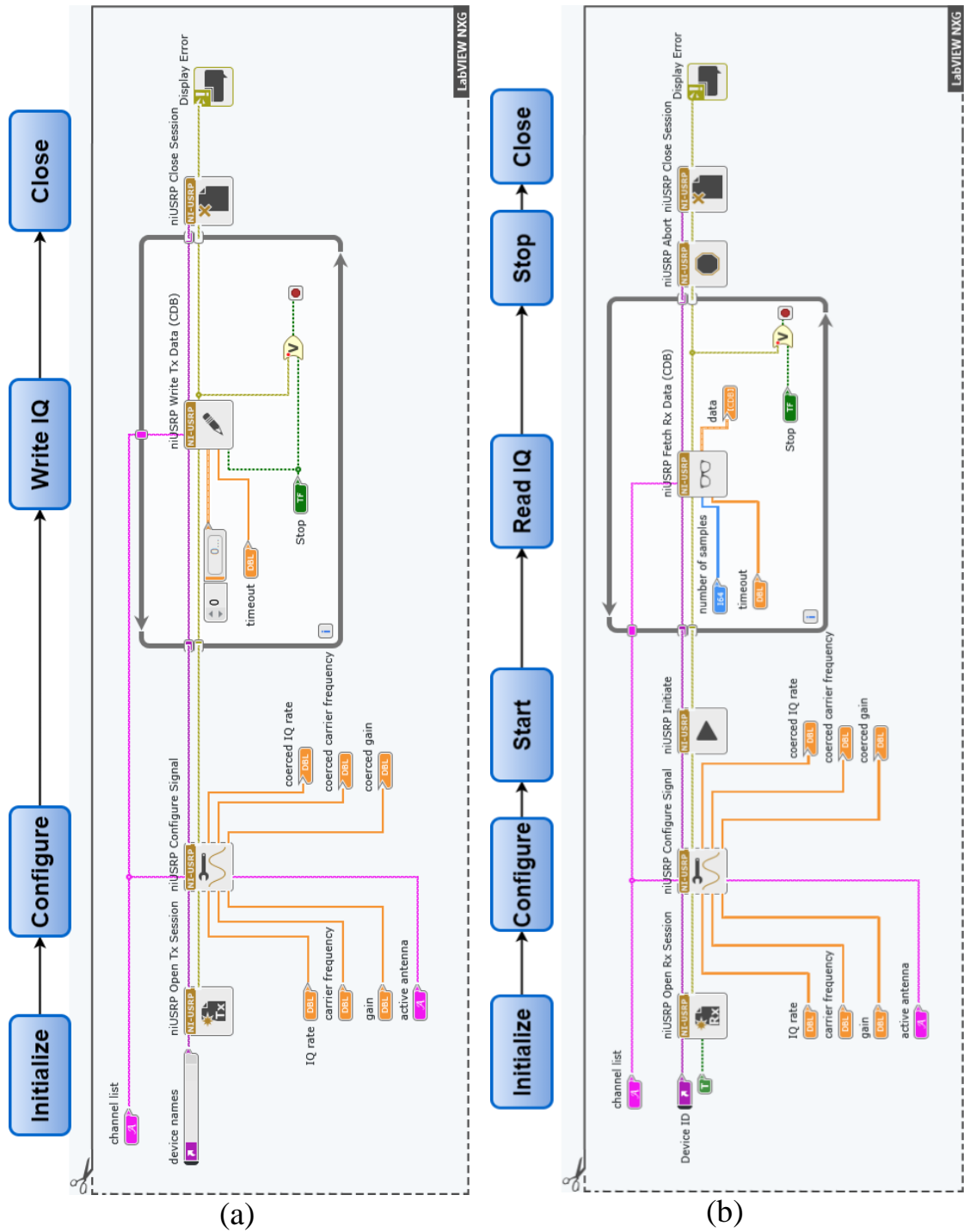


Figure (4.6) USRP nodes configuration in LabVIEW NXG: (a) transmitter
(b) receiver.

4.4 F-OFDM Practical Implementation

This section describes the main steps of transmitter and receiver for the two scenarios of the proposed F-OFDM waveform (mentioned in chapter 3, sub-section 3.4.4) using a single USRP device with the assistance of LabVIEW NXG USRP nodes and other external devices to verify the F-OFDM performance.

4.4.1 Hardware Requirements

- a. USRP-X310.
- b. PC supports Ethernet connection.
- c. Spectrum Analyzer.
- d. Two Antennas (Log-periodic operate from 850 MHz to 6500 MHz).
- e. Ethernet and SMA cables.

4.4.2 Equal-Sized Sub-bands F-OFDM Practical Implementation

The implementation is based on the same specifications and assumptions presented in the simulation part in chapter 3 subsection (3.4.4.1) using the proposed window 2 filter design. At the first step, the data to be sent is prepared for transmission, which involves the processes (input bit generation, QAM modulation, IFFT algorithm, CP insertion, filtering, and combination of the signals of different specifications). The transmitter block is built on a separate VI in LabVIEW. The modulated signal is stored in a Tag as shown in figure (4.7). For the traditional OFDM signal, the identical approach is presented without the filtering stage.

A new VI was built in the next step for setting up the signal to transmit and receive from/to the USRP device. At the transmitter side, the IQ signal is read from the transmitter Tag whereas the received signal is written in the received Tag. In this VI, the IQ signal is sent to the USRP TX channel, which then forwards it to the propagation channel. The returned signal is routed through the USRP RX channel and then to the receiver via the network cable.

The signal configuration is shown in figure (4.8), while the setting parameters are listed in table (4.1).

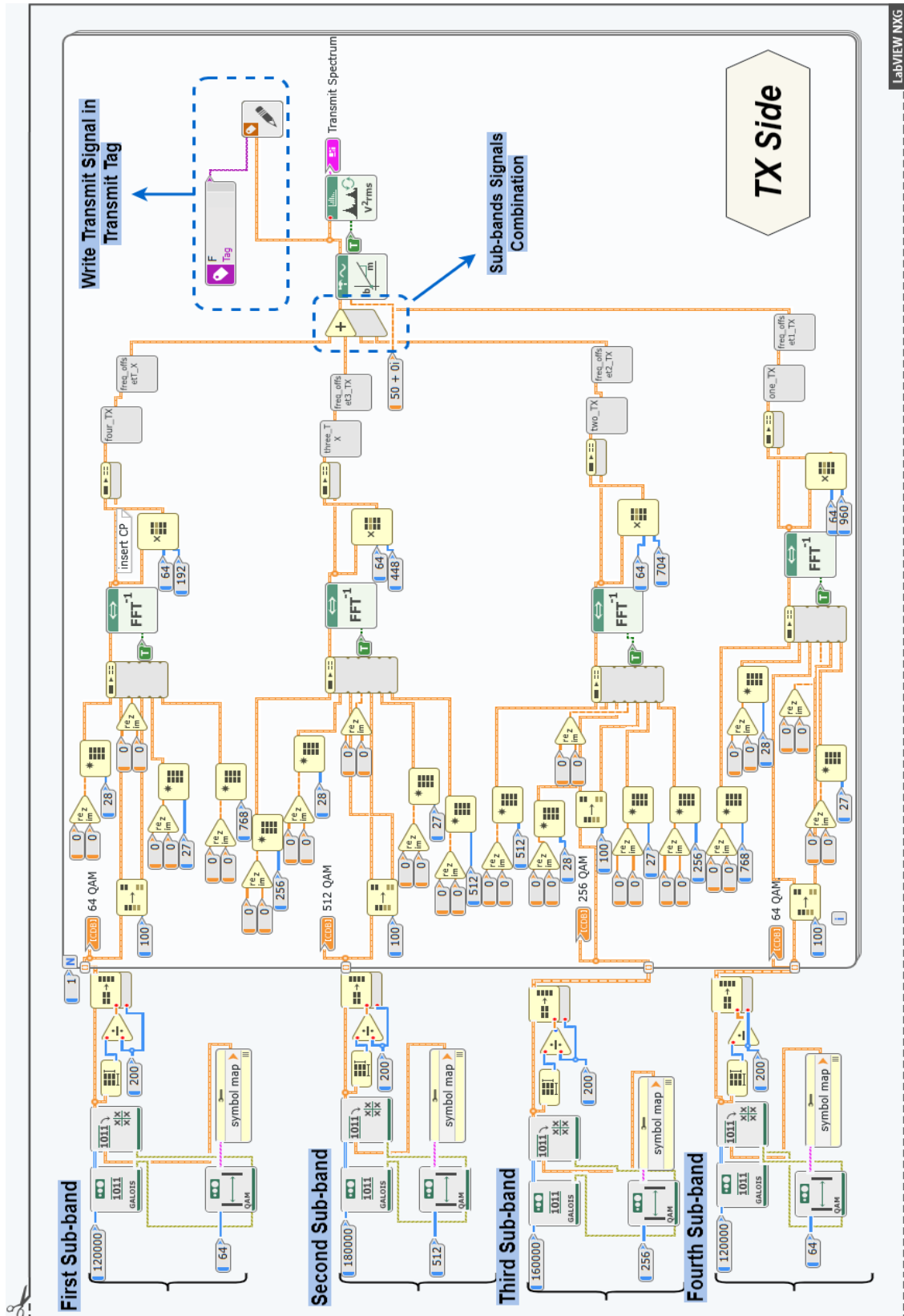


Figure (4.7) F-OFDM equal-sized sub-bands transmit signal process through USRP.

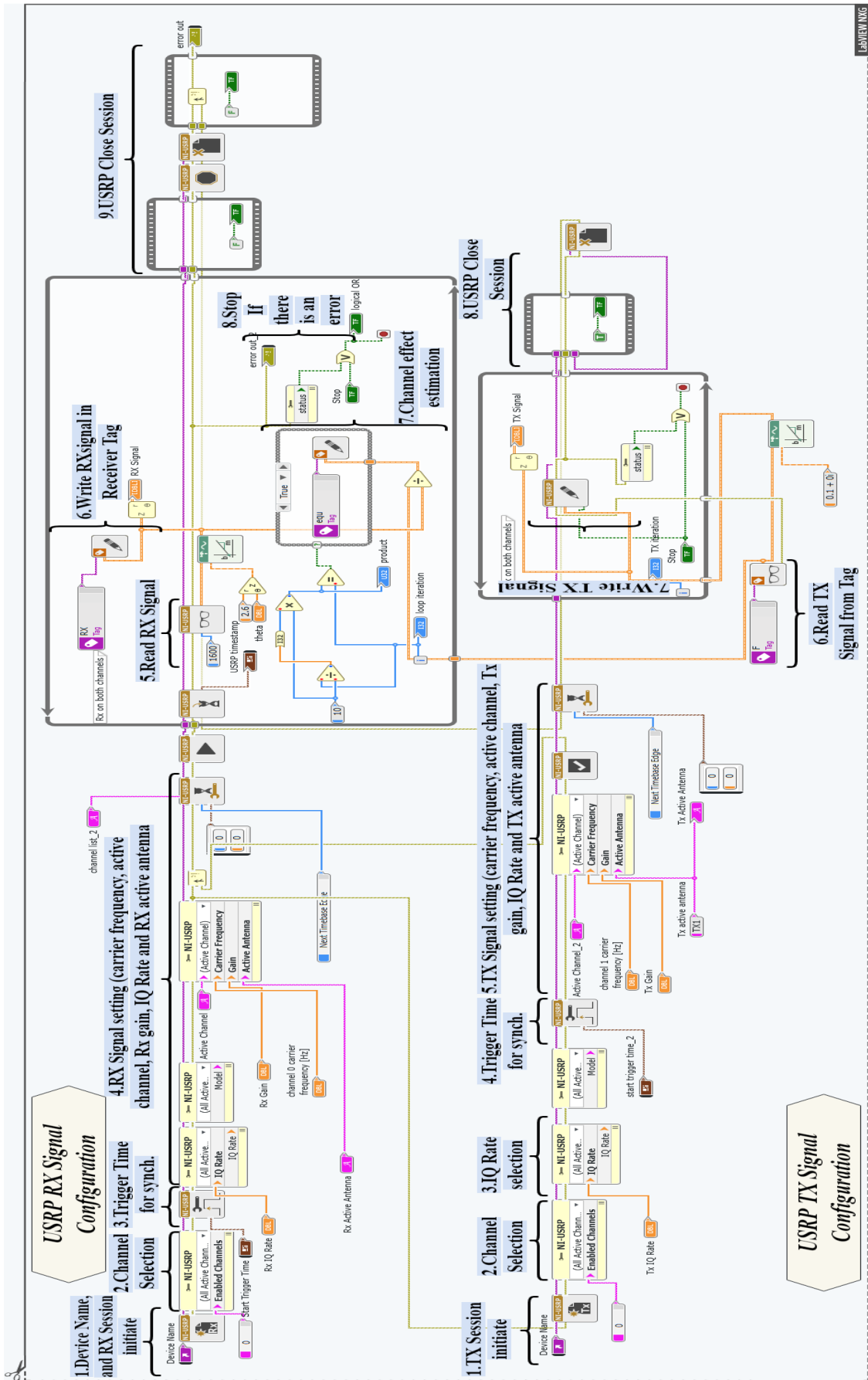


Figure (4.8) LabVIEW NXG diagram of transmit/receive signal setup.

Table (4.1) Transmitting/Receiving setting parameters for USRP.

| Parameter | Transmitting Setting | Receiving Setting |
|-------------------------------|----------------------|--------------------|
| Device name (IP: Port Number) | 192.168.10.2:49152 | 192.168.10.2:49151 |
| IQ Rate | 15.36 MHz | 15.36 MHz |
| Carrier frequency | 915 MHz, 3.4 GHz | 915 MHz, 3.4 GHz |
| Active Channel | 0 | 0 |
| Active Antenna | TX1 | RX2 |
| Gain | 20 | 1 |

As in the simulation, the signal to be transmitted is free of reference signals for synchronization and channel estimation, which needs to be studied in certain algorithms that are currently outside the scope of research. To achieve the synchronization between the transmitting and receiving nodes, the signals are configured by the (niUSRP Configure Time Start Trigger) node on both transmitting and receiving sides.

Because of the multipath phenomenon, the signal distorts (phase and amplitude) while being transmitted over the communication channel. To compensate for this distortion at the receiver, the channel characteristics estimator is required. The equalizer is built on the basis of finding the estimated transfer function of the channel by sending the information known by both the sender and receiver. The equalization is simply achieved by multiplying the received signal with the inverse transfer function of the channel to complete the receiver process. The entire receiving procedure is presented in the new VI by reading the received signal from the received Tag in the same project in LabVIEW.

Following the equalization stage, the receiver performs the opposite procedures of the transmitter, which involves filtering, signal modification due to the effect of filtering, CP removal, the FFT algorithm execution, and demodulation as shown in figure (4.9).

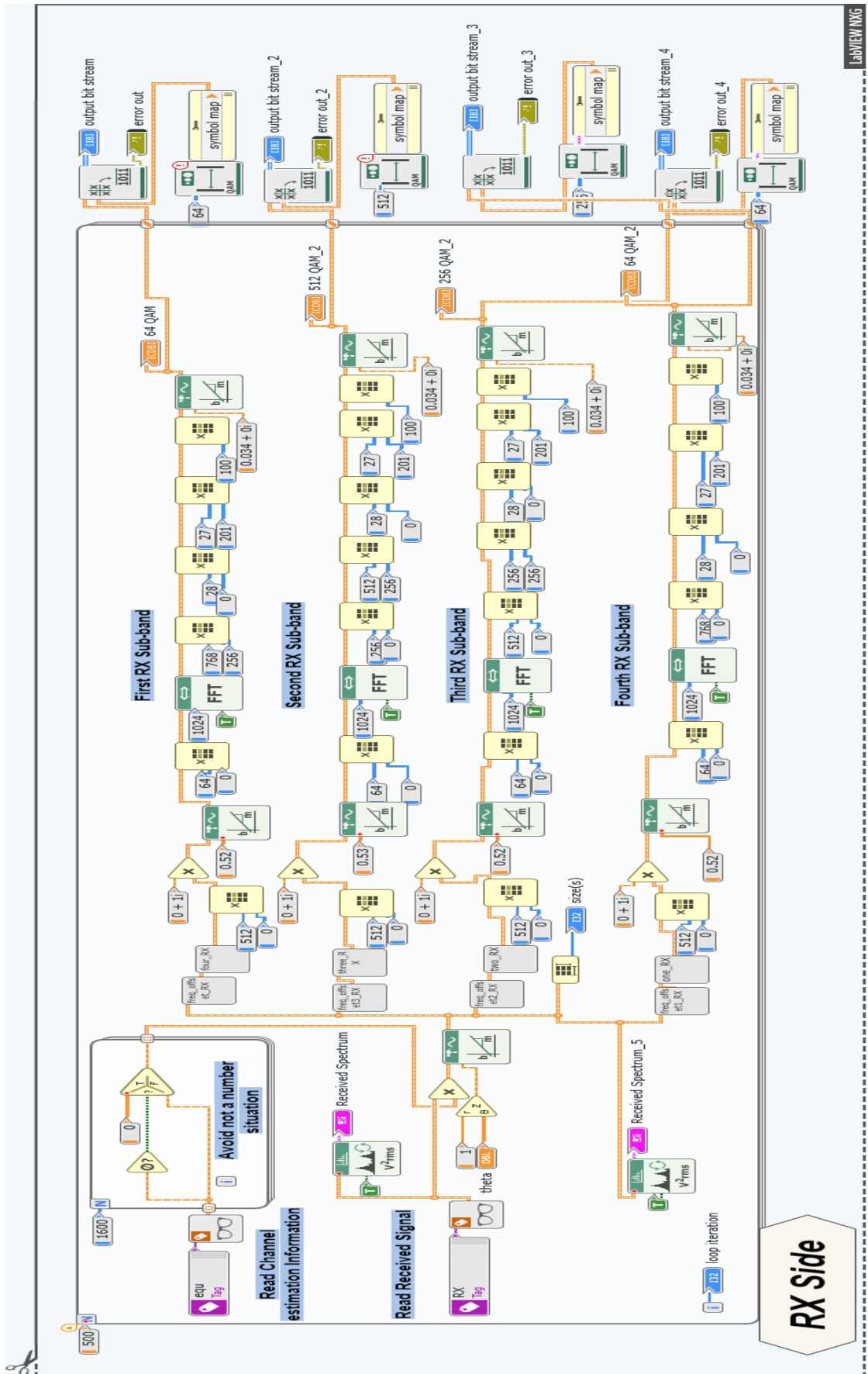


Figure (4.9) F-OFDM equal-sized sub-bands received signal process through USRP.

Figure (4.10) shows the hardware testbed of F-OFDM with network connection for equal-sized sub-bands. The USRP is connected to the PC using 1GigE cable, and the USRP is used to transmit and receive information to and from the channel via the antenna.

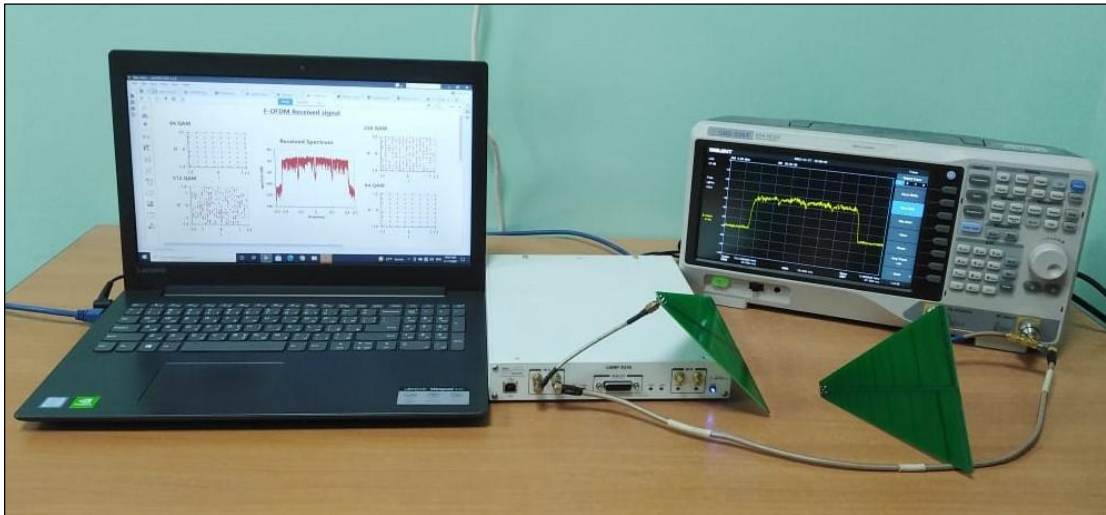


Figure (4.10) Testbed of the equal-sized sub-bands waveform F-OFDM.

Figure (4.11) illustrates a summary of the transmitting and receiving processes using the USRP device. The transmitted power spectrum and the constellation diagrams of the four sub-bands in both OFDM and F-OFDM are illustrated in figures (4.12-a) and (4.12-b), respectively, while the receiving spectrum (before equalizer) and proper constellation diagrams are illustrated in figures (4.13-a) for OFDM and (4.13-b) for F-OFDM.

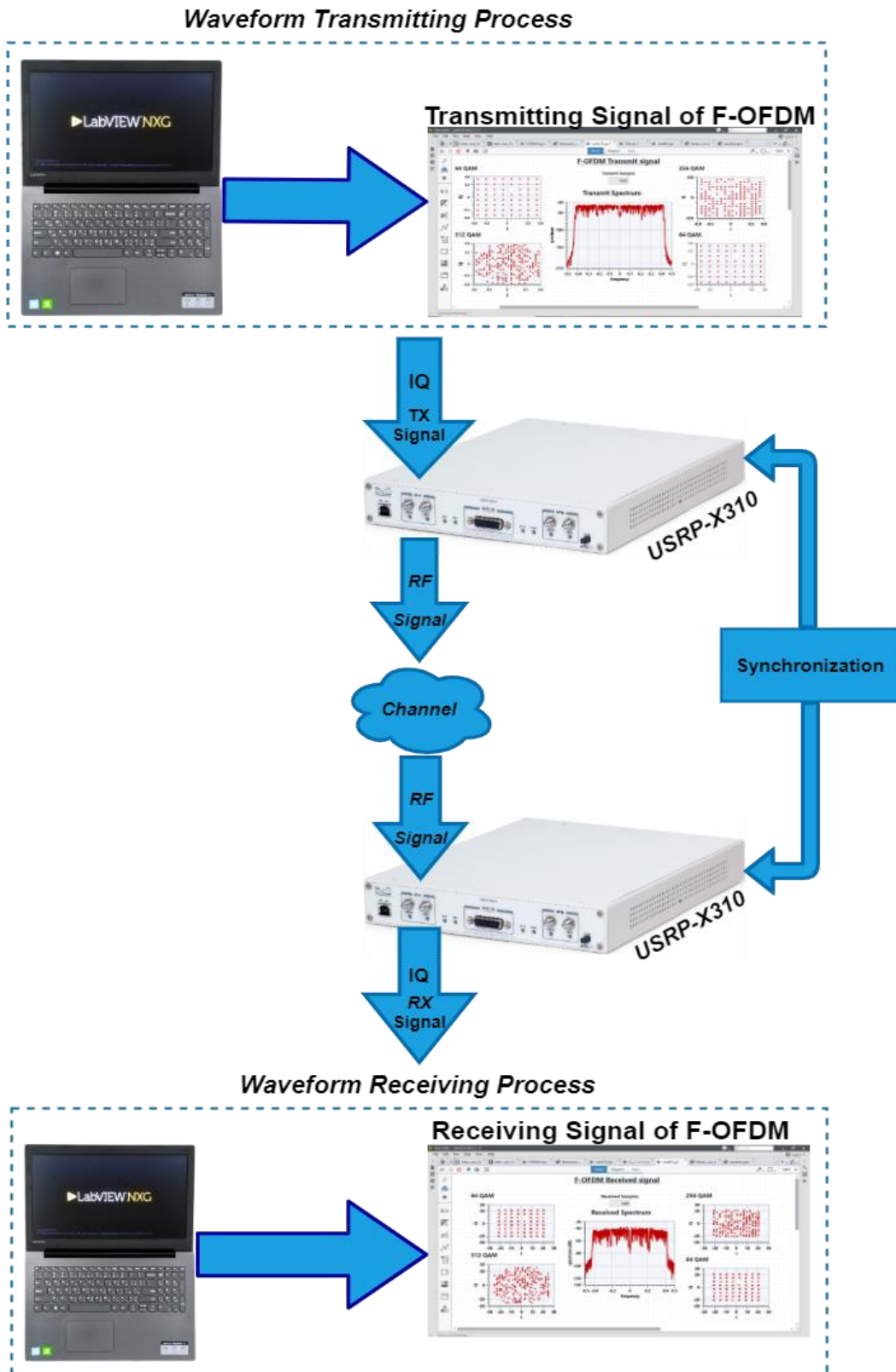
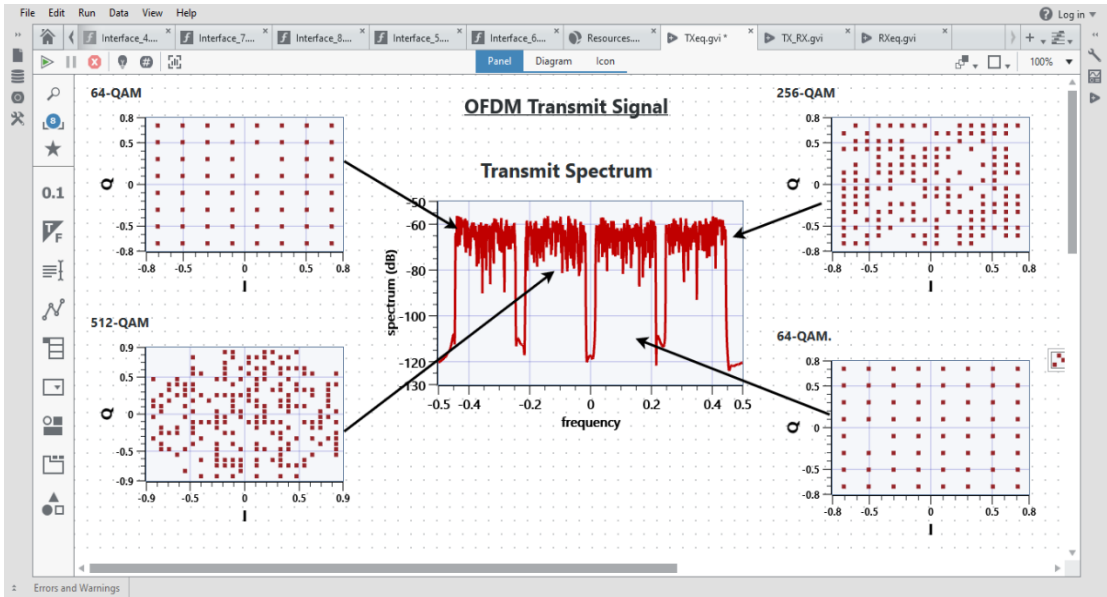
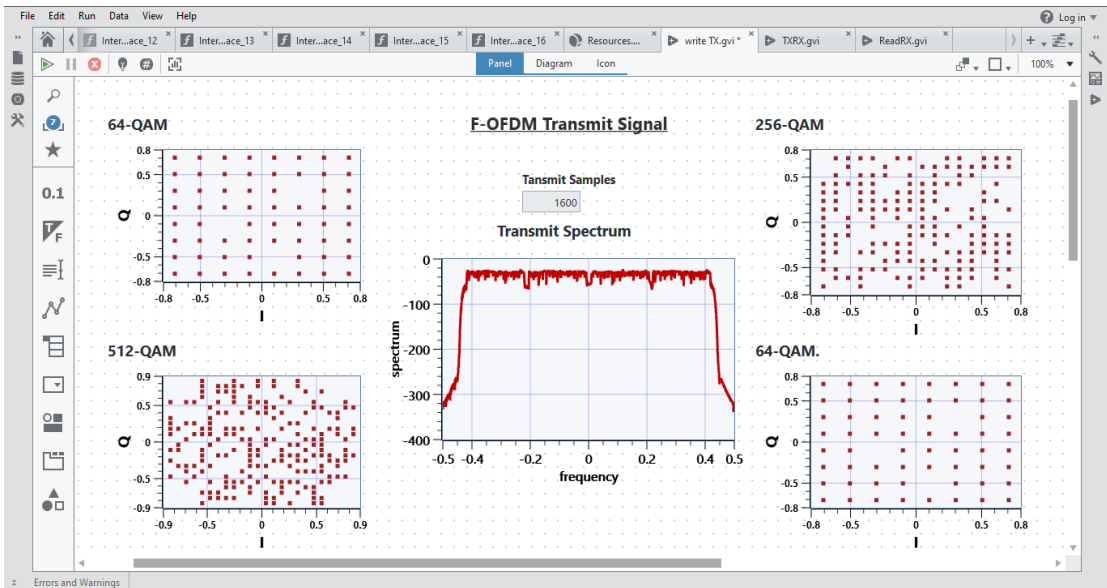


Figure (4.11) Transmit/Receive process summary for equal-sized sub-bands F-OFDM.

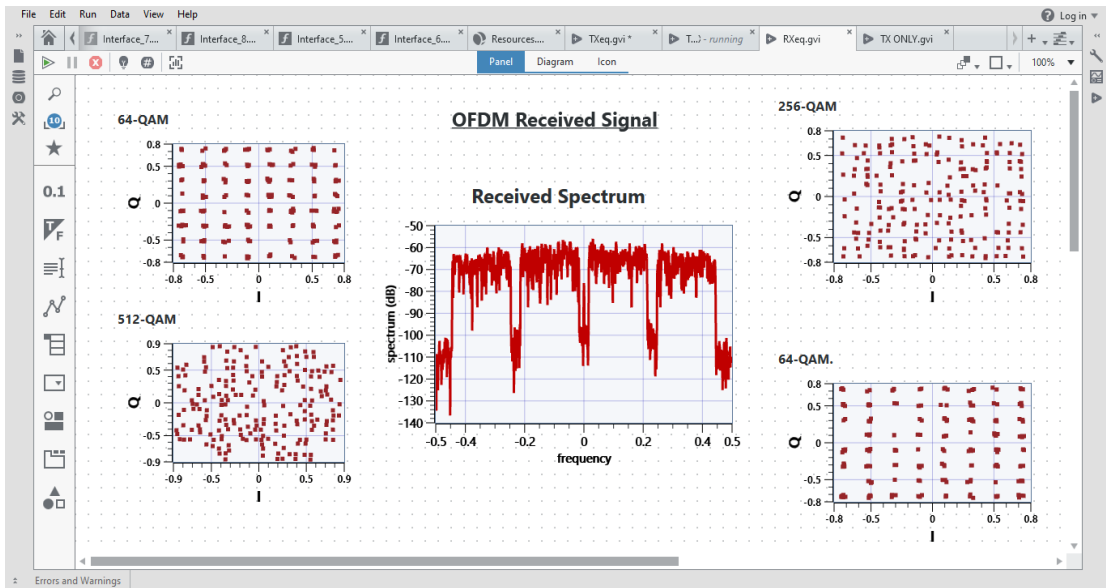


(a)

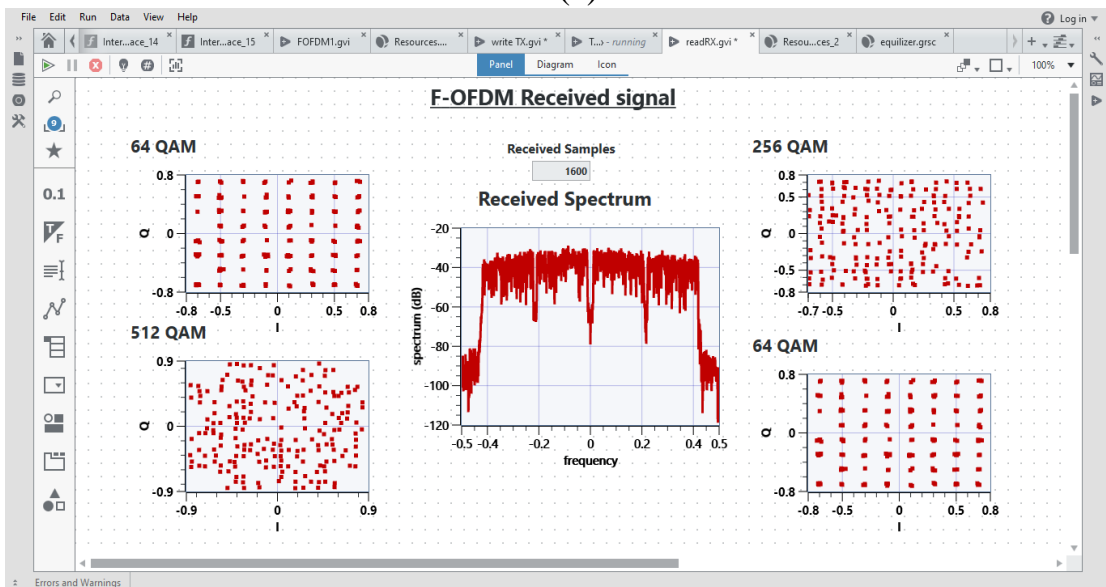


(b)

Figure (4.12) Equal-sized sub-bands waveform transmit signal spectrum and constellation diagrams: (a) OFDM (b) F-OFDM.



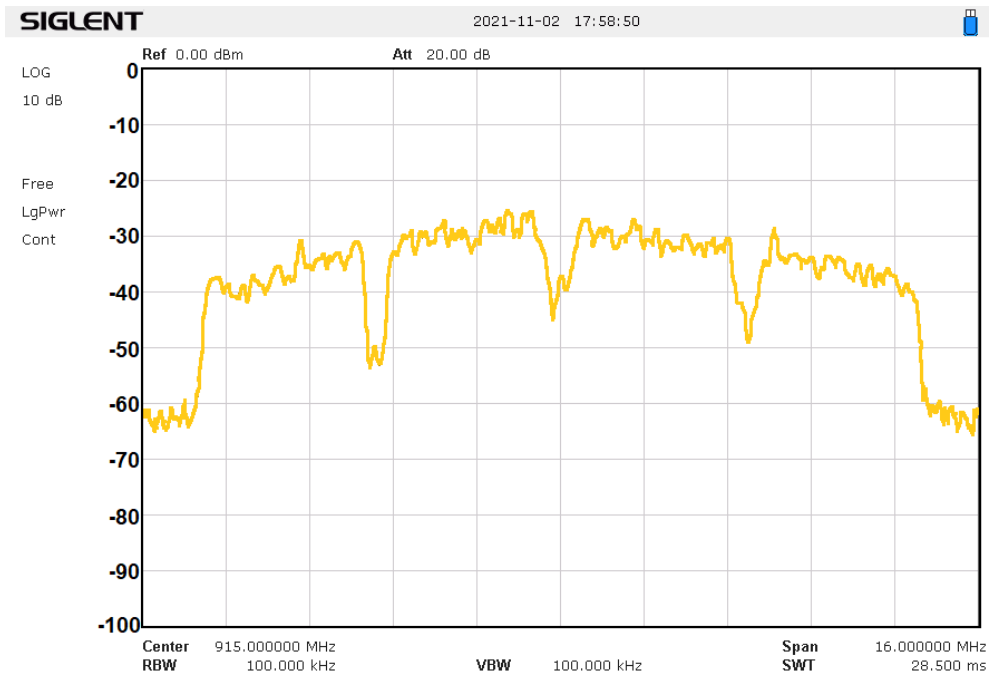
(a)



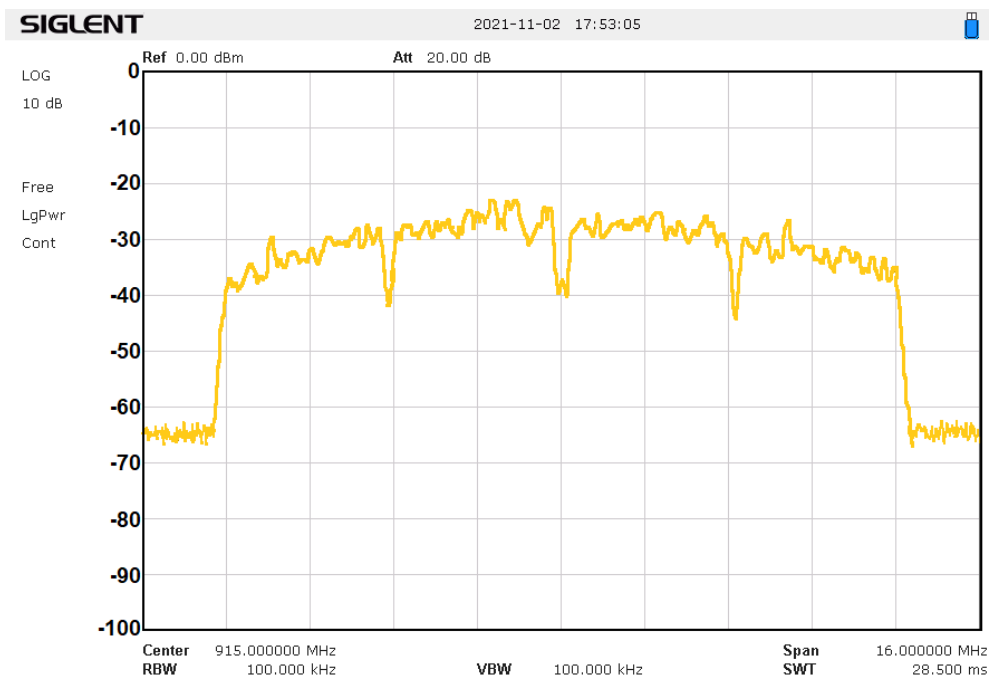
(b)

Figure (4.13) Equal-sized sub-bands waveform receive signal spectrum and constellation diagrams: (a) OFDM (b) F-OFDM.

The power spectrum of the transmitted equal-sized sub-bands waveform at 915MHz is measured using a Siglent SSA3032X spectrum analyzer and illustrated in figure (4.14), while the transmitted power spectrum at 3.4 GHz is measured using an Anritsu MS2665C spectrum analyzer and illustrated in figure (4.15). It is obvious that a significant enhancement in sidelobe power (OOBE) is due to the effect of using F-OFDM with respect to traditional OFDM.

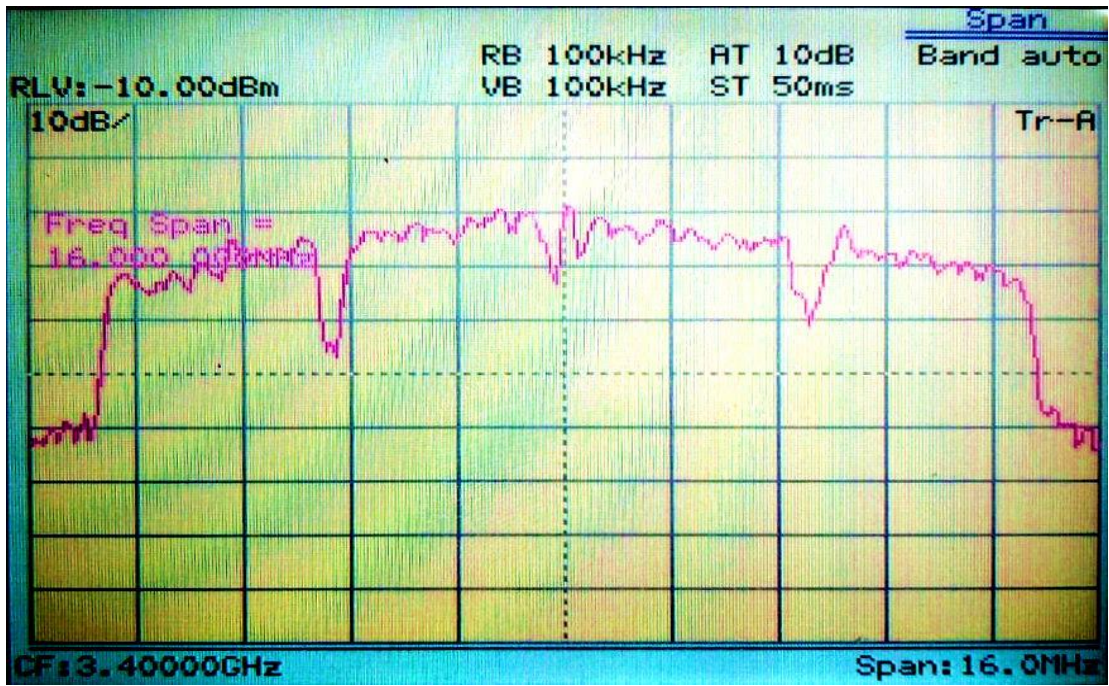


(a)

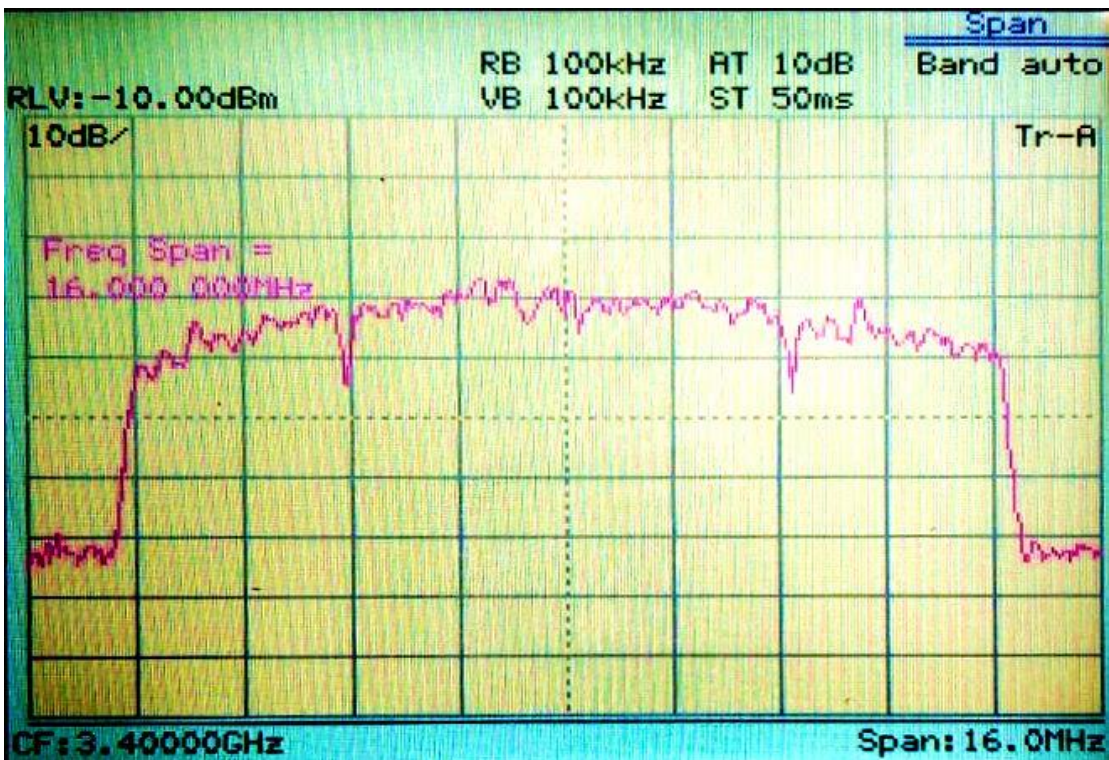


(b)

Figure (4.14) Equal-sized sub-bands waveform power spectrum at 915 MHz: (a) OFDM (b) F-OFDM.



(a)



(b)

Figure (4.15) Equal-sized sub-bands waveform power spectrum at 3.4 GHz: (a) OFDM (b) F-OFDM.

4.4.3 Unequal-Sized Sub-bands F-OFDM Practical Implementation

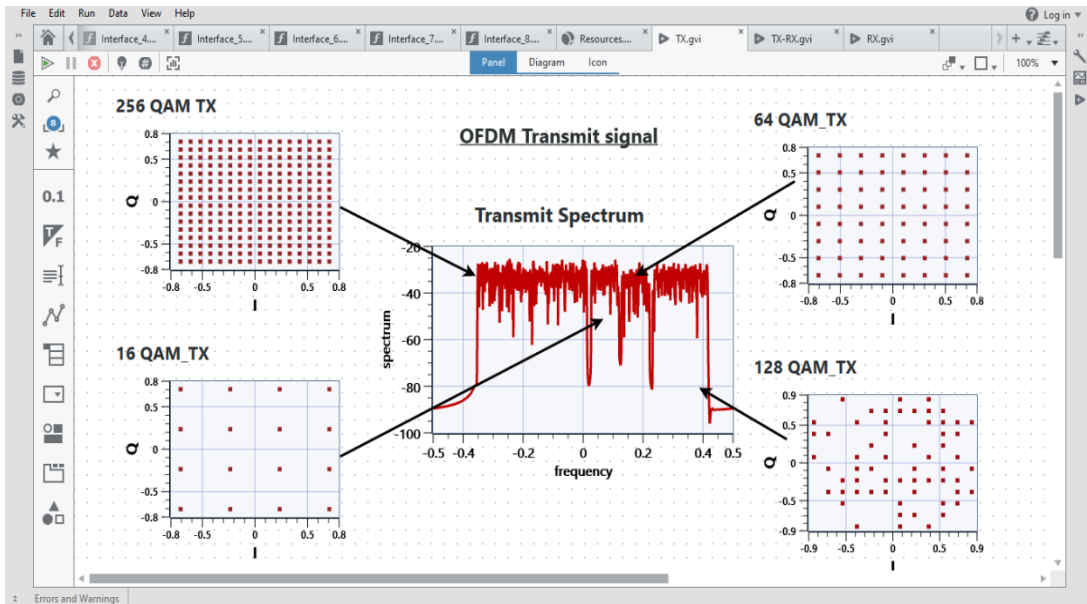
The same steps used for the equal-sized sub-bands are also used for the unequal-sized sub-bands. The unequal sub-bands are designed based on the same specifications as the simulation part in chapter three subsection (3.4.4.3). The data to be transmitted is prepared for transmission in the VI file of LabVIEW with the processes starting from bit generation, modulation with different orders, the IFFT algorithm performing following the insertion of CP, and finally the filtering process. The signals from different sub-bands are combined and transmitted. The transmit signal is stored in a Tag as in the same step for the equal-sized sub-bands. In the case of OFDM, the signal is transmitted without the filtering process.

A new VI is presented for signal configuration for transmitting and receiving the F-OFDM signal. The same signal setting is adopted in the table 1. The transmitted signal is read from the transmitted Tag, while the received signal from the USRP is written on the received Tag.

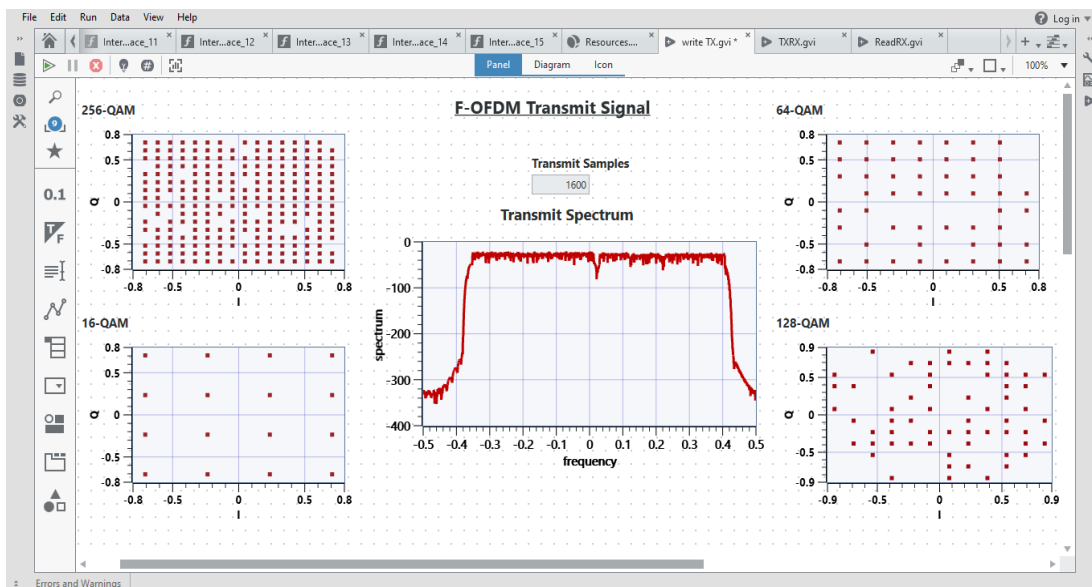
For synchronization and equalization, the same procedures used in the equal-sized sub-bands are reused in the unequal-sized sub-bands for proper receipt. In the final VI, the received signal is read from the received Tag and equalized. In the final step, the processes of each sub-band are started with the filtering process, equalizing the distortion produced by the filter, CP removing, FFT performing, and finally the demodulation stage.

The diagram of the signal configuration is the same as the equal-sized sub-bands waveform, which is illustrated in figure (4.8).

The transmitted power spectrum of the unequal-sized waveform and the constellation diagrams in both OFDM and F-OFDM are illustrated in figures (4.16-a) and (4.16-b), respectively, while the received spectrum and the equalized constellation diagrams are illustrated in figures (4.17-a) for OFDM and (4.17-b) for F-OFDM.

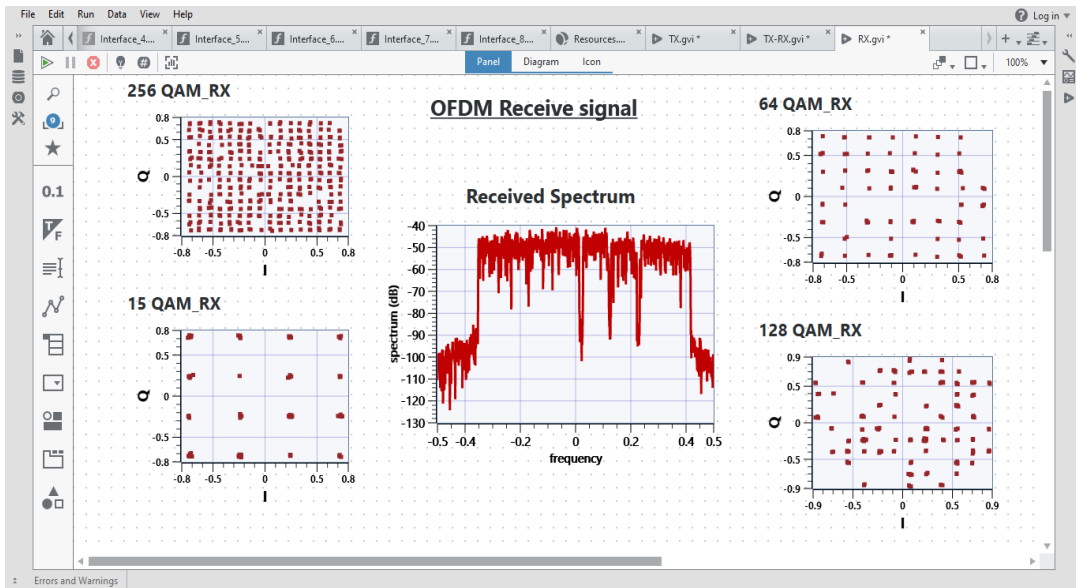


(a)

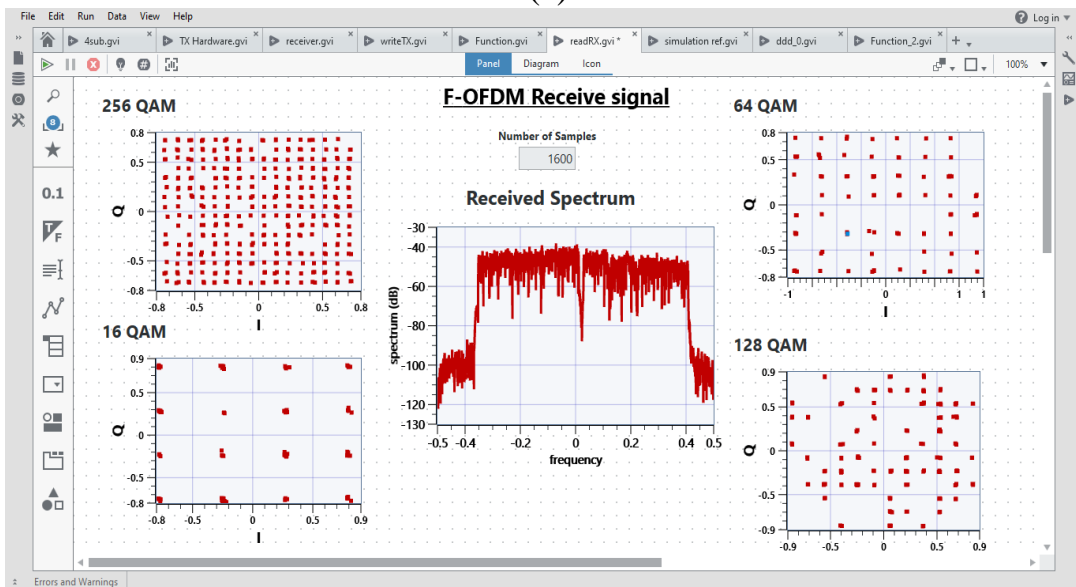


(b)

Figure (4.16) Unequal-sized sub-bands waveform transmit signal spectrum and constellation diagrams: (a) OFDM (b) F-OFDM.



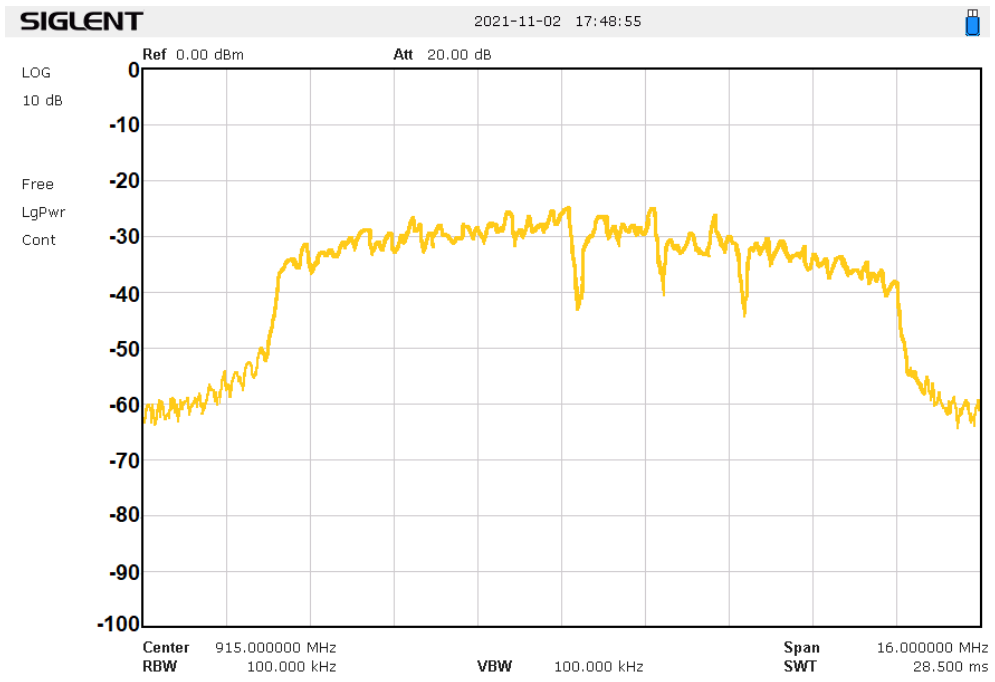
(a)



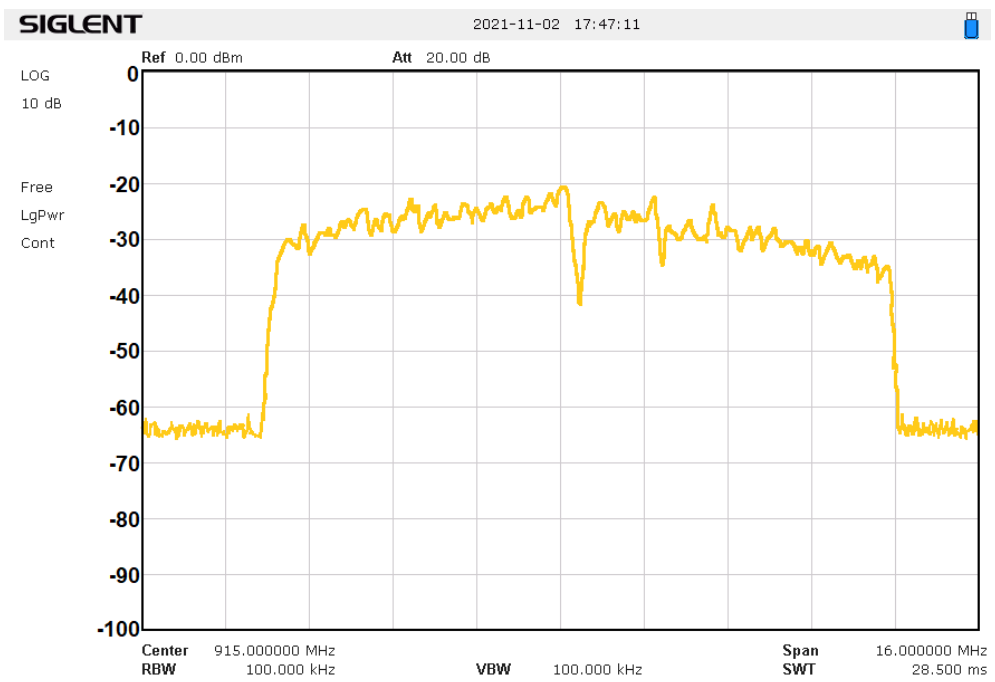
(b)

Figure (4.17) Unequal-sized sub-bands waveform receive signal spectrum and constellation diagrams: (a) OFDM (b) F-OFDM.

The power spectrum of the unequal-sized sub-bands waveform transmitted at the same spectrum analyzers used in the equal-sized waveform at 915 MHz and 3.4 GHz operation frequencies is illustrated in figures (4.18) and (4.19), respectively. It is evident that the use of F-OFDM results in a significant improvement in sidelobe power (OOBE) as compared to traditional OFDM.

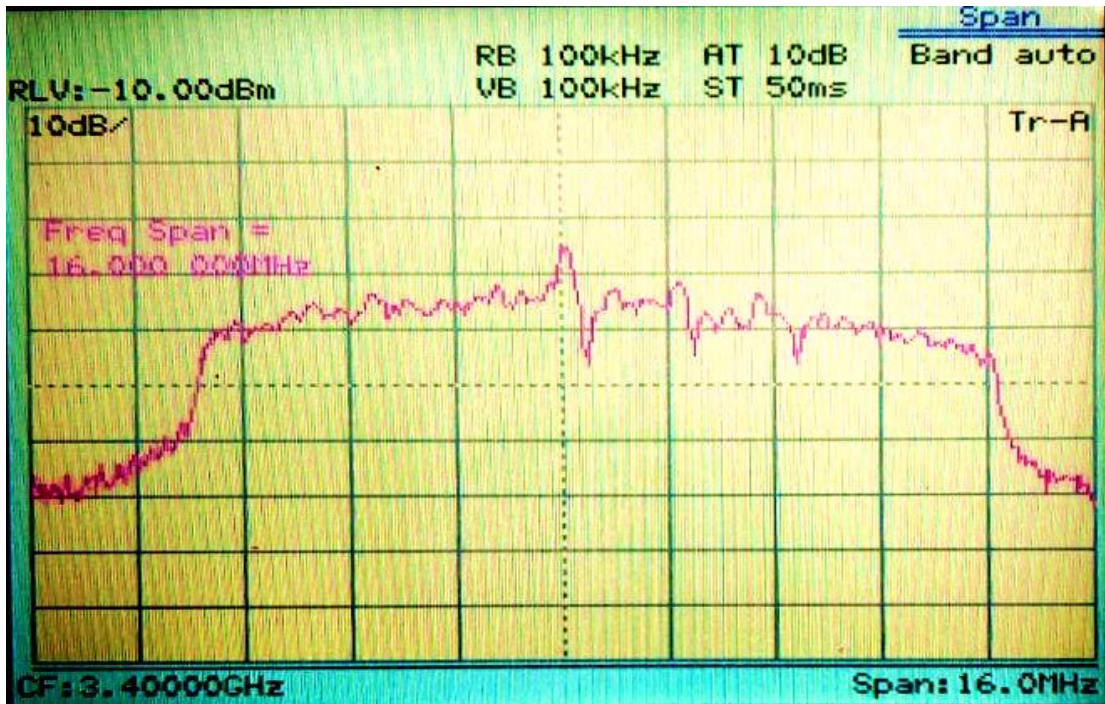


(a)

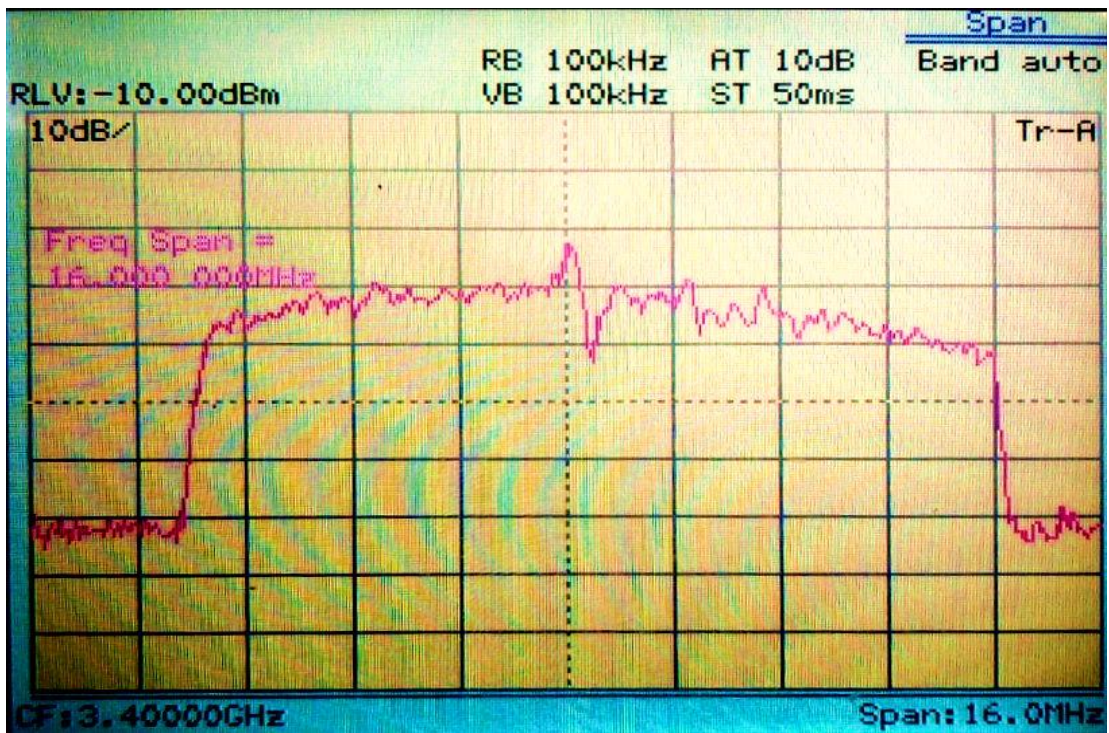


(b)

Figure (4.18) Unequal-sized sub-bands waveform power spectrum at 915 MHz: (a) OFDM (b) F-OFDM.



(a)



(b)

Figure (4.19) Unequal-sized sub-bands waveform power spectrum at 3.4 GHz: (a) OFDM (b) F-OFDM.

4.4.4 Spectrum Efficiency Enhancement

Comparing with OFDM, the enhancement achieved in SE for equal-sized and unequal-sized sub-bands F-OFDM waveform are 5% and 5.6%, respectively. The normalized enhancement SE in comparison to OFDM is shown in figure (4.20), which is relatively equal to the simulation part for the two scenarios.

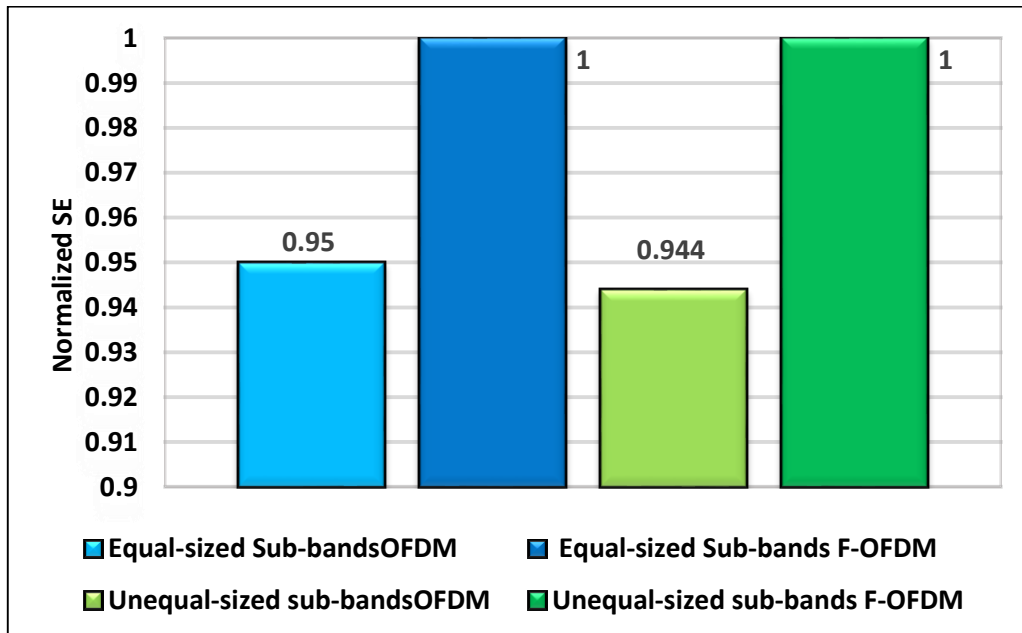


Figure (4.20) Normalized SE for the equal-sized and unequal-sized sub-bands F-OFDM in practical.

CHAPTER FIVE

CONCLUSION RESULTS AND SCOPE FUTURE DEVELOPMENT

5.1 Conclusion

The selection of the appropriate physical layer multicarrier waveform is a crucial task for achieving the desired coverage and throughput for wireless communication systems. An advanced OFDM design base filtering was recommended for the 5G air interface to improve spectrum localization, interference reduction, and allowing for asynchronous transmission. F-OFDM was presented in this thesis with two scenarios of spectrum fragmentation, one equal-sized sub-bands and the other unequal-sized using various kinds of Window-Sinc filters. Two software simulators were employed, MATLAB-Simulink and LabVIEW NXG, to design the waveform and evaluate the performance. Furthermore, some practical implementations were performed on the proposed scenarios by transmitting and receiving over a real communication channel using the SDR-USRP platform. The following is a summary of the conclusions obtained from this study:

1. The F-OFDM waveform model is more flexible and scalable, which can support various sets of numerology for each sub-band with mixed capability depending on the service requirements.
2. Various Window-Sinc filter forms have been successfully adopted. To enhance the performance, two new time-domain window functions were proposed, with the combination of two and three window functions. Hanning with Blackman and Hanning-Blackman with BlackmanHarris as proposed windows 1 and 2 respectively. The proposed window filters accomplished high OOB performance compared with the traditional window functions and OFDM.

3. Higher SE enhancement was achieved for the two proposed scenarios. By reducing the guard band, the maximum SE enhancement when using proposed window 2 was 5.2% and 5.8% with comparison to OFDM for the first and second scenarios, respectively.
4. According to the simulation, the larger sub-band size requires a larger guard band, and higher QAM order sub-bands also require a larger guard band.
5. All utilized window function forms have almost the same performance in terms of BER with different OOB reduction.
6. The obtained BER results give the impression that at lower values of SNR, the BER of F-OFDM has almost the same performance as OFDM, while at higher values of SNR the performance is different, which depends on the designed filter, and it is usually diverged from OFDM. It is recommended to use such technology (Application) for low SNR system.
7. As an average, the F-OFDM sub-bands have a higher PAPR in comparison with OFDM. To overcome this problem, some PAPR reduction techniques can be used.
8. The USRP wireless communication system offers more versatility, flexibility, and efficiency when it comes to dealing with communications techniques in practice. The practical work (transmitting and receiving) of the designed waveform is carried out with signal processing in LabVIEW and implementation using a single device of USRP.
9. In practical implementation, the SE enhancement of the two proposed scenarios using proposed window 2 were 5% and 5.6% for the first and second scenarios, respectively, which are similar to that in simulation.

5.2 Future Works

1. Implementing the proposed waveform solution completely on the FPGA of the USRP for faster processing (offloading).
2. Designing and building a full synchronized F-OFDM with a various channel estimation methods.
3. Designing the waveform with multi sub-band (more than four sub-bands).
4. Using another type of communication channel.
5. Designing different waveforms for each sub-band.

REFERENCES

- [1] A. M. Hamed and R. K. Rao, "Spectral and Energy Efficiencies in mmWave Cellular Networks for Optimal Utilization," *Wireless Communications and Mobile Computing*, vol. 2018, p.11, Jan. 2018, doi:10.1155/2018/3097094.
- [2] A. Bohli and R. Bouallegue, "A New Sensing Strategy for 5G Mobile Networks: Towards Spectral and Energy Efficiency Trade off," 2016 IEEE 30th International Conference on Advanced Information Networking and Applications (AINA), March 2016, pp. 155-159, doi: 10.1109/AINA.2016.11.
- [3] A. Zaidi et al., *5G Physical Layer Principles, Models and Technology Components*, Academic Press-Elsevier, 1st ed., 2018.
- [4] P. Banelli et al., "Modulation Formats and Waveforms for the Physical Layer of 5G Wireless Networks: Who Will be the Heir of OFDM?," *IEEE Signal Processing Magazine*, vol. 31, no. 6, pp. 80-93, Nov. 2014, doi: 10.1109/MSP.2014.2337391.
- [5] J. Wang et al., "Spectral Efficiency Improvement With 5G Technologies: Results From Field Tests," *IEEE Journal on Selected Areas in Communications*, vol. 35, no. 8, pp. 1867-1875, Aug. 2017, doi: 10.1109/JSAC.2017.2713498.
- [6] J. Li, E. Bala, and R. Yang, "Resource block Filtered-OFDM for future spectrally agile and power efficient systems," *Physical Communication*, vol. 11, pp. 36–55, June 2014, doi: 10.1016/j.phycom.2013.10.003.
- [7] J. Abdoli, M. Jia and J. Ma, "Filtered OFDM: A new waveform for future wireless systems," 2015 IEEE 16th International Workshop on Signal Processing Advances in Wireless Communications (SPAWC), July 2015, pp. 66-70, doi: 10.1109/SPAWC.2015.7227001.
- [8] X. Zhang et al., "Filtered-OFDM - Enabler for Flexible Waveform in

- the 5th Generation Cellular Networks,” 2015 IEEE Global Communications Conference (GLOBECOM), Dec. 2015, pp. 1-6, doi: 10.1109/GLOCOM.2015.7417854.
- [9] X. Cheng et al., “A Filtered OFDM Using FIR Filter Based on Window Function Method,” 2016 IEEE 83rd Vehicular Technology Conference (VTC Spring), May 2016, pp. 1-5, doi: 10.1109/VTCSpring.2016.7504065.
- [10] D. Wu et al., “A Field Trial of f-OFDM toward 5G,” 2016 IEEE Globecom Workshops (GC Wkshps), Dec. 2016, pp. 1-6, doi: 10.1109/GLOCOMW.2016.7848810.
- [11] R. Gerzaguet et al., “Block-filtered OFDM: A new promising waveform for multi-service scenarios,” 2017 IEEE International Conference on Communications (ICC), May 2017, pp. 1-6, doi: 10.1109/ICC.2017.7996399.
- [12] C. An, B. Kim and H. Ryu, “WF-OFDM (windowing and filtering OFDM) system for the 5G new radio waveform,” 2017 IEEE XXIV International Conference on Electronics, Electrical Engineering and Computing (INTERCON), Aug. 2017, pp. 1-4, doi: 10.1109/INTERCON.2017.8079635.
- [13] L. Y. X. Yang, “Filtered-OFDM System Performance Research Based on Nuttall’s Blackman-Harris Window,” 2017 IEEE 17th International Conference on Communication Technology (ICCT), Oct. 2017, pp. 687-691, doi: 10.1109/ICCT.2017.8359724.
- [14] L. Zhang et al., “Filtered OFDM systems, algorithms, and performance analysis for 5G and beyond,” IEEE Transactions on Communications, vol. 66, no. 3, pp. 1205-1218, March 2018, doi: 10.1109/TCOMM.2017.2771242.
- [15] M. Yang, Y. Chen and L. Du, “Interference Analysis and Filter Parameters Optimization for Uplink Asynchronous F-OFDM

- Systems,” *IEEE Access*, vol. 7, pp. 48356-48370, Apr. 2019, doi: 10.1109/ACCESS.2019.2910592.
- [16] S. Gökceli et al., "Software-Defined Radio Prototype for Fast-Convolution-Based Filtered OFDM in 5G NR," 2019 European Conference on Networks and Communications (EuCNC), June 2019, pp. 235-240, doi: 10.1109/EuCNC.2019.8802008.
- [17] S. Roy and A. Chandra, “Interpolated Band-pass Method Based Narrow-band FIR Filter: A Prospective Candidate in Filtered-OFDM Technique for the 5G Cellular Network,” *TENCON 2019 - 2019 IEEE Region 10 Conference (TENCON)*, Oct. 2019, pp. 311-315, doi: 10.1109/TENCON.2019.8929601.
- [18] K. S. Chandran and C. K. Ali, “Filtered-OFDM with Index Modulation for Mixed Numerology Transmissions,” 2020 6th International Conference on Advanced Computing and Communication Systems (ICACCS), March 2020, pp. 306-310, doi: 10.1109/ICACCS48705.2020.9074243.
- [19] M. A. Taher, H. S. Radhi, and A. K. Jameil, “Enhanced F-OFDM candidate for 5G applications,” *Journal of Ambient Intelligence and Humanized Computing*, vol. 12, pp.635-652, May 2020, doi: 10.1007/s12652-020-02046-3.
- [20] M. Liu et al., “Design of filters based on generic function model for reducing out-of-band emissions of the F-OFDM systems,” *International Journal of Electronics and Communications*, vol. 139, p. 153908, Sept. 2021, doi: 10.1016/j.aeue.2021.153908.
- [21] S. Mukhtar, and G. R. Begh, “Performance Analysis of Filtered OFDM Based Downlink and Uplink NOMA System over Nakagami-m Fading Channel,” *Journal of Telecommunications and Information Technology*, vol.66 , no. 2, pp. 11-23, 2021, doi:10.26636/jtit.2021.148020.

- [22] S. Ahmadi, 5G NR architecture, technology, implementation, and operation of 3GPP new radio standards, 1st ed., Academic Press-Elsevier, 2019.
- [23] Huawei White Paper, “5G: New Air Interface and Radio Access Virtualization,” Apr. 2015, [Online] Available: https://www.huawei.com/minisite/has2015/img/5g_radio_whitepaper.pdf (accessed Jan. 23, 2022).
- [24] IMT Vision–Framework and overall objectives of the future development of IMT for 2020 and beyond, Rec. ITU-R 2083-0, International Telecommunication Union, Geneva, Switzerland, Sept. 2015.
- [25] A. Hikmaturokhman, K. Ramli and M. Suryanegara, “Spectrum Considerations for 5G in Indonesia,” 2018 International Conference on ICT for Rural Development (IC-ICTRuDev), Oct. 2018, pp. 23-28, doi: 10.1109/ICICTR.2018.8706874.
- [26] E. Dahlman, S. Parkvall, and J. Skold, 5G NR the next generation wireless access technology, 2nd ed., Academic Press, Elsevier, 2021.
- [27] M. Nekovee and R. Rudd, “5G Spectrum Sharing,” 12th International Conference on Cognitive Radio Oriented Wireless Networks (CROWNCOM 2017), Lisbon, Portugal, 20-22 Sept. 2017. <http://sro.sussex.ac.uk/id/eprint/68889>.
- [28] F. Ouyang, Digital Communication for Practicing Engineers, 1st ed., John Wiley & Sons, 2019, doi: 10.1002/9781119598138.
- [29] J. Boccuzzi, “Introduction to Cellular Mobile Communications,” Electronics,” in: Multiple Access Techniques for 5G Wireless Networks and Beyond, vol. 159, M.Vaezi, Z. Ding, H. V. Poor Ed., Berlin, Germany: Springer, 2019, Ch.1, pp. 3-37, doi: 10.1007/978-3-319-92090-0_1.

- [30] J. Iqbal et al., "Comparison of Spectral Efficiency Techniques in Device-to-Device Communication for 5G," *IEEE Access*, vol. 7, pp. 57440-57449, May 2019, doi: 10.1109/ACCESS.2019.2914486.
- [31] S. Deshpande, "Introduction to MIMO and Massive MIMO," in *Fundamentals of Network Planning and Optimisation 2G/3G/4G: Evolution to 5G*, A. R. Mishra Ed., John Wiley & Sons Ltd, 2nd ed., pp.325-335, 2018, doi: 10.1002/9781119331797.app2.
- [32] H. Gamage, N. Rajatheva and M. Latva-aho, "Channel coding for enhanced mobile broadband communication in 5G systems," 2017 European Conference on Networks and Communications (EuCNC), June 2017, pp. 1-6, doi: 10.1109/EuCNC.2017.7980697.
- [33] A. Meriem, "Study and simulation of Sparse Code Multiple Access (SCMA) for 5G New Radio," MSc. thesis, University of Echahid Hamma Lakhdar El-Oued, Algeria, 2019. [Online]. Available: <http://dspace.univ-eloued.dz/bitstream/123456789/3372/1/621.382-074.pdf>.
- [34] V. P. Klimentyev and A. B. Sergienko, "A low-complexity SCMA detector for AWGN channel based on solving overdetermined systems of linear equations," 2016 XV International Symposium Problems of Redundancy in Information and Control Systems (REDUNDANCY), Sept. 2016, pp. 61-65, doi: 10.1109/RED.2016.7779331.
- [35] H. Schulze and C. Luders, *Theory and Applications of OFDM and CDMA Wideband Wireless Communications*, 1st ed., John Wiley & Sons Ltd, 2005.
- [36] T. Hwang et al., "OFDM and Its Wireless Applications: A Survey," *IEEE Transactions on Vehicular Technology*, vol. 58, no. 4, pp. 1673-1694, May 2009, doi: 10.1109/TVT.2008.2004555.
- [37] S. Weinstein and P. Ebert, "Data Transmission by Frequency-Division Multiplexing Using the Discrete Fourier Transform," *IEEE*

- Transactions on Communication Technology, vol. 19, no. 5, pp. 628-634, Oct. 1971, doi: 10.1109/TCOM.1971.1090705.
- [38] A. Yazar, M. Elkourdi, H. Arslan, “Waveform Designs for Cognitive Radio and Dynamic Spectrum Access Applications,” in Handbook of Cognitive Radio, W. Zhang Ed., Singapore, Springer, 2019, pp. 63-86, doi: 10.1007/978-981-10-1394-2_3.
- [39] N. Marchetti et al., “OFDM: Principles and Challenges,” in New Directions in Wireless Communications Research, V. Tarokh Ed., 1st ed., Boston, MA, Springer, 2009, Ch.2, pp. 29-62, doi: 10.1007/978-1-4419-0673-1_2.
- [40] Y. S. Cho et al., MIMO-OFDM Wireless communications with MATLAB, 1st ed., John Wiley & Sons, 2010, doi: 10.1002/9780470825631.
- [41] C. D. Parekha and J. M. Patel, “Overview on synchronization in OFDM systems,” 2016 International Conference on Advances in Computing, Communication, & Automation (ICACCA) (Spring), Apr. 2016, pp. 1-6, doi: 10.1109/ICACCA.2016.7578862.
- [42] 5G-RANGE, “Physical layer of the 5G-RANGE – Part II”, Deliverable 3.2, Work Package 3, Feb. 2019. [Online] Available: <https://ec.europa.eu/research/participants/documents/downloadPublic?documentIds=080166e5c1bc5112&appId=PPGMS> (Accessed Jan. 22, 2022).
- [43] P. P. Ann and R. Jose, “Comparison of PAPR reduction techniques in OFDM systems,” 2016 International Conference on Communication and Electronics Systems (ICCES), Oct. 2016, pp. 1-5, doi: 10.1109/CESYS.2016.7889995.
- [44] A. A. Zaidi et al., “Waveform and Numerology to Support 5G Services and Requirements,” IEEE Communications Magazine, vol.

- 54, no. 11, pp. 90-98, Nov. 2016, doi: 10.1109/MCOM.2016.1600336CM.
- [45] M. Gupta, A. S. Kang, and V. Sharma, "Comparative Study on Implementation Performance Analysis of Simulink Models of Cognitive Radio Based GFDM and UFMC Techniques for 5G Wireless Communication," *Wireless Personal Communications*, pp. 1-31, Aug. 2020, doi:10.1007/s11277-020-07561-2.
- [46] A. Ijaz et al., "Analysis of Candidate Waveforms for 5G Cellular," in *Towards 5G Wireless Networks A Physical Layer Perspective*, H. K. Bizaki Ed., IntechOpen, 2016, Ch.1, pp. 3-25, doi: 10.5772/66051.
- [47] L. Zhang et al., "Subband Filtered Multi-Carrier Systems for Multi-Service Wireless Communications," *IEEE Transactions on Wireless Communications*, vol. 16, no. 3, pp. 1893-1907, March 2017, doi: 10.1109/TWC.2017.2656904.
- [48] 3GPP, TSG RAN WG1 Meeting #85, "f-OFDM scheme and filter design, May 2016. [Online]. Available: <https://www.3gpp.org/DynaReport/TDocExMtg--R1-85--31662.htm> (accessed Jan. 23, 2022).
- [49] E. W. Hansen, *Fourier Transforms Principles and Applications*, 1st ed., John Wiley & Sons Ltd, 2014.
- [50] F. J. Harris, "On the use of windows for harmonic analysis with the discrete Fourier transform," *Proceedings of the IEEE*, vol. 66, no. 1, pp. 51-83, Jan. 1978, doi: 10.1109/PROC.1978.10837.
- [51] A. Nuttall, "Some windows with very good sidelobe behavior," *IEEE Transactions on Acoustics, Speech, and Signal Processing*, vol. 29, no. 1, pp. 84-91, Feb.1981, doi: 10.1109/TASSP.1981.1163506.
- [52] K. M. M. Prabhu, *Window functions and their applications in signal processing*, 1st ed., CRC Press, 2014, doi: 10.1201/9781315216386.

- [53] Matlab MathWorks, F-OFDM vs. OFDM Modulation, <https://www.mathworks.com/help/comm/ug/f-ofdm-vs-ofdm-modulation.html> (accessed Jan. 23, 2022).
- [54] NI-National Instruments, <https://www.ni.com/en-lb.html> (accessed Jan. 23, 2022).
- [55] J. Mitola III., “Software Radios: Survey, Critical Evaluation and Future Directions,” *IEEE Aerospace and Electronic Systems Magazine*, vol. 8, no. 4, pp. 25-36, 1993, doi: 10.1109/62.210638.
- [56] W. Liu et al., “Advanced spectrum sensing with parallel processing based on software-defined radio,” *EURASIP Journal on Wireless Communications and Networking*, vol. Sept. 2013, no.1, pp.1-15, 2013, doi:10.1186/1687-1499-2013-228.
- [57] YOTTVOLT, Ettus Research SDR Solutions, <https://www.yottavolt.com/ettus-research-sdr-solutions/> (accessed Jan. 23, 2022).
- [58] Knowledge Base, Ettus Research, https://kb.ettus.com/Knowledge_Base (accessed Jan. 23, 2022).
- [59] J. R. Machado-Fernández, “Software defined radio: Basic principles and applications,” *Revista Facultad de Ingeniería*, vol. 24, no. 38, pp. 79-96, Jan. 2015, doi: 10.19053/01211129.3160.
- [60] E. Grayver, *Implementing Software Defined Radio*, 1st ed., Springer, New York, NY, 2013, doi 10.1007/978-1-4419-9332-8.

APPENDIX-A

Time-Domain Window Functions Equations

Filters are one of the signal processing components that process the signal by removing undesired frequency components. One kind of digital filter is FIR, which has several methods for designing it, and one of these methods is the window method. The design of this type of filtering is based on multiplying the infinite impulse response of the sinc function with finite time-domain window functions. Different kinds of window functions were utilized in chapter three to design digital FIR filters. According to the following equations below, the representation of time and frequency response performed in MATLAB, figure (3.6):

1. Hanning Window

The window is defined in the following equation below:

$$w(n) = 0.5 \left[1 - \cos\left(\frac{2\pi n}{N}\right) \right] \quad (1)$$

2. Blackman Window

The window is defined in the following equation below:

$$w(n) = a_0 - a_1 \cos\left(\frac{2\pi n}{N}\right) + a_2 \cos\left(\frac{4\pi n}{N}\right) \quad (2)$$

$$a_0 = \frac{1-\alpha}{2}; a_1 = \frac{1}{2}; a_2 = \frac{\alpha}{2}. \alpha = 0.16 (a_0 = 0.42, a_1 = 0.5, a_2 = 0.08).$$

3. Nuttall Window

The window is defined in the following equation below:

$$w(n) = a_0 - a_1 \cos\left(\frac{2\pi n}{N}\right) + a_2 \cos\left(\frac{4\pi n}{N}\right) - a_3 \cos\left(\frac{6\pi n}{N}\right) \quad (3)$$

$$a_0 = 0.3635819; \quad a_1 = 0.4891775; \quad a_2 = 0.1365995; \quad a_3 = 0.0106411.$$

4. BlackmanHarris

The window is defined in the following equation below:

$$w(n) = a_0 - a_1 \cos\left(\frac{2\pi n}{N}\right) + a_2 \cos\left(\frac{4\pi n}{N}\right) - a_3 \cos\left(\frac{6\pi n}{N}\right) \quad (4)$$

$$a_0 = 0.35875; a_1 = 0.48829; a_2 = 0.14128; a_3 = 0.01168.$$

5. Gaussian Window

The window is defined in the following equation below:

$$w(n) = \exp\left(-\frac{1}{2}\left(\frac{n-\frac{N}{2}}{\frac{\sigma N}{2}}\right)^2\right), 0 \leq n \leq N. \quad (5)$$

$$\sigma \leq 0.5.$$

6. Hanning- Blackman window (Proposed Window 1)

This window was proposed by multiplying the Hanning equation with the Blackman equation, and can be defined as the following below:

$$w(n) = 0.5 \left[1 - \cos\left(\frac{2\pi n}{N}\right)\right] \cdot [a_0 - a_1 \cos\left(\frac{2\pi n}{N}\right) + a_2 \cos\left(\frac{4\pi n}{N}\right)] \quad (6)$$

$$a_0 = \frac{1-\alpha}{2}; a_1 = \frac{1}{2}; a_2 = \frac{\alpha}{2}. \alpha = 0.16 (a_0 = 0.42, a_1 = 0.5, a_2 = 0.08)$$

7. Hanning-Blackman-BlackmanHarris window (Proposed Window 2)

This window was proposed by multiplying the Hanning-Blackman equation with the Blackman equation, and can be defined as the following below:

$$w(n) = 0.5 \left[1 - \cos\left(\frac{2\pi n}{N}\right)\right] \cdot [a_0 - a_1 \cos\left(\frac{2\pi n}{N}\right) + a_2 \cos\left(\frac{4\pi n}{N}\right)] \cdot [a_3 - a_4 \cos\left(\frac{2\pi n}{N}\right) + a_5 \cos\left(\frac{4\pi n}{N}\right) - a_6 \cos\left(\frac{6\pi n}{N}\right)] \quad (7)$$

$$a_0 = \frac{1-\alpha}{2}; a_1 = \frac{1}{2}; a_2 = \frac{\alpha}{2}. \alpha = 0.16 (a_0 = 0.42, a_1 = 0.5, a_2 = 0.08);$$

$$a_3 = 0.35875; a_4 = 0.48829; a_5 = 0.14128; a_6 = 0.01168.$$

APPENDIX-B

Matlab Code for single Band F-OFDM

```
function y = fcn(u) % function for filtering single band F-OFDM
N=512; % Filter Taps (1/2 FFT size of the OFDM signal)
x=floor(N/2);
b = 0.27*sinc(0.7465*(-x:x));
b = b.*blackman(513)'; % When using a Blackman filter for the others forms we
can exchange it with Gaussian, Hanning...etc.
filtTx = dsp.FIRFilter(b);
y=filtTx([u;zeros(N,1)]);

function y = fcn(u) % for RX
N=512;
x=floor(N/2);
b = 0.27*sinc(0.7465*(-x:x));
b = b.*blackman(513)';
filtTx = dsp.FIRFilter(b);
prototypeFilterInv = clone(filtTx);
y=prototypeFilterInv(u);
```

Matlab Code for Multiband F-OFDM

```
function y = fcn(u) % for TX
numFFT=1024;
N=512;
subbandSize=256;
x=floor(N/2);
b = 0.3*sinc(0.219*(-x:x)).*exp(-1i*2*pi*(0:N)/numFFT* ...
((1-1/2)*subbandSize+0.5+numFFT/2) ); % Offset to the desired sub-
band
b = b.*blackman(513)';
filtTx = dsp.FIRFilter(b);
y=filtTx([u;zeros(N,1)]);

function y = fcn(u) % for RX
numFFT=1024;
N=512;
subbandSize=256;
x=floor(N/2);
b = 0.3*sinc(0.219*(-x:x)).*exp(-1i*2*pi*(0:N)/numFFT* ...
((1-1/2)*subbandSize+0.5+numFFT/2) );
b = b.*blackman(513)';
filtTx = dsp.FIRFilter(b);
prototypeFilterInv = clone(filtTx);
y=prototypeFilterInv(u);
```

PUBLISHING

Below is a list of publications resulting from work carried out during this study:

- [1] Dia Mohamad Ali and Zhraa Zuheir Yahya, "5G F-OFDM Waveform Based Software-Defined Radio Technology," Proceedings of Engineering and Technology Innovation, vol. 20, pp. 68-80, January 2022, doi: <https://doi.org/10.46604/peti.2022.8887>. (Published)
- [2] Dia M. Ali and Zhraa Zuheir Yahya, "An Experimental Study of F-OFDM Spectrum Efficiency for 5G Applications," International Journal of Microwave and Optical Technology, vol.17, no.1, pp. 1-9, January 2022, doi: <https://doi.org/10.46581/IJMOT20218172247>. (Published)
- [3] Dia M. Ali and Zhraa Zuheir Yahya, "Flexible Sub-bands F-OFDM Configured for Spectrum Efficiency Enhancement in 5G System," Journal of Communications, vol. 17, no. 3, pp. 203-209, March 2022, doi: [10.12720/jcm.17.3.203-209](https://doi.org/10.12720/jcm.17.3.203-209). (Published)
- [4] Zhraa Zuheir Yahya and Dia M. Ali, "Multiband Filtered-OFDM Configured for 5G Spectrum Efficiency Improvement," 2nd International Conference on Engineering and Advance Technology (ICEAT 2022), 2022. (Accepted).

الخلاصة

يتعين على شبكات الجيل الخامس (5G) التعامل مع الخدمات والمتطلبات غير المتجانسة وفقاً لمعايير مشروع شراكة الجيل الثالث (3GPP) و الاتحاد الدولي للاتصالات (ITU). يعد الاستخدام الفعال للطيف أحد التحديات المهمة للجيل المستقبلي، والذي يتطلب تصميماً مرناً للطبقة المادية لتعزيز كفاءة الطيف (SE) لمجموعة واسعة من التطبيقات عبر الموارد الراديوية.

تقدم الأطروحة الحالية نموذجاً لشكل موجة شبه متعامد يسمى Filtered- Orthogonal Frequency Division Multiplexing (F-OFDM) من أجل الاستثمار الأمثل للطيف الترددي والارسال غير المتزامن. تم اقتراح سيناريوهين للنمذجة (نطاقات فرعية متساوية وغير متساوية الحجم) باستخدام برامج Matlab-Simulink و LabVIEW NXG. تم استخدام العديد من نماذج مرشح Window-Sinc للحد من خسارة طيف المستخدم / الخدمة ، ولتعزيز الأداء ، تم اقتراح شكلين من دوال النافذة.

أظهرت نتائج المحاكاة أن F-OFDM حقق أعلى نسبة تحسن لكفاءة الطيف بمقدار 5.2% و 5.8% باستخدام النافذة المقترحة الثانية في السيناريوهين الأول والثاني ، على التوالي، مقارنةً مع OFDM التقليدي. علاوةً على ذلك ، أظهر المحاكيان نفس سلوك معدل الخطأ للبت (BER) ، وتباعد أدائهما عن أداء OFDM عند القيم العالية من نسبة الإشارة إلى الضوضاء (SNR). كما زادت نسبة الذروة إلى متوسط القدرة (PAPR) بشكل طفيف نتيجة لتأثير المرشح.

تم استخدام Universal Software Radio Peripheral (USRP) X310 ، وهو أحد المنتجات المادية لتقنية Software Defined Radio (SDR) ، لتقييم أداء نماذج الارسال والاستلام المقترحة في بيئة داخلية حقيقية. تم تنفيذ بيئة الاختبار باستخدام جهاز USRP واحد وجهاز كمبيوتر شخصي مع معدات اخرى. تم إجراء التشغيل العملي على ترددات الموجات الحاملة 915 ميغاهرتز و 3.4 جيجاهرتز لإثبات مرونة تقنية SDR. كانت نتائج تحسينات كفاءة الطيف المكتسبة 5% و 5.6% للسيناريوهين الأول والثاني ، على التوالي ، مما يدعم صحة النتائج التي تم الحصول عليها في برامج المحاكاة.



وزارة التعليم العالي والبحث العلمي

جامعة نينوى

كلية هندسة الالكترونيات

قسم هندسة الاتصالات

تقصي كفاءة الطيف بتقنية F-OFDM لأنظمة الجيل الخامس

رسالة تقدمت بها

زهراء زهير يحيى

إلى

مجلس كلية هندسة الالكترونيات

جامعة نينوى

كجزء من متطلبات نيل شهادة الماجستير

في

هندسة الاتصالات

بإشراف

أ.م.د. ضياء محمد علي



وزارة التعليم العالي والبحث العلمي

جامعة نينوى

كلية هندسة الالكترونيات

قسم هندسة الاتصالات

تقسي كفاءة الطيف بتقنية F-OFDM لأنظمة الجيل الخامس

زهراء زهير يحيى

رسالة ماجستير علوم في هندسة الاتصالات

بإشراف

أ.م.د. ضياء محمد علي